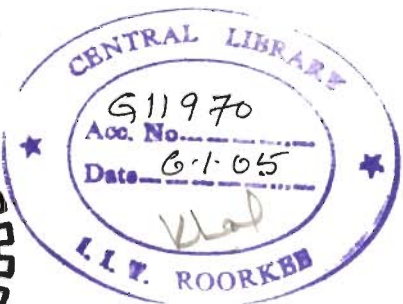# GIS-BASED STUDY FOR ROUTE PLANNING IN LANDSLIDE SUSCEPTIBLE TERRAIN

A THESIS

Submitted in fulfilment of the
requirements for the award of the degree
of
DOCTOR OF PHILOSOPHY
in
EARTH SCIENCES

By

ASHIS KUMAR SAHA

DEPARTMENT OF EARTH SCIENCES
INDIAN INSTITUTE OF TECHNOLOGY ROORKEE
ROORKEE-247 667 (INDIA)

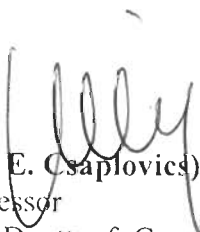JULY, 2004

CANDIDATE'S DECLARATION

I hereby certify that the work which is being presented in the thesis entitled **"GIS-BASED STUDY FOR ROUTE PLANNING IN LANDSLIDE SUSCEPTIBLE TERRAIN"** in fulfilment of the requirement for the award of the degree of **DOCTOR OF PHILOSOPHY** and submitted in the **Department of Earth Sciences, Indian Institute of Technology Roorkee**, is an authentic record of my own work carried out during a period from January 2000 to July 2004 under the supervision of **Prof. R. P. Gupta, Dr. M. K. Arora and Prof. E. Csaplovics.**

The matter presented in this thesis has not been submitted by me for the award of any other degree of this or any other University/Institute.

Date: 14.07. 2004

(ASHIS KUMAR SAHA)

This is to certify that the above statement made by the candidate is correct to the best of our knowledge.

14.7.04

(Dr. E. Csaplovics)
Professor
IPF, Deptt. of Geosciences
TU – Dresden
Dresden (GERMANY)

(Dr. M. K. Arora)
Associate Professor
Deptt. of Civil Engineering
IIT Roorkee
Roorkee (INDIA)

(Dr. R. P. Gupta)
Professor
Deptt. of Earth Sciences
IIT Roorkee
Roorkee (INDIA)

The Ph.D. viva voce examination of **Mr. Ashis Kumar Saha**, Research Scholar, has been held on 10-9-2004

Signature of Supervisors   Signature of H.O.D.   Signature of External Examiner

Abstract

Himalayas constitute the loftiest and the youngest mountain system on the Earth. Owing to their spread, elevation and general ruggedness, most of the regions in the Himalayas are not easily accessible, roads providing the only way of transport. Occurrence of landslides is one of the major problems in this region causing extensive damage to life, property and communication every year. It has been observed that most of the roads have been constructed disregarding the distribution of Landslide Hazard Zones in the region. Many sections of the roads get closed due to landslides in rainy season, thereby disconnecting many villages and towns in the area. Therefore, there is an immense need to develop a strategy utilising advanced techniques for route planning in landslide susceptible terrains, such as the Himalayas.

Remote Sensing and Geographic Information System (GIS) techniques, by virtue of their numerous advantages, appear to be an automatic choice to tackle this problem, which requires efficient processing, interpretation and analysis of a large amount of spatial data from a variety of sources.

The main objective of this research is to explore the potential of the advanced technologies – remote sensing and GIS, and to devise an automatic and intelligent approach for route planning in a hilly region prone to landslide hazards.

The study area covers a small region of about 550 km^2 in the Himalayas (Latitude 30°20'-30°34'N and Longitude 79°05'-79°22'E). It is a part of Chamoli and Rudraprayag districts of the newly formed state – Uttaranchal – of India. The terrain is highly rugged with elevations ranging from about 920 m to 4250 m above mean sea level. The river Alaknanda with its tributaries constitutes the drainage network in the area. Geologically,

the region comprises the Lesser Himalayas and the Higher Himalayas. Structurally, the region is complex due to the presence of various thrusts, faults and intense deformations.

The following datasets have been used to generate various thematic data layers:

a) Remote Sensing data: IRS-1C LISS-III multi-spectral, PAN and stereo-PAN

b) Survey of India toposheets at 1:50,000 scale (53 N / 2, 3, 6, 7)

c) Geological Map

d) Hill road design parameters (Indian Roads Congress 2001 recommendations)

e) Field data on existing landslides, landuse/landcover and ground control points (using GPS surveys)

The remote sensing data have been processed using ERDAS Imagine software. The BLUH software has been used for DEM generation from stereo-PAN image pair. The GIS analysis has been carried out using ILWIS software. A series of C++ programs have been written for route planning and the outputs have been suitably interfaced with the GIS derived themes.

The IRS-1C LISS-III multi-spectral and PAN data have been co-registered to sub-pixel accuracy with the topographic map using a large number of ground control points. The LISS-III data have been corrected for atmospheric path radiance using the 'dark-object subtraction technique'.

The Digital Elevation Model (DEM) of the study area has been generated using two methods. Firstly, an attempt has been made to generate a high resolution DEM from IRS-1C stereo-PAN image pair using BLUH software (University of Hannover, Germany). However, the DEM generated from this method could not be used subsequently as it suffered from inaccuracies due to steep slopes, differential forest cover and snow. In view of the above, the Survey of India topographic map (1:50,000) has been digitised at 40 m contour interval, interpolated and resampled to generate the DEM. Slope, aspect and relative relief maps are then derived from the DEM using standard processes in raster GIS.

Lithological and structural features have been extracted through digitisation of the geological map. The lineaments have been interpreted from 3 × 3 filter edge-enhanced LISS-III image and comparing the same with the geological map. At this stage, the structural features and lineaments are merged in a single layer and a distance buffer map is generated, which has been suitably reclassified. The drainage features have been digitised from topographic map and classified according to Strahler's ordering of streams. A drainage density map has also been generated.

Landuse/landcover map has been generated by multi-source image classification of IRS-1C LISS-III image using logical channel approach. Multi-source classification has been adopted to reduce the effect of shadows cast by high mountain peaks in the region. Nine landuse/landcover classes that have impact on landslide activities in the region have been considered. These classes are: dense forest, sparse vegetation, agriculture, fallow land, barren land, settlements, fresh sediments, water body and snow. Normalised Difference Vegetation Index (NDVI) image and DEM have been included in the classification process to reduce the effect of shadows in the region and to improve the separability among various classes. The most common classification algorithm - Maximum Likelihood Classifier – has been adopted to perform multi-source classification. It has been found that landuse/landcover map obtained from the combination of green, red and SWIR bands of LISS-III image, NDVI and DEM data layers produces the maximum overall accuracy of 92.06%. Post-classification filtering and editing has also been carried out to reduce the noise in the form of stray pixels in the map.

The PAN-sharpened LISS-III image (based on IHS transform) together with substantial field observations has been used to produce a landslide distribution map. A new statistical approach for the preparation of LHZ map has been developed and applied for the region considering several thematic layers including topographic slope, aspect, relative relief, lithology, structure-buffers, drainage density and landuse/landcover. The weight

factors have been calculated by overlaying the landslide distribution map on various thematic layers, and using a modified Landslide Nominal Hazard Factor (m-LNHF) method. The weighted thematic layers have been algebraically added to generate Landslide Hazard Index (LHI) map. A new statistical procedure has been applied to classify the LHI map into various hazard zones.

For calculating the cost of road development and maintenance, the thematic layers considered are: landslide occurrence map classified according to size, landslide hazard zones, higher order drainage (to consider bridge construction cost), landuse/landcover and lithology. The data layers have been integrated using an ordinal scale weighting-rating method. The thematic layers have been arranged in a hierarchical way, in order of increasing cost and a weight number (from 0 to 9) is given to each layer. Similarly, each class within a layer has been given an ordinal rating. These weighted layers have been aggregated to generate a thematic cost map in which the pixel value implies the thematic cost to move through the pixel.

The above thematic cost layer is a kind of isotropic cost layer and does not incorporate the costs due to neighbourhood distance and the terrain gradient, which are direction dependent. To consider these aspects, the neighbourhood schemes have to be used. In raster GIS, these schemes can be related to the movements similar to those in the game of chess, namely Rook's, Bishop's and Knight's patterns. In view of the steep topographic slopes of the area, the above existing neighbourhood schemes may not suffice and so two more possible moves (not existing in the game of chess) have been conceived and have been named here as Knight31 and Knight32. In this process, a total of 32 unique neighbourhoods are possible. The neighbourhood distance between the source and connected neighbour on the 3-D surface is calculated using the Euclidean distance formula.

The gradient between the connected neighbours is calculated and classified into various classes considering the limiting, ruling and exceptional gradient recommended by

the Indian Roads Congress (2001) for hill roads. The gradient classes have been converted into gradient costs. The neighbourhood movement cost (NM-cost) is computed from neighbourhood distance, gradient and thematic cost map, and gives the cost to move in to a connected neighbour from a source pixel.

Dijkstra's algorithm has then been used to find out the least-cost route between origin and destination points. The route thus generated has been converted into ILWIS readable segment map for its subsequent linking and integration with other thematic data layers.

A dedicated software, named as Landslide Safe Intelligent Route Finder (LaSIRF) has been developed (in C++) to compute NM-cost and to implement the Dijkstra's algorithm for finding out the least-cost route. Since, the current version of the software developed is computationally very intensive, its performance has been examined on a set of example areas, each of 1.5 km × 1.5 km size, extracted from the original study area with different types of terrain conditions and different landslide distribution patterns. This has validated the concept and the approach developed in this research. The results indicate that the algorithm wisely avoids the landslide zones as well as higher cost areas, falling on its way from the origin to the destination points. The approach developed in this study can be successfully implemented for route planning in hilly regions that are susceptible to landslides.

Acknowledgement

especially, **Jochen, Ulrich, Pradeep** and **Mike,** for making my stay comfortable and enjoyable.

Thanks are due to my friends, **Shantanu-da, Chandra-da, Umesh, Shekhar-da, Prem-da, Khan-da, Tamal, Partho, Amit, Pallov, Rajeev, Satvinder, Joshi, Sharif-da, Shashanka-da, Swapan-da, Suman, Kalyan, Ashish, Dulu, Vivek** and **Aniket** for being at an arm's distance throughout. Their companionship all along the vicissitudes of research helped me pull through with my work.

I cannot but express my heartfelt thanks to the people of Chamoli and Gopeshwar region for their help during field data collection.

The help extended by **Sarvesh Ji, Nair Ji** and other technical and non-technical staff of Department of Earth Sciences and Civil Engineering, IIT Roorkee is duly acknowledged.

Finally, my heart goes on a spin when I think of the contribution by my parents towards whatever little or much I have been able to achieve. Without their blessings and emotional strength I would have never seen this day.

Ashis Kumar Saha

Contents

List of Figures

List of Tables

Chapter 1

Introduction

1.1 Introduction

Himalayas being the youngest orogen of the world are very sensitive in terms of stability, seismicity and environment. Owing to their spread, elevation and general ruggedness, the regions in the Himalayas are not easily accessible, the only mode of transport being by roads. Prior to 1960, there were very few roads in the Himalayan region. Later, with the formation of Border Roads Organisation (BRO) in India, a major thrust was given to the development and maintenance of roads in this region also.

However, occurrence of landslides is one of the major problems in the Himalayas that cause extensive damage to life, property and communication every year. It has been observed that in general, most of the roads are constructed disregarding the distribution of Landslide Hazard Zones in the region. Therefore, a huge amount of money and manpower is spent for the maintenance of roads throughout the year. Moreover, several roads get closed due to landslides in rainy season, thereby disconnecting many villages and towns in

the area causing acute local civic miseries, besides hampering the developmental activities (Fig. 1.1). Hence, there is a tremendous need for proper planning of roads that considers efficient engineering design as well as consideration of geological factors in terms of slope stability and safety measures.

Suitable and efficient route planning, thus, has large-scale significance in hilly areas and therefore requires careful attention. Broadly, the route planning may be defined as 'the selection of the best possible route from a set of alternatives based on optimal costs and various considerations at command'. The basic objectives of planning hill roads in Indian scenario may be summarised as (Tiwari, 1981):

a) For the development of hilly areas, and for maintaining better communication and supplies to these areas

b) Extending urban amenities in the hilly areas

c) For the development of border roads for strategic purposes

d) To provide access to remote hilly areas - for tourists, nature lovers and from pilgrimage point of view.

1.2 Factors Affecting Routes (Development and Maintenance) in the Himalayas

Route development in hilly areas is a difficult job as the terrain plays an important role in route planning. A hill road has to traverse a longer path with numerous curves and turnings to meet the elevation requirements, in contrast to the roads in the plain areas, which are usually straight and with shortest distance. Therefore, during hill road planning a number of factors ought to be taken into consideration (Tiwari, 1981; Khanna and Justo, 1987). These include:

a) Distance from source to destination

b) Geological safety and soundness

c) Stability of slopes and landslide hazards

Figure 1.1: (a) Field photograph showing a road passing through an active landslide zone in the study area. (b) Disrupted traffic due to road blockade caused by a fresh landslide.

d) Drainage crossings and extent of waterways

e) Necessity of passing through obligatory points, *e.g.,* villages, *etc.*

f) Topography and gradient

g) Need for special structures, *e.g.,* bridge, tunnel, retaining wall, *etc.*

h) Value of land

i) Construction cost, cut-and-fill, *etc.*

j) Availability of construction material

All the above factors are required to be given due attention for efficient and accurate route planning in hilly areas.

1.3 Conventional Route Planning Practice and its Limitations

Although all the above factors ought to be considered during route planning, the hill roads are generally planned without considering the geological hazards, the only or major consideration usually being the topography and the length of the road.

The conventional route planning practice followed widely in India is based on manual method. A reconnaissance survey carried out based on Survey of India toposheets at scale commonly 1:50,000 and contour interval ≈50 m constitutes a major part of the route alignment planning as it helps in deciding subsequent detail surveys for actual road construction. On the base (contour) map, traces are drawn with a divider to demarcate the possible routes at specified gradient. In this way, various alternative routes are drawn and the same are comparatively evaluated in terms of length and cost of the route to identify the best route. Hence, the process is largely manual, tedious and time consuming. Therefore, there is always a high possibility that not all the possible routes are considered and only the easiest, as per convenience, which may not be the best, is selected.

Introduction of the aerial photogrammetric techniques has resulted in overcoming some of the limitations of the conventional manual route planning approach. The aerial

photographs provide a synoptic overview as well as the three-dimensional perspective view of the terrain. It also helps the specialists to work in the laboratory and reduces the necessity of tiresome field investigations. The photogrammetric plotting instruments can also be used to generate contours and plot the suitable route alignments. A detailed review of photogrammetric techniques for route planning can be found in Linkwitz (1961).

Still, however, in the manual route planning, geological aspects, particularly landslide distribution, which is a key factor, is not taken into consideration, which in turn may lead to recurring problems of landslide activity in the route alignment. Besides, in the manual approach it is also nearly impossible to concurrently consider all the thematic factors (as mentioned in the previous section), which are spatial in nature.

Hence, there is a great need to plan roads using computer-assisted methodology that may consider various parameters including landslide hazards.

1.4 Remote Sensing – GIS Advantages

With the availability of satellite remote sensing data at many different spatial, spectral and temporal resolutions, it has now become possible to efficiently and accurately collect and analyse a variety of spatial attributes, such as geology, structure, landuse/landcover, lineaments, *etc.* of an area. The advantages of remote sensing data can be enumerated as (Cracknell, 1993; Cracknell, 1998; Navalgund, 2001; Lillesand and Kiefer, 1999; Gupta, 2003) –

    a) Synoptic overview of the terrain

    b) Repetitive coverage of the area

    c) Unbiased recording of events

    d) Data availability in digital form

    e) Cost-effective technology

    f) Multi-spectral information

g) Stereoscopic viewing and 3-dimensional capability (for selective satellite sensors)

The Geographic Information System (GIS) and advanced computing facilities offer numerous advantages in multi-geodata handling, such as (Aronoff, 1989):

a) Storage of large quantities of data in cost-effective and efficient digital formats and their fast retrieval

b) Capability of integrating different types of data in a single analysis

c) Ability to perform complex spatial analysis rapidly

d) Usefulness in planning and decision-making

Therefore, remote sensing and GIS techniques, by virtue of their numerous advantages, appear to be the automatic choice to tackle the problem of route planning, which requires efficient processing, interpretation and analysis of large amount of spatial data of great variety.

1.5 Objective of the Research

The main objective of this research is to tap the potential of the advanced technologies – remote sensing and GIS, and to devise an automatic and intelligent approach for route planning in a hilly region that are prone to landslides. The objective includes developing a methodology to combine and optimise various parameters related to route planning in GIS environment supplemented with the coding of data analysis techniques in C++ programming language. The resulting alternative route should be cost effective in terms of development and maintenance.

1.6 Methodology - Overview

This study has been carried out using an integrated remote sensing – GIS approach. In the following section, the broad methodology adopted in the present study has been outlined (Fig. 1.2). Detailed description of the methodologies has been given at relevant places in the chapters to follow.

Data and Software Used: The following data sets have been used to generate various thematic data layers corresponding to factors responsible for route planning in a region:

a) Remote Sensing data: IRS-1C LISS-III multi-spectral, PAN and Stereo-PAN

b) Survey of India toposheets (1:50,000 scale)

c) Geological map

d) Hill road design parameters (Indian Roads Congress recommendations, 2001)

e) Field data on landslides, landuse/landcover and ground control points (using GPS surveys)

The processing of remote sensing data has been done using ERDAS Imagine software. The BLUH software has been used for DEM generation from stereo-PAN image pairs. The GIS analysis has been carried out using ILWIS software. A series of C++ programs have been written for route planning and the outputs have been suitably interfaced with the GIS derived thematic data layers.

In this work, particular emphasis has been placed on various aspects of landslides and landslide hazard zones, which is the key for successful route planning in hilly areas. For this purpose, a suitable test site has been selected in the Himalayas. A large number of thematic data layers have been generated and analysed. These include topographic data (including elevation, slope, aspect and relative relief), drainage, geology (lithology and structure), landuse/landcover, landslide distribution and landslide hazard zonation.

Data Pre-processing: In order to analyse such a large amount of data both in digital and paper form at a common geo-reference system, their accurate registration is a pre-requisite. Therefore, all the data layers have been co-registered with the base map constituting Survey of India (SOI) topographic maps. The multi-spectral LISS-III data has also been corrected for atmospheric path radiance.
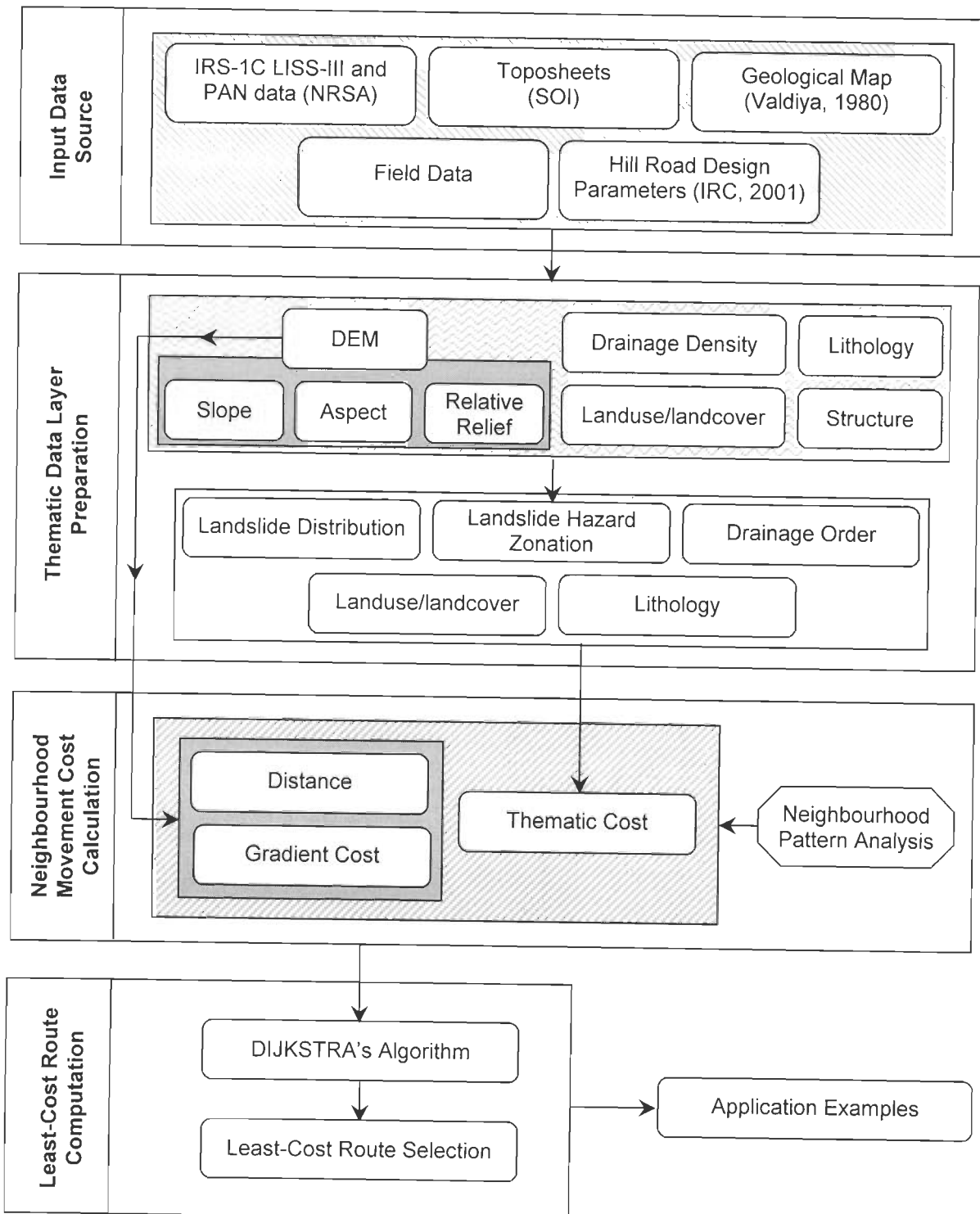
Figure 1.2: Flow diagram showing the broad methodology adopted in this study.

Thematic Data Layer Preparation: The geo-referenced database has been used for various thematic data layer preparation. The elevation contours have been digitised on-screen, rasterised and interpolated to generate digital elevation model (DEM). An attempt has also been made to generate a DEM from stereo-PAN data analysis using photogrammetric techniques; however, the same could not be used due to severe distortions. The topographic map derived DEM has therefore been used to generate slope, aspect, relative relief and shaded relief maps. The geological map has been digitised to extract lithological and structural information. The drainage network is digitised from the topographic map and is used to calculate the drainage density. The IRS-1C LISS-III image has been processed for linear feature enhancement to generate a lineament map. Multi-source classification using IRS-1C LISS-III remote sensing data and DEM derived layers has been performed to produce landuse/landcover map. The IRS-1C LISS-III and PAN data have also been used to generate merged product to map landslide distribution. These data layers have further been processed and statistically integrated to generate a Landside Hazard Zonation map.

Neighbourhood Movement Cost Calculation: Thematic data layers (namely, landslide distribution, landslide hazard zonation, drainage order, landuse/landcover and lithology) have been integrated to generate a thematic cost map, which takes into account the nominal costs pertaining to the development and maintenance of roads. To consider the cost of movement due to gradient from a particular pixel to a connected neighbour, the DEM has been utilised and the gradient has been calculated using Euclidean rule. The gradient data and distance factors have been suitably integrated with the thematic cost. The integrated cost is named as Neighbourhood Movement cost (NM-cost).

Least-Cost Route Calculation: A dedicated C++ software, named here as Landslide Safe Intelligent Route Finder (LaSIRF) has been written to implement the Dijkstra's Algorithm (Dijkstra, 1959) to determine the least-cost route between a given source

and destination. The route generated by the software is then converted to a segment map and imported in the GIS database.

A few example areas representing different terrain conditions and landslide hazard zones have been considered as case studies to demonstrate the utility of the approach developed in this research for route planning.

1.7 Organisation of the Thesis

In this chapter, after introducing the problem, the research objectives and an overview of the broad methodology have been set out. Chapter 2 provides a review on landslides and various landslide hazard zonation techniques, which have assisted in adopting a suitable methodology for this study. In Chapter 3, the study area and the data sources used have been described. Chapter 4 describes in detail the preparation of various thematic data layers based on recent and new techniques. In Chapter 5, the details of methodology developed for data integration for thematic cost calculation has been presented. The description of route planning approach developed in this study has been provided in Chapter 6. A few representative case studies have also been presented here to validate and examine the efficacy of the approach developed in this research. Finally, Chapter 7 provides summary and conclusions.

Chapter 2

Landslides and Landslide Hazard Zonation – A Review

2.1 Introduction

Among the various natural hazards, landslides are the most widespread and damaging hazard. They cause loss of life and property, damage to natural resources (*e.g.*, vegetation, land and soil) and hamper developmental projects like roads, bridges and communication lines, *etc.* It has been estimated that, on an average, the damage caused by landslides in the Himalayan range costs more than US$ one billion besides causing more than 200 deaths every year, which overall is considered as 30 percent of such types of losses occurring world-wide (Naithani, 1999). Malpa landslide of August 1998 and Uttarkashi landslide of September to October 2003 are burning examples in the Himalayas that have caused large-scale human tragedies, material damage and associated environmental–social hazards.

The Himalayan terrain possesses a high susceptibility to landslides, mainly owing to a complex geological setting combined with contemporary crustal movements, varying slopes and relief, heavy rainfall, along with ever-increasing human interference in the ecosystem. Mitigation of disasters caused by landslides can be taken up, only when

detailed knowledge about the expected frequency, character and magnitude of mass movements in an area is available. For a quick and safe mitigation measure and future strategic planning, identification of landslide prone areas (Landslide Hazard Zonation), therefore, becomes a pre-requisite.

Although, it may not be possible to predict a landslide event in space and time, an area may be segmented into near-homogeneous domains and ranked according to degrees of potential hazard due to mass-movements (Varnes, 1984). Such maps are called Landslide Hazard Zonation (LHZ) maps (also referred to as Landslide Susceptibility maps). The landslide hazard and/or risk assessment and zonation are generally based on two fundamental assumptions (Aleotti and Chowdhury, 1999). Firstly, landslides always occur in the same geological, geomorphological, hydrogeological and climatic conditions as in the past, and secondly, the main conditions that cause landslides are controlled by identifiable physical factors.

The LHZ maps are useful in several ways (Anbalagan, 1992), for example,

a) These maps assist planners in the selection of favourable sites for development schemes, such as buildings, dams and road construction. Even if the hazardous areas cannot be avoided altogether, their recognition in the initial stages of planning may help adopt suitable precautionary measures.

b) These maps also assist in identifying and delineating hazard-prone areas, so that environmental regeneration programs can be initiated and suitable mitigation strategies may be adopted.

The evaluation of landslide hazard is a complex task as the occurrence of landslides is dependent on many factors (Brabb, 1991). In the last few decades, several field-based hazard zonation studies with manual integration of data have been carried out in the Himalayas (*e.g.,* Brabb, 1984; Anbalagan, 1992; Pachauri and Pant, 1992; Gupta *et al.,* 1993; Virdi *et al.,* 1997; Pachauri *et al.,* 1998, *etc.*). However, these approaches have

several drawbacks, such as the extent of the area covered is generally small and manual overlay of thematic maps is tedious and thus, has poor integration capability.

The application of remote sensing data coupled with Geographic Information System (GIS) analysis has tremendously helped preparation of LHZ maps with greater efficiency and accuracy than before. This is primarily due to the fact that through this technology, it is possible to collect, manipulate and analyse a variety of spatial and non-spatial data about the causative factors (such as lithology, structure, landcover, geomorphology, vegetation, *etc.*) responsible for triggering the landslide activity in a region (Varnes, 1984; Gupta and Joshi, 1990; Carrara *et al.*, 1991; McKean *et al.*, 1991; Nagarajan *et al.*, 1998; Gupta *et al.*, 1999; Rautela and Lakhera, 2000; Saha *et al.*, 2002).

2.2 Factors Responsible for Instability of Slopes

The factors that are responsible for instability of slopes are mainly of two types: natural and anthropogenic, which can be further subdivided as follows (Varnes, 1984; Dikau *et al.*, 1996; Naithani, 1999):

A) Natural-   (a) Inherent: i. Lithology of slope material

                                    ii. Structure

                                    iii. Geomorphology

                                    iv. Vegetation

                                    v.   Hydrogeologic conditions

                     (b) External: i. Seismicity

                                    ii. Climate

                                    iii. Undercutting by river and sea waves

B) Anthropogenic-   (a) Landuse change

                     (b) Unplanned construction

Lithology: Lithology reflects the physical and chemical behaviour of a rock. The composition, fabric, texture, grainsize, type of origin, *etc.*, of the rocks determines their permeability, shear strength, susceptibility to physical and chemical weathering that in turn affects the slope stability.

Structure: Structure includes the features of inhomogeneity and discontinuity in rocks or soils at scales larger than hand specimen. Since landslides are gravitational phenomena, the pre-existing weak planes in the form of joint planes, bedding and other structures are the pre-requisites for landslides to occur. Generally, the joints dipping towards the valley are responsible for inducing the landslides.

Geomorphology: An important geomorphologic character is the presence or absence of pre-existing landslides, as this governs the behaviour of the terrain. The slope angle has a direct bearing on instability as the gravitational forces are accentuated with increasing slope angle. The relative relief has a similar effect as the weight of the slope material (*i.e.,* the weight increases with the increase in relative relief). Slope aspect (*i.e.,* direction in which slope faces) and its curvature, both down slope and across slope, may have a local effect on slope stability.

Vegetation: Vegetation is an important factor in controlling the erosion of the slopes. A thickly vegetated slope reduces the action of climatic agents, such as rain, and prevents erosion because of natural anchorage provided by the tree roots. The grass cover drastically reduces the subsurface seepage of rainwater and thereby keeps the slope safe. On the other hand, barren slopes are more prone to erosion and thus, the landslides.

Hydrogeologic conditions: The presence of water increases the pore water pressure and decreases the shear strength. Therefore, the hydrogeological conditions indicating the nature of distribution of subsurface water within the geological units are also important.

Seismicity: The earthquake shocks are responsible for many landslides as the vibrations due to earthquake may induce instability, particularly in loose and unconsolidated material on steep slopes.

Climate: The climatic pattern due to change in latitude, longitude and altitude may also influence landslide activity. For example, in Arctic regions, frost action and extreme ranges in temperature may induce rock-fall hazards. High rainfall in tropical and subtropical climate may activate landslides, *e.g.,* in the Himalayas.

Undercutting action of river and sea waves: The under-cutting by river and sea waves may cause rock fall hazard.

Landuse change: The landuse change, such as deforestation, conversion of vegetated slopes into built up area, *etc.* may also result into the occurrence of landslides.

Unplanned construction: The removal of lateral support and overloading of slopes by human activities is an important cause of slope failure in many areas, *e.g.,* cutting for roads, housing, excavation quarrying and open pit mines, *etc.*

2.3 Input Data for Landslide Hazard Zonation

Based upon the factors responsible for slope instability and landslide hazard, a variety of input data can be used for landslide hazard zonation. The requirement of input spatial thematic maps with different classes of associated factors depends largely upon the scale at which the LHZ map is to be prepared. Accordingly, regional scale (<1:100,000), medium scale (1:25,000 – 1:50,000) and large scale (>1:10,000) maps may be generated. van Westen (1994) provides an overview of the data types that can be used for studies at different map scales (Table 2.1).

Table 2.1: Overview of input data and their collection techniques
for landslide hazard analysis (van Westen, 1994)

Data types	Summary of data collection techniques	Feasibility of data collection		
		Regional scale	Medium scale	Large scale
GEOMORPHOLOGY				
1. Terrain mapping units	Satellite image interpretation + walk over study	High	Moderate	Low
2. Geomorphological units	Aerial photo interpretation and field check	Moderate	High	High
3. Geomorphological subunits	Aerial photo interpretation and field check	Low	High	High
4. Landslides (recent)	Aerial photo interpretation and field descriptions	Low	High	High
5. Landslides (older period)	Aerial photo interpretation + collection of landslide records from newspapers, fire brigades, or church archives	Low	High	High
TOPOGRAPHY				
6. Digital elevation model	Collection of existing contour maps	Moderate	High	High
7. Slope map	Generated from a (DEM)	Moderate	High	High
8. Slope direction map	Generated from a DEM. No extra data collection required	Moderate	High	High
9. Breaks of slope	Aerial photo interpretation	Low	Moderate	High
10. Concavities/convexities	Generated from a DEM or detailed photo interpretation	Low	Low	High
ENGINEERING GEOLOGY				
11. Lithology	Checking of existing geological maps or by mapping if no data are available	Moderate	High	High
12. Material sequences	Produced from integration of other maps (geomorphological, geology, slope and DEM)	Low	Moderate	High
13. Sampling points	Field descriptions of soil and rock outcrops + Laboratory analysis of selected samples to characterize material types	Moderate	High	High
14. Faults and lineaments	Satellite image and aerial photo interpretation, and field work	High	High	High
15. Seismic events	Collection of existing seismic records	High	High	High
16. Isolines of seismic intensity	Questionnaires on the observed damage from earthquake(s)	Low	Moderate	High
LANDUSE/ LANDCOVER				
17. Infrastructure(recent)	Aerial photo interpretation and topographic map	Moderate	High	High
18. Infrastructure (older)	Aerial photo interpretation and topographic map	High	High	High
19. Land use map (recent)	Aerial photo interpretation and classification of satellite images and field check	Moderate	High	High
20. Land use map (older)	Aerial photo interpretation	Moderate	High	High
21. Cadastral blocks	Collection of existing cadastral maps and database	Low	Low	High
HYDROLOGY				
22. Drainage	Aerial photo interpretation and topographic map	High	High	High
23. Catchment areas	Aerial photo interpretation and topographic map or modelling from a DEM	Moderate	High	High
24. Meteorological data	Collection of existing meteorological stations	High	High	High
25. Water table	Field measurements of Ksat and modelling	Low	Low	Moderate

2.4 LHZ Methods – A Review

A number of methods for landslide hazard zonation have been proposed which can be grouped into six broad categories (Table 2.2). Detailed review of the methods can be found elsewhere (*e.g.,* van Westen, 1994; Aleotti and Chowdhury, 1999; Guzzetti *et al.,* 1999). Nevertheless, a brief review is provided here to understand the logic of each method.

Table 2.2: Various methods for Landslide Hazard Zonation
(After van Westen, 1994; Mantovani *et al.*, 1996)

LHZ method	Main feature	For example
1) Distribution Analysis	Direct mapping of mass movement features resulting in a map, which gives information only for those sites where landslides have occurred in the past.	Wieczorek (1984)
2) Qualitative Analysis	Direct or semi-direct methods in which the geomorphological map is renumbered to a hazard map or in which several maps are combined into one using subjective decision rules based on the experience of the earth scientist.	Saha *et al.* (2002)
3) Statistical Analysis	Indirect methods in which statistical analysis techniques are used to predict mass-movements from a number of parameter maps	Yin and Yan (1988); Gupta and Joshi (1990); Lee *et al.* (2002a); Carrara *et al.* (1991); Chung and Fabbri (1999)
4) Distribution-free methods	Neural networks and neuro-fuzzy methods, which do not depend on distributional assumptions of the data. Here, the weights are computed in an objective manner.	Arora *et al.*(2004); Elias and Bandis (2000)
5) Deterministic Analysis	Indirect methods in which parameters are combined in slope stability calculation	Okimura and Kawatani (1986)
6) Landslide Frequency Analysis	Indirect methods in which earthquakes and/or rainfall records or hydrological models are used for correlation with known landslide dates to obtain threshold values with a certain frequency	Capecchi and Focardi (1988)

2.4.1 Distribution Analysis

Distribution analysis is a simple method, which shows the distribution of existing landslides mapped from field investigations, aerial photo interpretation and/or historical records. These maps do not provide information on predictive behaviour of future landslide activity. GIS techniques can only be used for transferring maps to digital format. This method is most suitable for medium to large-scale landslide hazard zonation. Although this kind of landslide inventory map preparation is a time-consuming and difficult affair, these maps may be useful for preliminary studies of an area. The case studies using this method may be found in Wieczorek (1984) and Jha (1991).

2.4.2 Qualitative Analysis

In the qualitative analysis, a set of subjective decision rules are applied to define weights and ratings based on the field knowledge and experience of earth science experts. This method has become very popular for regional and medium scale hazard zonation because of its fast, easy to use capability where a large number of input maps can be considered. The qualitative methods can broadly be grouped into two categories: (a) field-geomorphological analysis and (b) index map overlay/combination. In field-geomorphological analysis, a hazard zonation map is prepared on the basis of examination of various parameters and subjective rules driven by the geomorphologist (*e.g.*, Rupke *et al.* 1988). GIS is used here only as a drawing tool (*e.g.*, van Westen *et al.*, 2000).

In the index map overlay/combination method, the GIS techniques are used for thematic data layer generation, assigning of weights to each parameter classes/maps and overlay operation. In this method, a numerical value or weight is assigned to each thematic data layer. Within the thematic data layer, there are different classes with a rating assigned to each. The weighting-rating may either be based upon the experience of the earth scientist (Saha *et al.*, 2002) or on the logical analytic model (Bughi *et al.*, 1996), where on-

site monitoring of slope deformation data helps to calibrate the weights. These maps are then overlaid or combined by algebraic operations to prepare an LHZ map.

2.4.3 Statistical Analysis

To remove the subjectivity associated with qualitative analysis methods, various statistical methods have also been employed for LHZ studies. These methods compare the spatial distribution of landslides with the parameters that are being considered (Aleotti and Chowdhury, 1999). These methods can broadly be classified into three types: bivariate, multivariate and probabilistic prediction models.

2.4.3.1 Bivariate Statistical Analysis

The bivariate models are based on the overlay of parameter maps and calculation of landslide densities. In this case, each individual parameter or thematic data layer is considered at a time to calculate the weight factor and can be easily implemented in a GIS environment. Three such methods, Information Value (InfoVal) method (Yin and Yan, 1988; van Westen 1997), Landslide Nominal Risk Factor (LNRF) method (Gupta and Joshi, 1990) and Weight of Evidence method (developed by Bonham-Carter *et al.* (1988) for gold prospecting) are widely used in medium scale landslide hazard analysis.

a) Information Value Method

van Westen (1997) used a statistical method for Landslide Hazard Zonation, which considers the probability of landslide occurrence within certain area of each class of thematic data layer. This method is regarded as a simplification of the method in Yin and Yan (1988), in which the weights of a particular class in a thematic map are determined as:

$$W_i = \ln\left(\frac{Densclas}{Densmap}\right) = \ln\frac{Npix(S_i)/Npix(N_i)}{\sum_{i=1}^{n} Npix(S_i)\bigg/\sum_{i=1}^{n} Npix(N_i)} \qquad (2.1)$$

where, W_i denotes the weight given to the ith class of a particular thematic data layer (*e.g.,* Granite or Limestone in the thematic layer 'Lithology'); *Densclas* denotes the landslide density within the thematic class; *Densmap* denotes the landslide density within the entire thematic layer; *Npix(S_i)* denotes the number of pixels, which contain landslides, in a certain thematic class; *Npix(N_i)* denotes the total number of pixels in a certain thematic class and n is the number of classes in a thematic map.

Thus, the weight is calculated for various classes of each thematic data layer. The thematic data layers are then overlaid and added to prepare a Landslide Hazard Index (LHI) map. Near-equal subdivision of LHI cumulative frequency curve into five classes yields zones of different landslide hazards (*i.e.,* very high, high, moderate, low and very low). However, the boundaries may be adjusted subjectively to refine the LHZ map (van Westen, 1997).

b) Landslide Nominal Risk Factor (LNRF) Method

In this method, the Landslide Nominal Risk Factor (LNRF) (Gupta and Joshi, 1990) is determined and is related to the weight of each class of thematic maps considered for the preparation of LHZ map, as follows:

$$LNRF_i = \frac{Npix(S_i)}{\left(\sum_{i=1}^{n} Npix(S_i)\right)\Big/n} \tag{2.2}$$

where, *Npix(S_i)* denotes the number of pixels containing landslides in i^{th} thematic class and n is the number of classes present in the particular thematic data layer.

A higher value of LNRF (*i.e.,* LNRF >1) implies more susceptibility to landslides than the average; an LNRF value <1 indicates less susceptibility to landslides; whereas, an LNRF value =1 indicates a thematic class with an average landslide susceptibility.

Gupta and Joshi (1990) regrouped the LNRF values broadly into three classes for each thematic data layer, and assigned weights 0, 1 and 2 for LNRF<0.67 (low risk), 0.67<LNRF<1.33 (medium hazard) and LNRF>1.33 (high risk) respectively. The thematic data layers were overlaid and aggregated to prepare a LHI map. The LHI map is then classified into three hazard zones: low, medium and high keeping equal intervals of LHI values.

c) *Weight of Evidence Model*

The weight of evidence model uses Bayes rules for conditional probability to calculate weights for binary input thematic data layers. A test of conditional independence has to be performed for the selection of the factors to be used for landslide susceptibility/hazard mapping. The weights of the thematic data layers are then added and the final map provides the posterior probability of occurrence of landslides for each pixel. The detailed formulation of this method along with a case study can be found in Lee *et al.* (2002a).

2.4.3.2 Multivariate Statistical Analysis

Multivariate methods consider relative contribution of each thematic data layer to the total hazard within a defined area. Multiple regression analysis and discriminant analysis are generally used to analyse the thematic data layers (Carrara *et al.*, 1977; Chung and Fabbri, 1999; Clerici *et al.*, 2002). These methods are time-consuming considering the data collection, handling of large volumes of data and analysis. In order to use this method, external statistical software packages are generally used to support the GIS packages.

2.4.4 Distribution-free Methods

Recently, neural network (Arora *et al.*, 2004; Lee *et al.*, 2004) and neuro-fuzzy (Elias and Bandis, 2000) methods have also been used to generate LHZ maps. These methods are free from any distributional assumptions or bias of the data, rather the weights

are computed in an objective manner. GIS is mainly used for thematic data layer generation. The analysis of the data layers for the generation of LHZ maps is usually performed using external artificial neural network and fuzzy logic tools, such as those available in MATLAB software.

Table 2.3: Summary of the feasibility and usefulness of various methods for LHZ at three working scales (Modified after Mantovani *et al.*, 1996)

LHZ methods	Regional scale		Medium scale		Large scale		Role of GIS
	Feasibility	Usefulness	Feasibility	Usefulness	Feasibility	Usefulness	
Distribution Analysis	Moderate	Useful	Good	Useful	Good	Useful	Moderate
Qualitative Analysis	Good	Useful	Good	Limited use	Good	No use	Moderate
Statistical Analysis	Low	No use	Good	Useful	Good	Limited use	High
Distribution-free methods	Low	No Use	Good	Useful	Good	Limited use	High
Deterministic Analysis	Low	No Use	Low	Limited use	Moderate	Useful	High
Landslide Frequency Analysis	Moderate	Limited use	Good	Useful	Good	Limited use	Low

2.4.5 Deterministic Analysis

The deterministic landslide hazard analysis is only applicable to large-scale hazard zonation or site-specific geotechnical studies. In this case, slope stability factors are calculated for a particular portion with the help of mathematical models considering various datasets measured directly from the site. These factors include soil layer thickness, soil strength, depth below the terrain surface of potential sliding surfaces, slope angle, pore pressure conditions, ground water level map, *etc.* (Nilsen and Brabb, 1977; van Westen, 1994). GIS and 3-D modelling software are generally used to determine the stability

factors in different cross-sections. A detailed review can be found in Aleotti and Chowdhury (1999).

2.4.6 Landslide Frequency Analysis

The landslide frequency analysis is aimed at providing information on the probability of occurrence at a specific location within a certain time period considering the triggering agents, such as rainfall and earthquakes (van Westen, 1994; van Asch *et al.*, 1999). This method is suitable for large and medium scale studies provided daily rainfall data and landslide record are available for a large span of time.

A summary of the feasibility and usefulness of applying various LHZ methods has been given in Table 2.3. It may be mentioned here that for regional and medium scale LHZ studies, the methods based on qualitative and statistical analysis have extensively been employed. The qualitative methods have the disadvantage of utilising arbitrary weights. Therefore, to introduce objectivity in weight assignment and for landslide hazard zonation, statistical analysis and distribution-free methods may be more appropriate than others. In this study, two bivariate statistical methods namely Information Value and LNRF (with some modification) have been implemented for the generation of LHZ map in a raster based GIS environment and their results compared. The LHZ map, thus generated, has been used as a data layer for route planning studies which is the prime objective of this research.

Chapter 3

Study Area and Data Sources

3.1 General

Almost the whole Himalayan belt is prone to landslides. Therefore, a region in the Garhwal Himalayas covering parts of Chamoli and Rudraprayag districts has been selected for this study. This region represents a typical high-altitude rugged terrain, affected by a large number of landslides. The area is also prone to earthquakes, which may again lead to reactivation of the existing landslides (Ravindran and Philip, 1999; Saraf, 2000). The region provides access to the important Hindu pilgrimage centres of Badrinath and Kedarnath, which attract millions of devotees and tourists every year. Besides, there are also several tourist places and trekking routes (*e.g.,* Chopta, Tungnath, Diuriya Tal, *etc.*) (Fig. 3.1). Thus, altogether there appears to be plenty of scope to develop new access routes to various tourist places in this region.

3.2 Study Area

3.2.1 Location

The study area is bounded by 30°20'N and 30°34'N latitudes and 79°05'E and 79°22'E longitudes (Fig. 3.2) covering about 550 km^2 and constitutes a part of Survey of India toposheet numbers 53N/2,3,6,7 (scale 1:50,000). Chamoli (30°24'08"N, 79°19'59"E) and Gopeshwar (30°24'48"N, 79°18'59"E) are the two major towns falling in the area. Chamoli is well connected by road with some of the important tourist destinations, *e.g.*, Rishikesh, Okhimath, Joshimath, *etc.*

3.2.2 Physiography and Drainage

The area represents a highly rugged mountainous terrain with altitudes varying from a minimum of 920 m to a maximum of 4250 m above mean sea level (msl). The highest and the lowest elevation points in the region are about 25 km apart. The Alaknanda river flowing through the south-eastern part of the study area with its tributaries constitutes the drainage network of the area. The Alaknanda river and its tributaries form a deep constricted V-shaped valley, which together with the high run-off and steep gradients indicates a young stage of geomorphological development of the region. Generally, the tributary streams are at much higher elevation (approximately 40 m to 100 m) than the main river. Several snow-covered peaks above 3800 m are also present, lying mostly in the north-eastern part of the study area.

The drainage network in this region mainly follows the geological-structural features. The drainage order goes upto the 6th order (Strahler's scheme, 1964) on 1:50,000 scale. Some of the important tributaries are Balasuti Nadi, Amrit Ganga, Kyar Gad, Kakra Gad and Kyunja Gad. Besides, several natural springs also exist in the area. In general, the drainage pattern may be referred to as angular to rectangular (Fig. 3.2).

(a) Chopta – a tourist destination.

(b) A road through a forest.

(c) The famous temple of
Badrinath, access to which
must pass through the study area.

(d) An early morning view of the
Kedarnath peak from Okhimath.

Figure 3.1: Some scenic views in this part of the Himalayas.
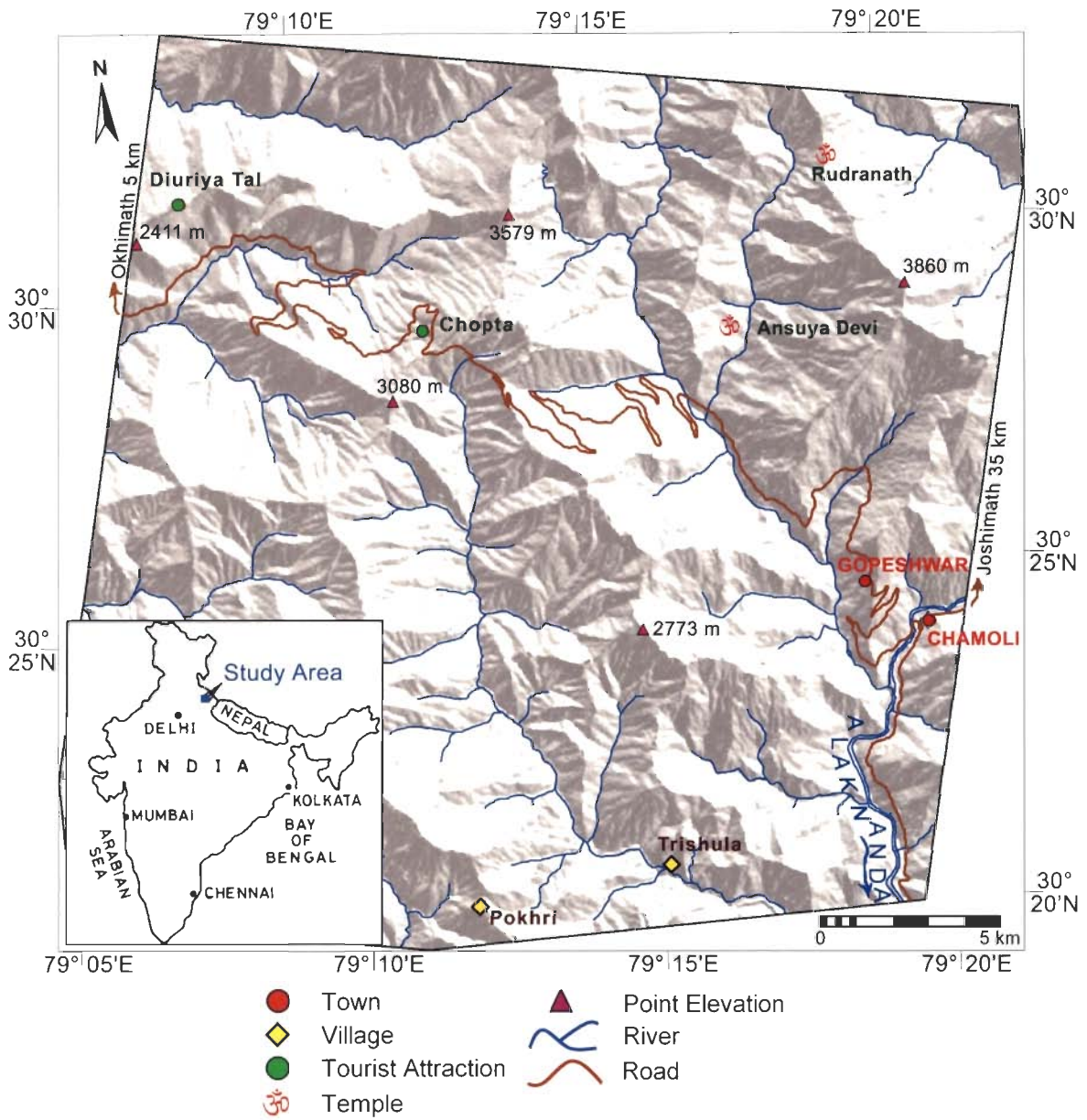
Figure 3.2: Location map of the study area (the background is a shaded relief model).

3.2.3 Climate

The climate of this region is characterised by a short and less severe hot weather followed by a colder and prolonged winter. The average summer temperature is about 25° C and winter temperature drops down to even sub-zero in the northern part of the study area. The rainfall in this region is mainly due to monsoon. The average annual rainfall varies from 140 cm to 160 cm. Snowfall occurs mostly in the northern part of this area during the winter months only.

3.2.4 Vegetation

There is a marked difference in density of vegetation in different parts of the area. In general, south facing slopes are more vegetated than the north facing slopes owing to differential solar insolation. The high altitude areas are snow covered, whereas medium altitudes are largely covered with pine trees. The cultivation is usually done on the terraces of the hill slopes with rice being the main crop grown in this region.

3.2.5 Geology

Geologically, the area falls mainly under Lesser Himalayas with some part lying under the Higher Himalayas. The Main Central Thrust (M.C.T.) or Vaikrita Thrust, passing through the northern part of the study area, separates the rocks of the Lesser Himalayas from those of Higher Himalayas. The geological setting of the area has been studied by many researchers (*e.g.,* Gansser, 1964; Valdiya, 1980) who have used different nomenclatures for the litho-units and structural discontinuities. In this study, the nomenclature followed by Valdiya (1980) has been used. Table 3.1 shows the litho-tectonic succession of the area. A regional geological map of this area adopted from Valdiya (1980) has been shown in Figure 3.3.

3.2.5.1 Lithology

The broad litho-tectonic units exposed in this area are described below (*cf.* Table 3.1):

Table 3.1: Litho-tectonic succession of the study area (Valdiya, 1980)

	Group	Formation	Rock Type
Higher Himalayas	Vaikrita Gr.	Joshimath Fm.	Sillimanite / Kyanite / Staurolite / Garnet / Biotite / Muscovite schist / gneiss / migmatites
	----------------------------------Vaikrita Thrust ----------------------------------		
Lesser Himalayas	Almora Gr.	Munsiari Fm	Granite-granodiorite and augen gneiss Schist, amphibolite, mylonitized granite-gneiss and augen gneiss.
	----------------------------------Munsiari Thrust----------------------------------		
	Ramgarh Gr.	Nathuakhan Fm.	Chlorite schist inter-bedded with quartzite
		Debguru Porphyroid	Quartz porphyry and granite porphyry
	----------------------------------Ramgarh Thrust ----------------------------------		
	Jaunsar Gr.	Nagthat-Berinag Fm.	Orthoquartzites, inter-bedded with slates.
	----------------------------------Krol/Berinag Thrust----------------------------------		
	Tejam Gr.	Deoban Fm.	Cherty dolomite and dolomite limestone

N.B.   *Age of all the formations is Precambrian*

a) Lesser Himalayan Rocks

Deoban Formation of Tejam Group is exposed in small portions in the south-western part of the study area. The litho-unit comprises of stromatolite bearing cherty dolomite and dolomitic limestone with intercalations of grey slates and limestone. Nagthat-Berinag Formation of Jaunsar Group is exposed in the south central part of the study area overlying Deoban Formation. This formation is characterised by orthoquartzites, which are locally pebbly or conglomeratic and interbedded with greenish and purple slates. Nagthat-Berinag Formation is overlain by Ramgarh Group and Almora Group.
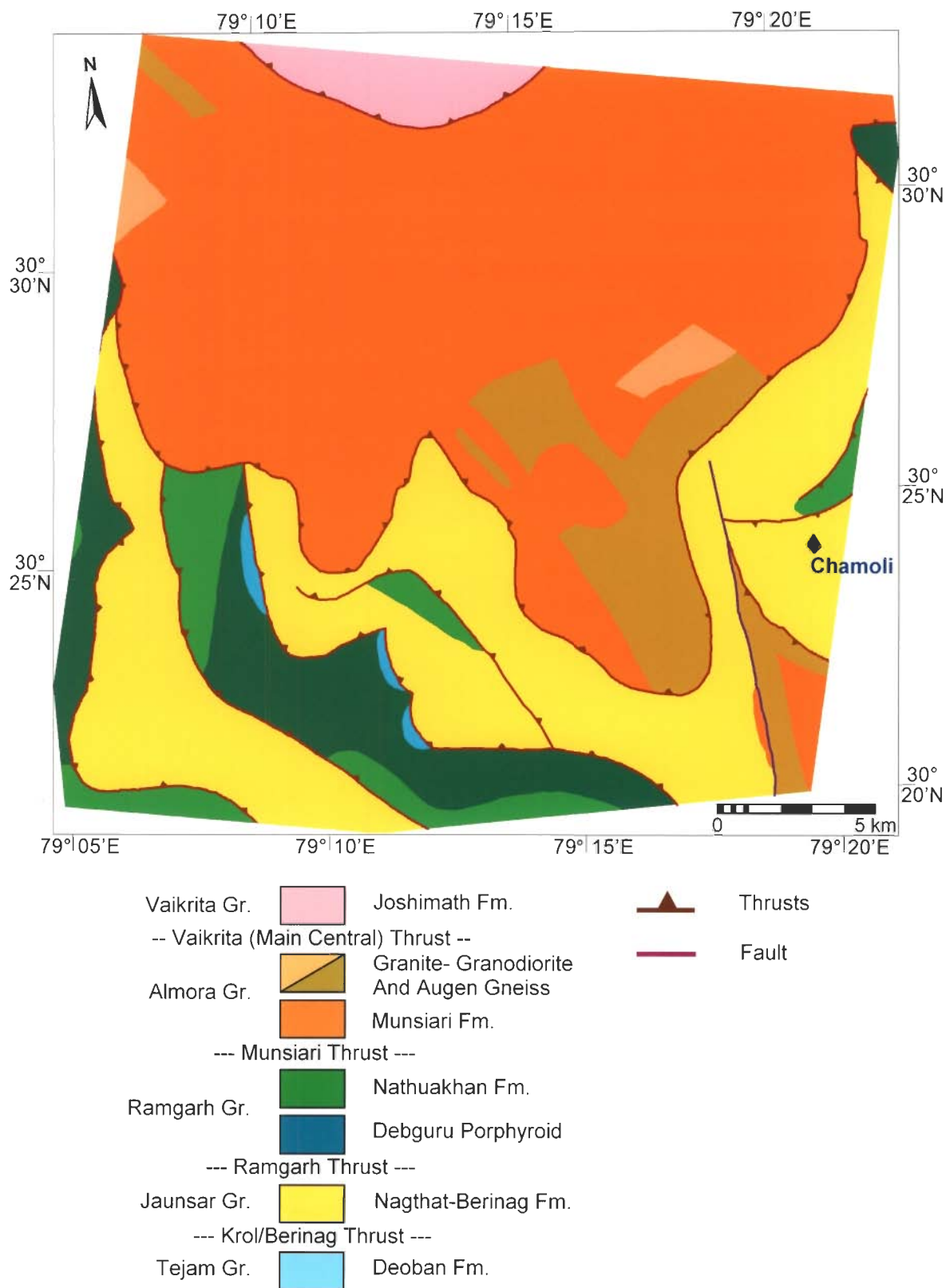
Figure 3.3: Geological map of the study area (Valdiya, 1980).

Ramgarh Group of rocks is exposed in the southern part of the study area. Quartz porphyry and porphyritic granite rocks of Debguru Porphyroid are mainly exposed in this area. Debguru Porphyroid is overlain by Nathuakhan Formation, which is characterised by chlorite, sericite schist interbedded with very fine-grained quartzite. Ramgarh Group is underlain and overlain by Ramgarh Thrust and Munsiari Thrust, respectively.

Munsiari Formation of Almora Group is exposed in the central and northern part of the study area. There is a lot of controversy of its association either with Lesser or Higher Himalayan groups. Munsiari Formation is considered as a part of Lesser Himalayan sequence as mentioned in Valdiya (1980). This formation is characterised by schists, amphibolite, granite-granodiorite and augen gneiss, which is mylonitised in some areas.

b) *Higher Himalayan Rocks*

Joshimath Formation of Vaikrita Group is exposed in the northernmost part of the study area. This formation is characterised by sillimanite / kyanite / staurolite / garnet / biotite / muscovite schist / gneiss and migmatites.

3.2.5.2 Structure

Structurally, the study area is highly complex with several thrusts and folds. There are two major thrusts present in this area (Fig. 3.3). The Munsiari Thrust separates Lesser Himalayan Formations from overlying Higher Himalayan Munsiari Group of rocks. The Vaikrita or Main Central Thrust (M.C.T.) separates the Munsiari Formation from the overlying Joshimath Formation. The thrust zones are highly crushed and show unstable slopes along the strike. The rocks of Tejam Group are exposed within a window demarcated by Krol/Berinag Thrust. Ramgarh Group is overlying the Jaunsar Group separated by Ramgarh Thrust. Several irregularly oriented faults are also present. The rock groups in the area are highly folded. The major trend of the fold axes is NW-SE.

3.3 Data Used

The data used in this study can be broadly divided into three main categories: (a) remote sensing data, (b) ancillary data and (c) field data.

3.3.1 Remote Sensing Data

The study has mainly utilised remote sensing data from the Indian Remote Sensing (IRS) Satellite acquired from the National Remote Sensing Agency (NRSA), Hyderabad, India.

The IRS data have widely been used in recent times in a variety of applications - in geosciences, landuse/landcover mapping, hydro-geomorphological mapping, urban planning, biodiversity characterisation, disaster management, *etc.* The scope of applications of IRS data can be found in Navalgund (2001) and Gupta (2003).

Table 3.2: Remote sensing data used in this study

| Characteristics | IRS-1C sensors data used | | | |
| | LISS-III | PAN | Stereo-PAN | |
			Left image	Right image
Path/Row	97/49	97/49	97/49	97/49
Date of acquisition	26.11.1998	10.11.2001	22.11.1998	11.11.1998
Format	BIL	BSQ	BSQ	BSQ
Sun Azimuth (degree)	163.28	160.92	162.84	163.06
Sun Elevation (degree)	36.31	40.17	38.18	39.93
Tilt Angle (degree)	0	1.96	-22.27	23.20

The data used in this study are mainly from IRS-1C mission. It operates in a polar, sun-synchronous orbit at an altitude of 817 km. Its local equatorial crossing time is 10:30 AM in the descending mode. The satellite payload consists of three sensors, namely Panchromatic camera (PAN), Linear Imaging Self-Scanning Sensor (LISS-III) and Wide Field Sensor (WiFS) (Navalgund and Kasturirangan, 1983; *www.nrsa.gov.in*). Table 3.2

shows the list of IRS-1C data used in this study. Figure 3.4 shows the schematic representation of the area coverage by various satellite data used here.

The IRS-1C LISS-III and PAN sensor characteristics are given in Table 3.3. The LISS-III sensor collects multi-spectral data in four bands, *viz.,* green, red, near infrared (NIR) and shortwave infrared (SWIR). The panchromatic camera provides data in a single broad band with a ground resolution of 5.8 m and is highly useful in recognising ground objects. The PAN camera can be steered upto ± 26°, which can be used to acquire stereo pairs for DEM generation, and also improves the revisit capability upto 5 days.
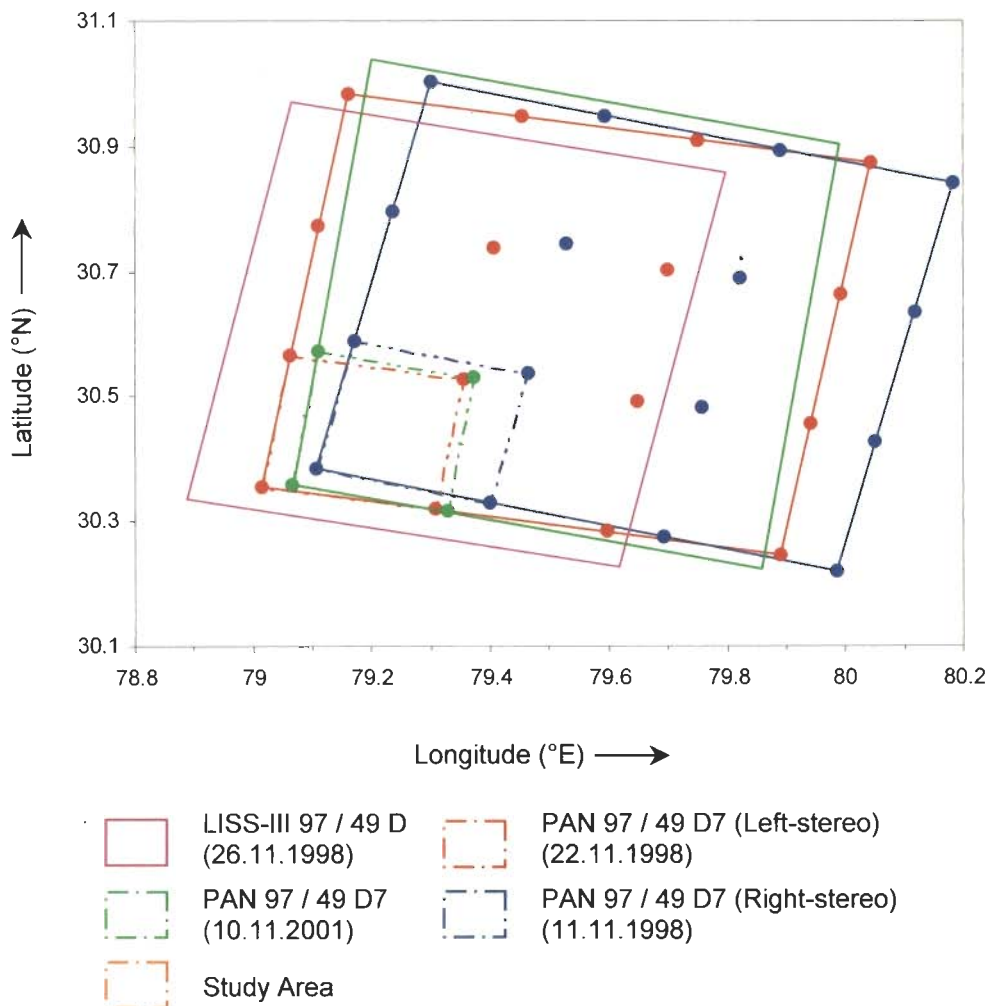
Figure 3.4: IRS - satellite data coverage of the study area.

In this study, the LISS-III and PAN data have been used for landuse/landcover classification, lineament mapping and landslide mapping. The stereo-PAN data have been used to generate DEM of the study area.

Table 3.3: IRS-1C sensor characteristics (*www.nrsa.gov.in*)

Characteristics	LISS-III sensor	PAN sensor
Spectral Bands	4	1
Spectral ranges	B2: 0.52 - 0.59 µm	
	B3: 0.62 - 0.68 µm	0.50 - 0.75 µm
	B4: 0.77 - 0.86 µm	
	B5: 1.55 - 1.70 µm	
Spatial Resolution	B2-B4 : 23.5 m B5 : 70.5 m	5.8 m
Swath	B2-B4 : 141 km B5 : 148 km	70 km
Quantization	7 bit	6 bit
Repetitivity	24 days	Upto 5 days (in stereo mode)
Steerability	-	± 26°

3.3.2 Ancillary Data

The ancillary data, namely - topographic maps, geological map and road design parameters have been collected from various sources and used in this study. A brief description of these data and their sources has been given in Table 3.4.

Table 3.4: Ancillary data used in this study

Data type	Specification	Source
1) Topography	Toposheet Nos. 53N/2, 3, 6, 7 Scale: 1:50,000	Survey of India (1960's)
2) Geology	Scale: 1:326,000	Valdiya, 1980
3) Hill road design parameters	Ruling, limiting and exceptional gradient specifications	Indian Roads Congress, IRC: 52-2001

The Survey of India toposheets form the base map of the study area. A large number of information has been extracted from the topographic map, *e.g.,* contours and point elevations, drainage network, roads, *etc.* Geological map has been used to collect information on lithology and structural features, *e.g.,* thrusts and faults. The hill road design parameters have been used in route planning.

3.3.3 Field Data

Collection of field data is very important for any remote sensing and GIS based study. Extensive field data have been collected during December 2001 and November 2003. The early winter period was preferred for field data collection as this coincides with the period in which remote sensing data used in this study was acquired.

The main purposes of field data collection are as follows:

a) To get information on existing landslide distribution

b) To collect training and testing data samples for landuse/landcover classification and distribution

c) Differential GPS survey to collect ground control points for stereo-PAN data processing and calibration.

Field photographs and details of the ground check have been incorporated at relevant places in subsequent chapters.

Chapter 4

Thematic Data Layer Preparation

4.1 Introduction

The thematic data layer or thematic map is a major component of GIS database. A thematic data layer displays the locations of a single attribute or the relationships among several selected attributes of a particular theme, such as soil, landuse/landcover, lineaments, *etc.* (Demers, 2000). Generation of accurate thematic data layers has been the key to the research reported in this thesis. Therefore, novel and new methods, as appropriate, have also been used and developed to prepare a number of data layers pertinent to the study. As a result, a major component of the research has also been devoted to this. A large number of thematic data layers, *viz.*, Digital Elevation Model (DEM), lithology, landuse/landcover, drainage order, landslide distribution and landslide hazard zonation (LHZ) map, have been generated using remote sensing and GIS techniques. The purpose of these thematic layers is to assist in estimating the thematic cost for route planning. This chapter deals with various aspects of data capturing, pre-processing and advanced processing techniques to generate various primary (which are directly derived

from data-sets, *e.g.,* lithology or landslide distribution map) and secondary (which need substantial data processing, *e.g.,* LHZ map) thematic data layers.

The work involved has been categorised into the following sections:

a) Pre-processing of remote sensing data

b) Generation of Digital Elevation Model (DEM) and derivation of secondary attributes, such as slope, aspect, *etc.*

c) Extraction of lithology and structure from geological map and LISS-III image interpretation

d) Generation of drainage order and drainage density map

e) Landuse/landcover map generation using multi-source classification of LISS-III image and ancillary data layers - Normalised Difference Vegetation Index (NDVI) and DEM

f) Preparation of landslide distribution map using remote sensing images and field data

g) LHZ map preparation using a novel method based on statistical analysis.

4.2 Pre-processing of Remote Sensing Data

The digital data acquired from remote sensing satellites need to be processed to derive useful information about the Earth's surface features. A digital image is a two-dimensional data array of brightness values representing spectral response of the scene captured. It typically comprises of small equal-sized areas called pixels (picture elements), which form the ground resolution cell. A digital image often contains distortions with respect to its geometry and radiometry (*e.g.,* atmospheric effects). Therefore, the data needs to be pre-processed to rectify for various distortions. The rectified image is then subjected to a number of image processing operations, such as contrast enhancement, ratioing, classification, *etc.* for extracting useful information related to the Earth's environment (Fig. 4.1).
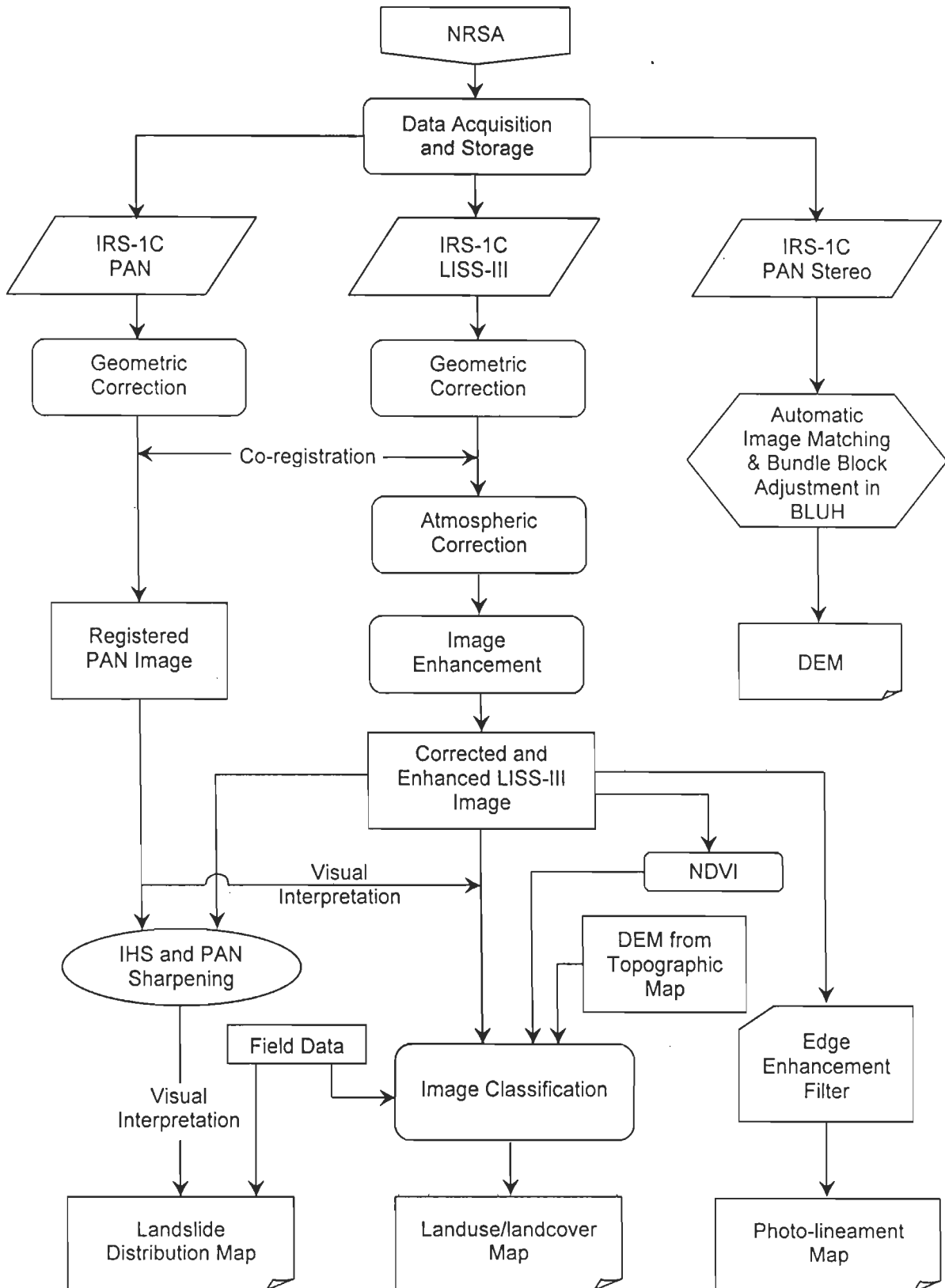
Figure 4.1: Methodology overview for digital image processing of the remote sensing data adopted in this study.

4.2.1 Geometric Correction

Raw digital images contain geometric distortions, which render them unusable unlike maps, which are drawn at unique scale and orthographic projection. The geometric distortions in images may occur due to several reasons, such as Earth's curvature, panoramic distortion, *etc.* The goal of geometric correction is to correct for these distortions to produce an image with the geometric integrity of a map.

A common procedure is to use the method of rubber-sheet stretching that has been explained in many standard texts (*e.g.,* Mather, 1999; Gupta, 2003). A number of ground control points (GCPs) distributed evenly over the entire area are collected such that they can be easily located on both the image to be rectified and the reference map, such as a toposheet. A GPS survey is often carried out for accurate determination of coordinates of the GCPs.

In this study, the geometric correction of remote sensing data (IRS-1C LISS-III and PAN images) using the above procedure has been performed on ERDAS Imagine. For this, Survey of India toposheets (53 N/2,3,6,7 at 1:50,000 scale) have been scanned to convert the paper maps into digital format. The scanned toposheets have been geo-coded using the latitude and longitude information of the graticule intersections and reprojected to Lambert Conformal Conic (LCC) projection system with Modified Everest spheroid and datum (Table 4.1). A mosaic of these four geo-coded toposheets has been generated and used as reference map or "master" for geometric rectification of satellite images and geological maps.

a) Geometric correction of LISS-III image:

In view of the absence of other distinct features in the area, a total of 39 well-distributed drainage junction points identified from the geo-coded mosaic of toposheets have been taken as GCPs. The river migration or shift has been assumed negligible within a span of 40 years (*i.e.,* the time difference between the preparation of toposheets and the

remote sensing data) in such a high altitude terrain, and therefore, it is believed that GCPs will be accurate. An RMS error of 0.91 pixel has been obtained using 1st order polynomial model for geometric correction, which is well within the acceptable limit of one pixel for such type of study. The nearest-neighbour resampling method has been adopted to generate the final georeferenced LISS-III image, as this preserves the original brightness values in the output image.

Table 4.1: Properties of map projection system used

Projection	Lambert Conformal Conic (LCC)
Spheroid/Datum	Modified Everest
Longitude of Central Meridian	68° E
Latitude of Origin	32°30' N
False Easting	2743196.4 m
False Northing	914398.8 m

b) Co-registration of PAN with LISS-III image:

The co-registration of IRS-1C PAN with LISS-III image was necessary since the PAN image was visually interpreted for the extraction of existing landslides, and selection of training and testing datasets for landuse/landcover classification. Therefore, the PAN image has been co-registered with geo-referenced LISS-III image, using 60 GCPs, at an RMS error of 0.50 pixel using 1st order polynomial model and the nearest-neighbour resampling method.

4.2.2 Atmospheric Correction

The optical remote sensing data invariably contains the effect of selective atmospheric scattering and absorption of the solar radiation. In the visible – near infrared part of the electromagnetic spectrum, scattering is the most dominant process leading to path radiance. This has an additive role and affects the brightness values (Jensen, 1996).

The remote sensing data, therefore, need to be corrected. Although there are many techniques to perform this correction, the most widely used 'dark-object subtraction' technique (Chavez, 1988) has been adopted here to correct for atmospheric scattering. The technique is based on an empirical approach to rectify the data for path radiance. As the near-infrared (NIR) band gets completely absorbed in a deep and clear water body, the values over such pixels are used to estimate the path radiance. The corresponding (minimum) brightness value for NIR, green, red and shortwave infrared (SWIR) bands over deep and clear water body (*e.g.*, a lake called Diuriya Tal - 30°31'17"N, 79°07'40"E) are found and subtracted from all other brightness values in the respective bands to generate an image corrected for atmospheric path radiance. Figure 4.2 shows geometrically and atmospherically corrected colour infrared composite of LISS-III image.

4.3 Digital Elevation Model

Digital Elevation Model (DEM) is an important and basic component in many remote sensing and GIS-based applications. A DEM represents the spatial variation of elevation (*i.e.*, altitude or height) over an area. In this study, DEM has a large number of applications. The DEM has been used:

a) As an input parameter in multi-source classification for landuse/landcover map in order to reduce error in classification arising due to a large elevation differences.

b) To derive various terrain-related parameters (*viz.*, slope, aspect and relative relief) for preparation of Landslide Hazard Zonation (LHZ) map.

c) To calculate slope between neighbouring connected pixels while carrying out route planning. Since minor variations in slope are critical particularly for route planning, there is a need to develop a high resolution DEM of the study area.

Figure 4.2: IRS-1C LISS-III Colour Infrared Composite in a perspective view (NIR=R, Red=G, Green=B).
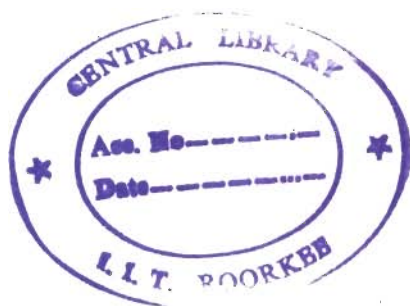
In this study, two different approaches have been used to generate the DEM:

a) Photogrammetry with IRS stereo-PAN satellite data and

b) Digitisation of Survey of India topographic maps.

4.3.1 DEM from Stereo-PAN Data

Stereo photogrammetry is an established technique that is widely used for topographical mapping and generation of DEM from aerial photographs (both digital and analogue) acquired at various scales. With the advent of satellite technology and design of stereo optical imaging sensors, it is now possible to generate DEM from perspective geometry of the satellite image pairs (Jacobsen, 1998). Several satellites carry optical sensors to collect stereo-images, *viz.,* SPOT, MOMS-2P, IRS-1C/1D PAN and ASTER. Examples of DEM generation from MOMS-2P data may be found in Rössner *et al.* (2000), from ASTER data in Cheng *et al.* (2003) and from SPOT data in Kratky (1989). The IRS-1C/1D stereo-PAN data have also been used to generate DEM, though sparingly, partly due to the problems in its stereo data acquisition capabilities. For example, Jacobsen (1997) has tested the IRS-1C stereo-PAN data for DEM generation using BLUH software, for a study area near Hannover, Germany and obtained a DEM with average planimetric accuracy in the range ± 5 m, and elevation accuracy of ± 10.6 m. Jayaprasad *et al.* (2002) used DATDEM software (developed by ISRO, India) to generate DEM using IRS-1C data in an area in Rajasthan, India and achieved an elevation accuracy about ± 19.03 m. Rao and Rao (2003) used PCI EASI/PACE software to generate DEM from IRS-1C data in Koyna, India and achieved an elevation accuracy of about ± 16 m. All these studies have been carried out in areas where elevations are generally low and the topography is fairly flat. There appears to be no published work on the use of this technique in high-altitude rugged terrain, such as the Himalayas. In this research, an attempt has been made to generate DEM from IRS-1C stereo-PAN image pair for the study area in Himalayas.

4.3.1.1 IRS-1C Stereo-PAN Data

The IRS-1C/1D PAN sensor has the capability to cover the ground stereoscopically by a rotation of the sensor upto ± 26° in across-track direction. The PAN image has a swath width of 70 km, which has been captured by 3 CCD line sensors having 4096 pixels each. The CCDs are oriented in an overlapping fashion. These sensors have geometric distortions due to different focal length, rotation against the image plane, shift in the image plane, *etc.* Hence, geometric calibration of the sensors is required to construct the stereo model (Jacobsen, 1997; Srivastava *et al.*, 2000).

A pair of IRS-1C stereo-PAN images (see Table 3.2 in Chapter 3) has been used to generate the DEM. The view angles of the two images are -22.27° and 23.20°, respectively. Based on the following relation (Rao and Rao, 2003),

$$Base / Height\ ratio\ (B/H) = tan|\theta_1| + tan|\theta_2| \qquad (4.1)$$

the B/H ratio has been estimated as 0.84. For topographic mapping, a B/H ratio between 0.6 and 1.2 is generally recommended. Thus, the value obtain for the stereo pair selected here is well within this range. Figure 4.3 shows the left and right PAN image pair of the study area used for DEM generation.

4.3.1.2 Software for Stereo-PAN Data Processing

There are only a few software for stereo image processing of IRS-1C PAN data. Although, the standard commercial image processing software like ERDAS Imagine and Geomatica from PCI have the capability to process these data, the modules are generally used as black boxes since users have little or no control over the processing operations. In this study, the BLUH (BundLe block adjustment University of Hannover) software, developed by University of Hannover, Germany, has been used to process the IRS-1C stereo-PAN data. Assistance from Dr. Karsten Jacobsen, one of the developers of this
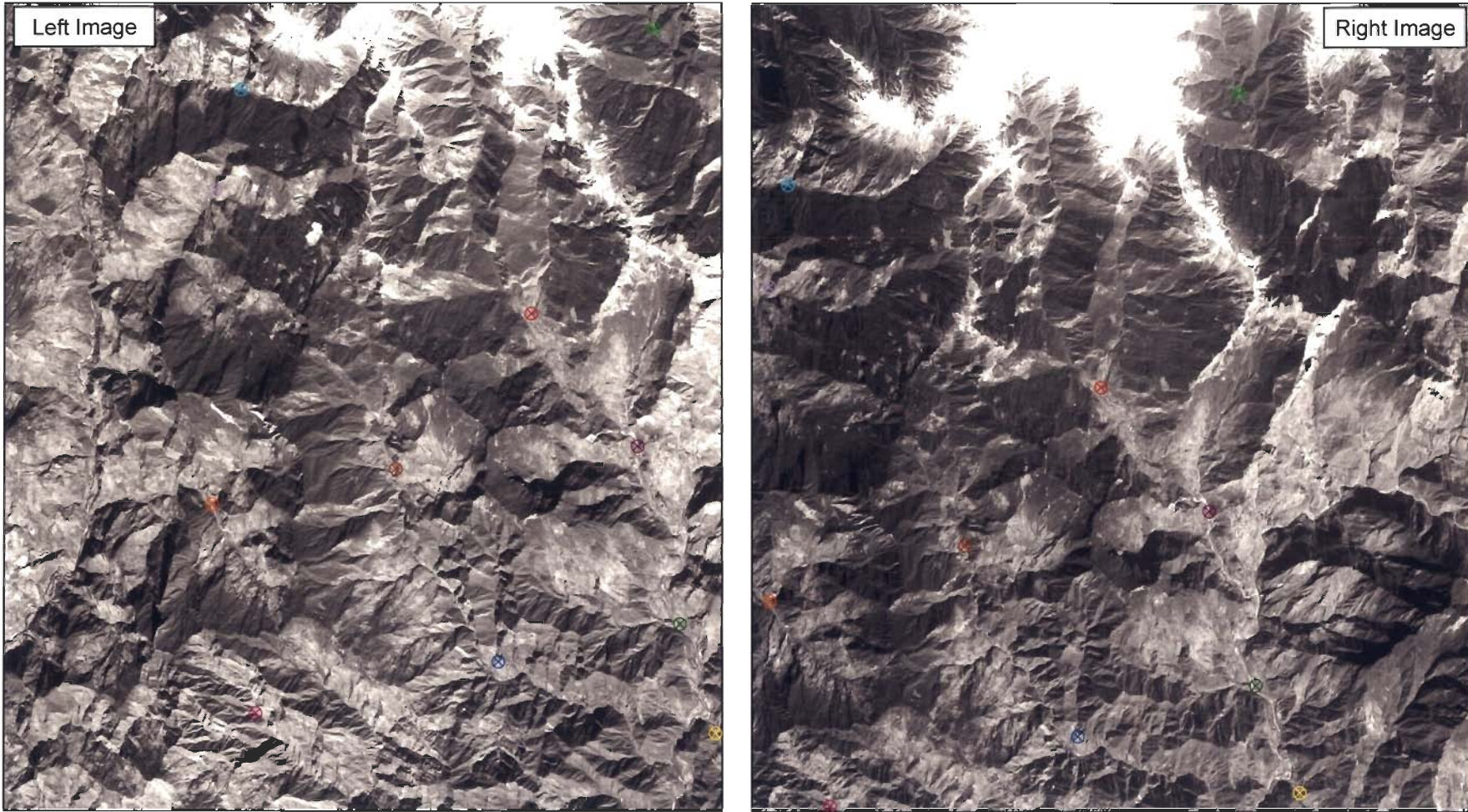
Figure 4.3: The pair of left and right PAN stereo images used for DEM generation. The selected tie points are marked on both the images.

software, has also been taken in data processing. The software is versatile and has wide possibility of user interaction to generate DEM (BLUH manual, 2002).

4.3.1.3 Bundle Block Adjustment

The BLUH software is based on bundle block adjustment technique for DEM generation. Bundle block adjustment is a rigorous and flexible method of block (an irregular grid of overlapping photos/images) adjustment. Determination of photo orientation is the most important aspect of photogrammetric mapping. But, it is not economical to determine the orientation of each photo individually or through a model based on control points. The bundle block adjustment is based on the fact that the rays from the projection centre to the photo points are building a bundle of rays. This information is used in photogrammetric data processing. Since the technique uses photo coordinates directly, it produces accurate results. The principal point of each photo is taken as the origin of the image coordinates. With the help of transformation equations and various calibration parameters, image geometry is established and thus the elevation can be determined.

Applying some special conditions, bundle block adjustment may be performed for perspective images acquired from space. Line scanners, such as IRS-1C have perspective geometry only in the sensor line. Satellite line scanner images are not perspective photos with one projection centre, as imaging is done line by line. As the sensor scans the ground and moves along the satellite track, the Earth also rotates, which makes the geometry more complex. Using a minimum of 4 control points (at least one at any corner), the image geometry may be established. Moreover, a large number of parameters are considered for adjustment of possible systematic errors, the details of which can be found in Kraus (1993), Jacobsen (1997) and BLUH manual (2002).

4.3.1.4 DEM Generation Using BLUH

There are two major steps involved in DEM generation using BLUH:

a) Image Matching for Tie Point Generation:

Automatic image matching (template matching) technique is used to find the homologous points in both images, which helps to reconstruct the geometry of the stereo image pair. Automatic image matching technique used in BLUH software is shown in Figure 4.4. The BLUH software also has the flexibility of radiometric normalisation of the image pair for better image matching.

To apply image-matching technique on the stereo-PAN image pair used in this study, 11 tie points have been identified on both the images by visual interpretation with the assistance of topographic map (Fig. 4.3). Subsequently, around 2000 manually edited points were added. After image matching, the result for a total of 773598 points shown in dark tone is presented in Figure 4.5. It can be seen that at numerous places, no image matching is possible (white areas indicate no information). Due to steep slopes, the same portion of the ground may not be visible on the two oppositely inclined images. The forest may have also caused poor contrast in the image. Further, as there is an 11-day difference between the dates of acquisition of the PAN stereo-pair, the snow cover may also have partially changed. All these factors may have resulted in poor image matching.

b) Bundle Block Adjustment and DEM Generation:

BLUH software has a set of special calibration parameters for IRS-1C/1D stereo image processing. These parameters are particularly required for the adjustment of geometric distortions present in the stereo-PAN sensor as mentioned in Section 4.3.1.1. The parameters also take into account the varying pixel sizes in the across track direction, irregular movement, satellite rotation, *etc.* The elevation at points in the areas having high image matching has been determined using BLUH. The software uses the coordinate

information from the tie-points. The point elevation data has been interpolated and resampled to a raster grid (50 m × 50 m) to generate a DEM of the study area (Fig.4.6).
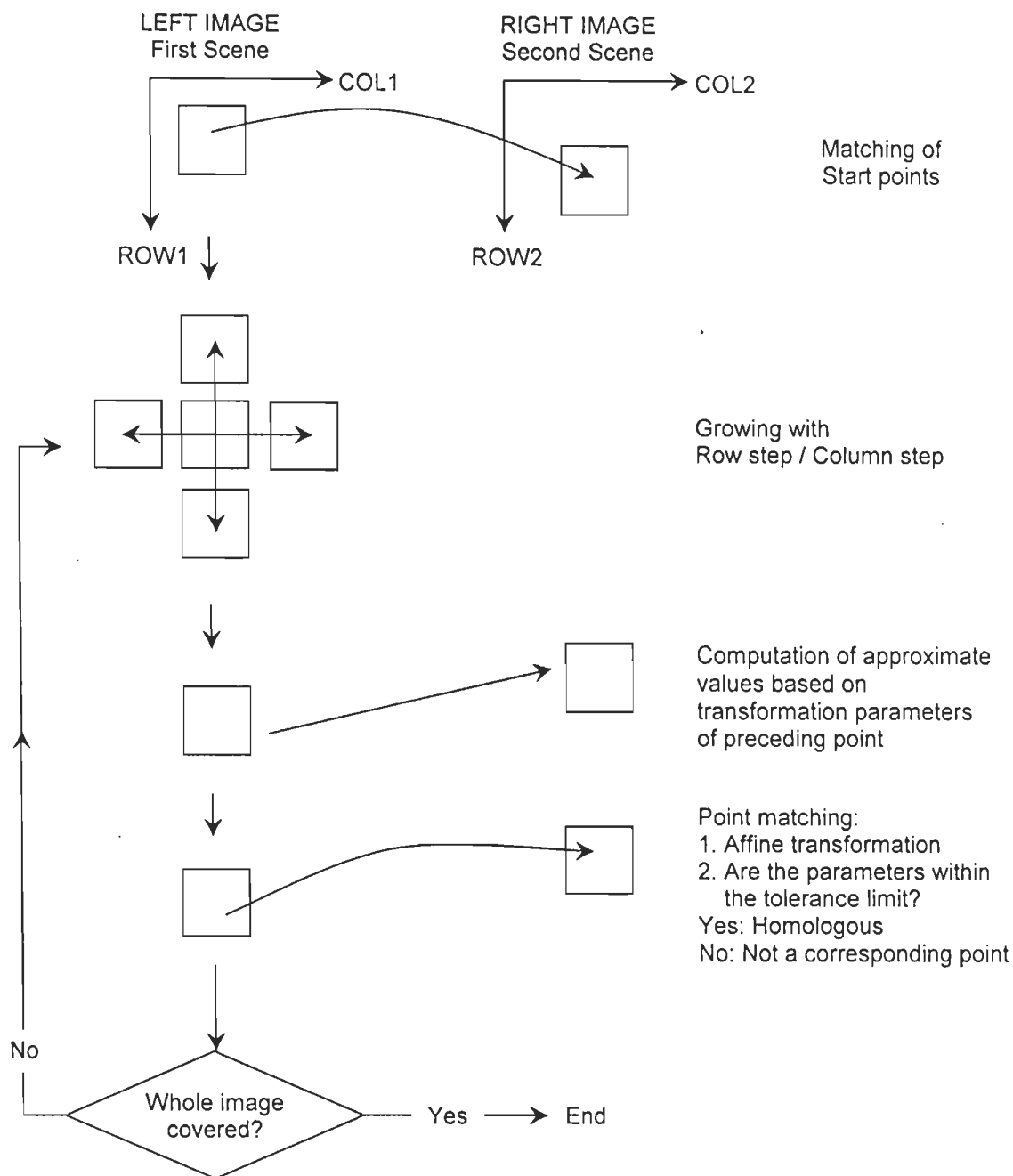
Figure 4.4: Automatic image matching procedure used in BLUH software (BLUH manual, 2002).

4.3.1.5 Assessment of the DEM Accuracy

Due to inaccurate image matching in several areas in this high altitude terrain, the DEM of only a partial area has been obtained. It is therefore, very difficult to assess the accuracy of this DEM. For accuracy assessment, a GPS survey in differential mode (using Leica geodetic GPS receivers) has been carried out to collect precise position and elevation of the points initially selected for tie point generation. A large part of the study area is inaccessible by roads, measurements at only 4 points were possible within a baseline distance of 15 km. Post-processing of the raw GPS data has been carried out using SKI software and the precise location and elevation (in the range of cm) of 4 points have been determined. The GPS produces the data in world geodetic system WGS84. BLUH software has the capability to convert it into local co-ordinate system (*i.e.*, Lambert Conformal Conic projection used in this study). Using data of these four control points, horizontal and elevation accuracy have been found as DX = ± 88.31 m, DY = ± 54.17 m and DZ = ± 69.61 m. This DEM accuracy is obviously not sufficient for a study like route planning. The elevation accuracy is predicted to be higher, where good correlation is established. Further, there are many pixels without any data (white areas in Fig. 4.5) and these appear as smooth areas in the interpolated DEM, which have been shown with the help of a Shaded Relief Model (SRM) in Figure 4.6.

From the above results and discussion, it can be inferred that the DEM generation using stereo-PAN image for high altitudes and in rugged terrains like the Himalayas is a difficult task and the accuracy is also limited. This is mainly due to non-availability of sufficient control points and poor image matching (mainly in steep slopes, forest and snow covered areas). Hence, this technique may not be suitable for DEM generation in such a terrain.
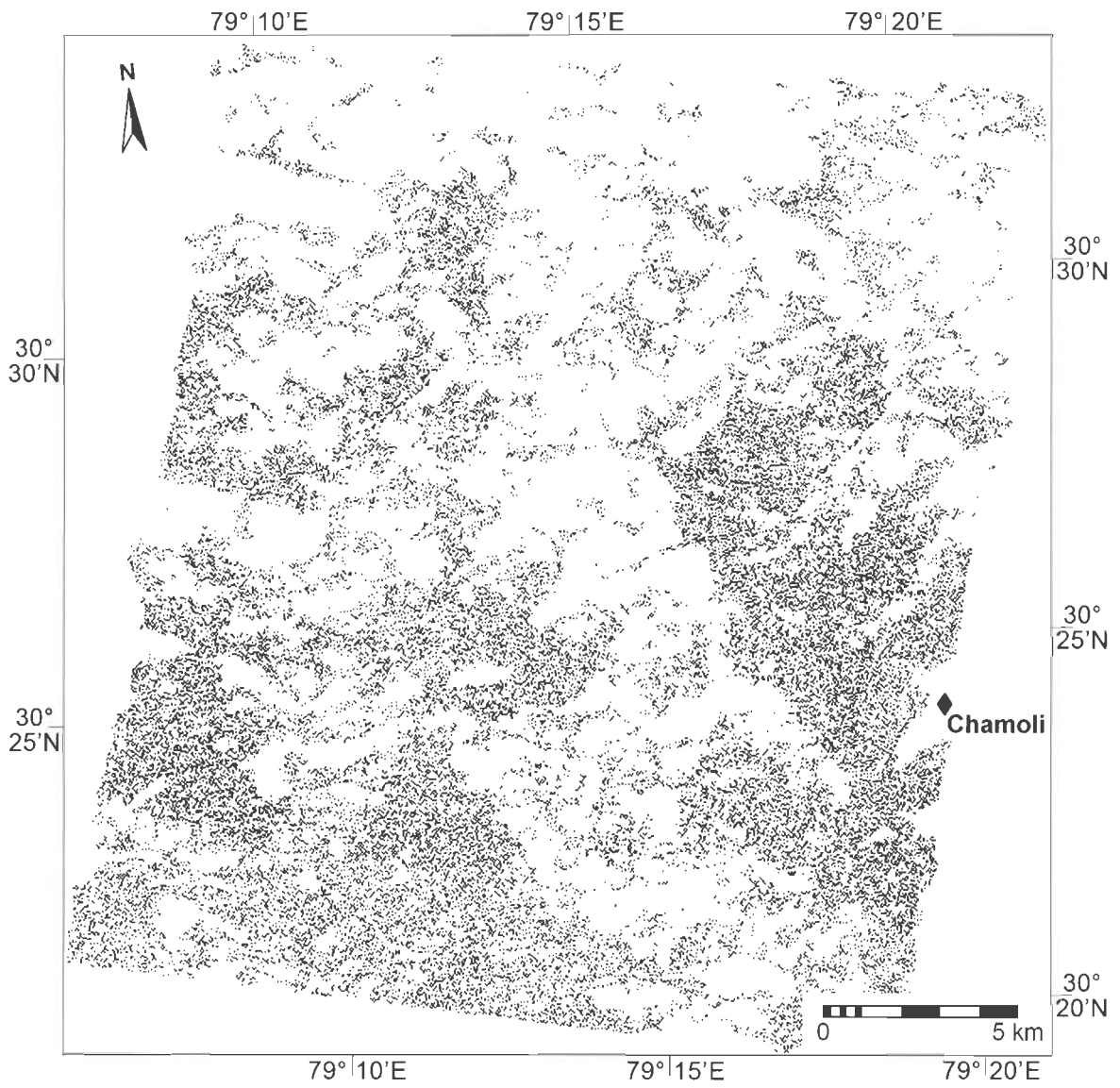
Figure 4.5: Map showing areas (white) for which homologous points could not be obtained using image-matching technique.
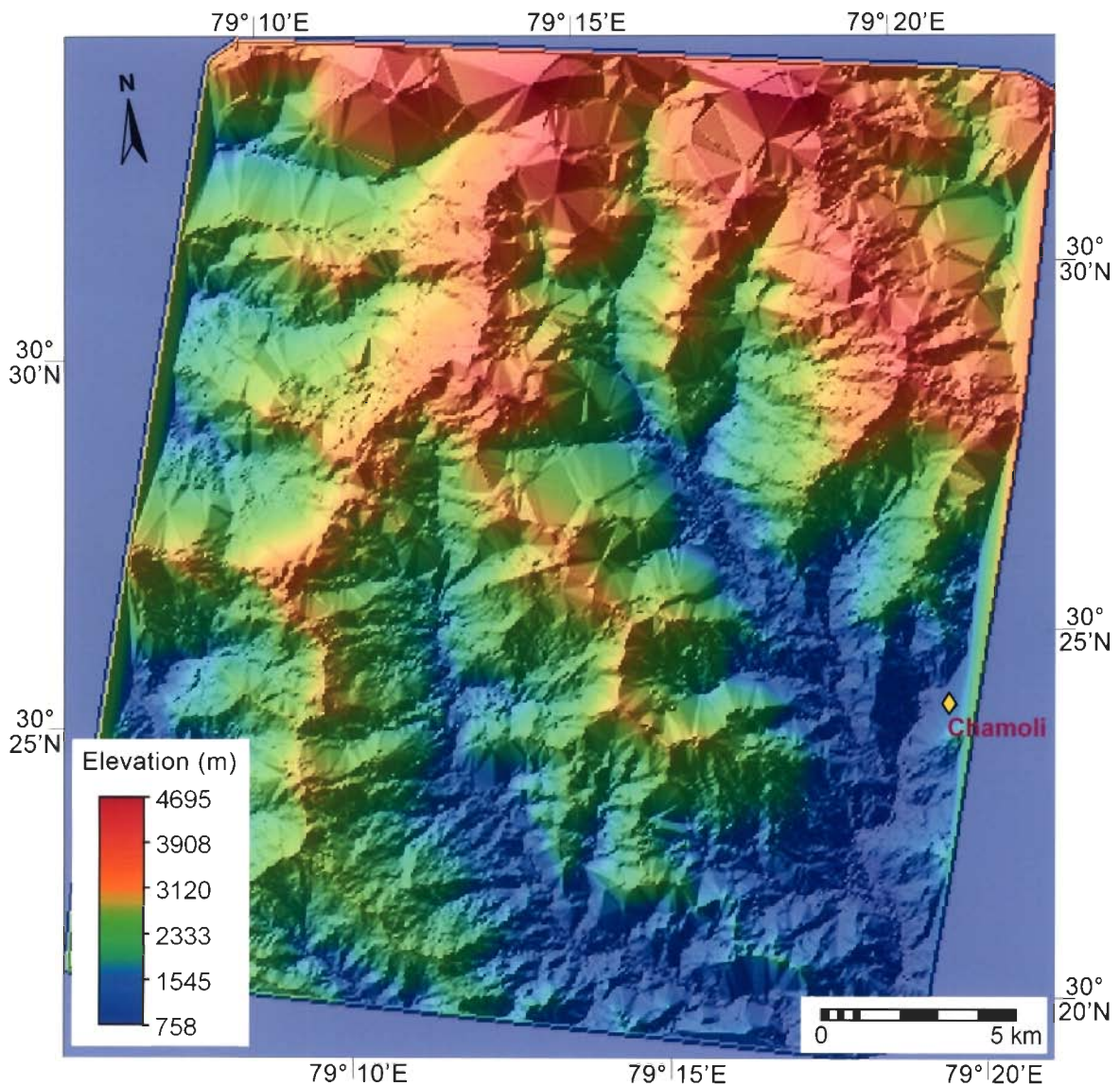
Figure 4.6: Shaded Relief Model (SRM) based on DEM generated from IRS-1C PAN stereo data with elevations in colour. Note that there are many areas, where no data exists and such areas appear as smooth regions resulting from interpolation.

4.3.2 DEM from Topographic Map

Due to the above problems in the DEM generated from IRS stereo-PAN data, the conventional topographic map digitisation technique has been implemented for generating DEM in this study. The Survey of India (SOI) topographic maps (scale 1:50,000) have been digitised onscreen at 40 m contour interval. The digitised contour map has been linearly interpolated using *Borgefors distance method* (ILWIS, 2001). In this method, the shortest distances of each undefined pixel from its two nearest contours are calculated, and the height value of the undefined pixel is calculated using the following equation:

$$H_P = H_2 + (d_2/(d_1+d_2) \times (H_1-H_2)) \tag{4.2}$$

where, H_P is the computed height of the output pixel, H_1 and H_2 are the height values of the higher and lower contour lines, and d_1 and d_2 are the shortest distances from higher and lower contour lines to the pixel.

DEMs at two different spatial resolutions corresponding to pixel sizes 23.5 m (to match the pixel size of IRS-1C LISS-III data) and 6 m (to match the pixel size of IRS-1C PAN data) (Fig. 4.7) have been generated in this study.

4.4 DEM-Based Derivatives

The topographic map based 6 m resolution DEM has been used to derive various terrain related parameters (*viz.,* slope, aspect and relative relief) that have been used for LHZ (see Section 4.10 in this chapter). The direction dependent slope or gradient between connected neighbours has also been calculated from DEM for route planning (to be used in Chapter 6).

4.4.1 Slope

Slope is an important parameter for stability consideration of the terrain. Slope can be designated as the first derivative of DEM. A slope map is a raster map in which the attribute of each pixel denotes the maximum slope at a particular location. In a raster GIS, two gradient maps in x (DXmap) and y (DYmap) directions have been prepared using DFDX and DFDY filters in ILWIS (ILWIS, 2001) (Fig. 4.8). The slope is calculated as follows:

$$Slope\ (in\ degrees) = tan^{-1}(\ (\ DXmap^2 + DYmap^2\ )^{1/2} / (Pixel\ Size)\ ) \qquad (4.3)$$

The slope map thus derived from DEM of the study area shows the range of variation of slopes from 0° to 80°, which have been further categorised into five classes for use as a parameter in landslide hazard zonation as recommended by Anbalagan (1992). Figure 4.9 represents the classified slope map of the study area.

4.4.2 Aspect

Aspect is referred to as the direction of maximum slope of the terrain surface. It influences solar insolation, which is strongly related to the distribution and density of vegetation on mountainous slopes. As vegetation provides anchorage to the ground, the stability of slope is also related to the aspect. The aspect map has also been generated using gradient maps (*i.e.,* DXmap and DYmap) prepared earlier, using the following equation:

$$Aspect = tan^{-1}(DXmap/DYmap) \qquad (4.4)$$

The aspect map thus generated shows direction from 0° to 360° azimuth with respect to the north (undefined values signify flat areas). The aspect values have been categorised into nine direction classes, namely N, NE, E, SE, S, SW, W, NW and Flat (Fig. 4.10).
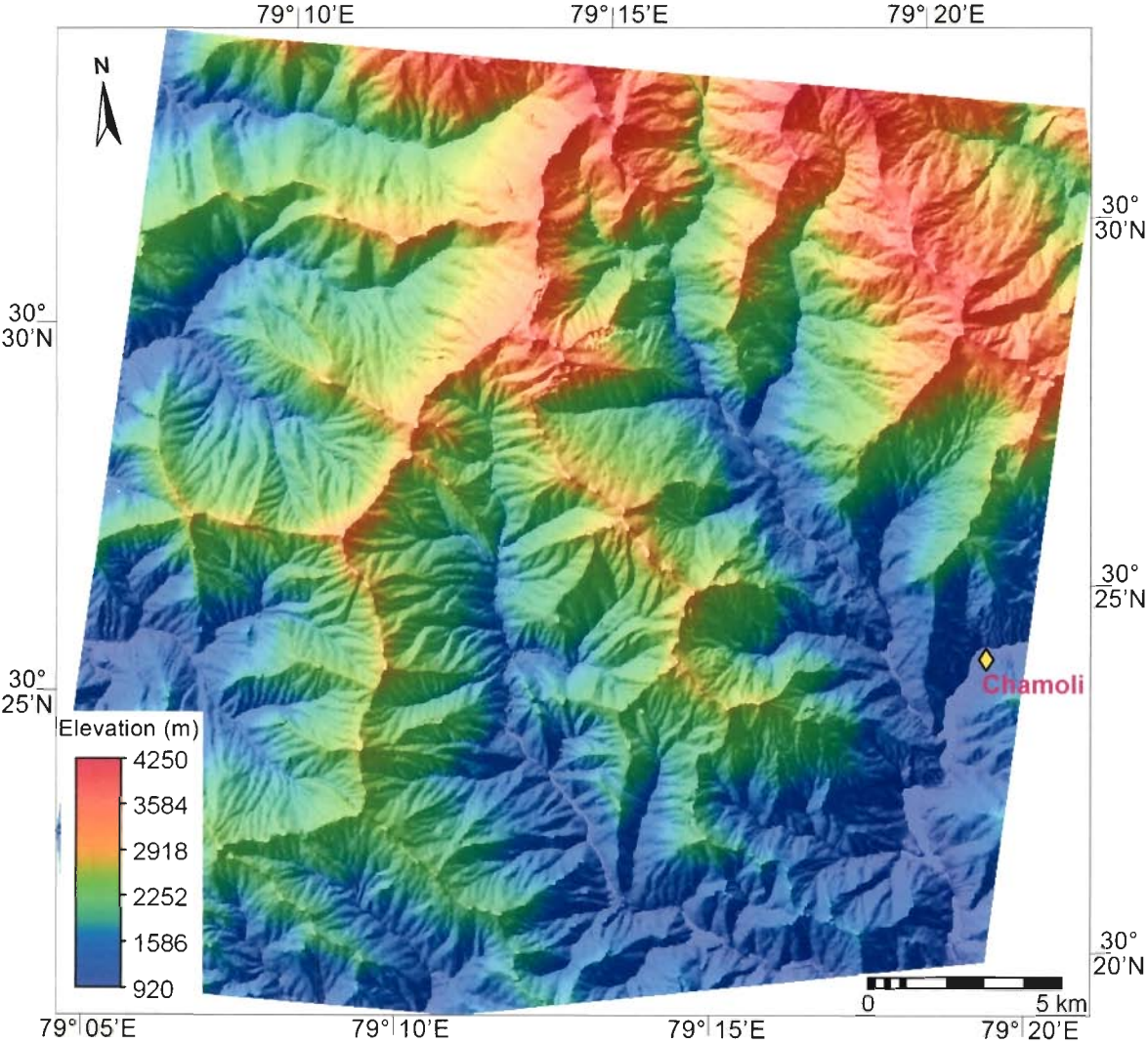
Figure 4.7: Shaded Relief Model (SRM) based on DEM generated from digitisation of topographic map. Interpolation and resampling have been performed to 6 m pixel size.

DFDY filter
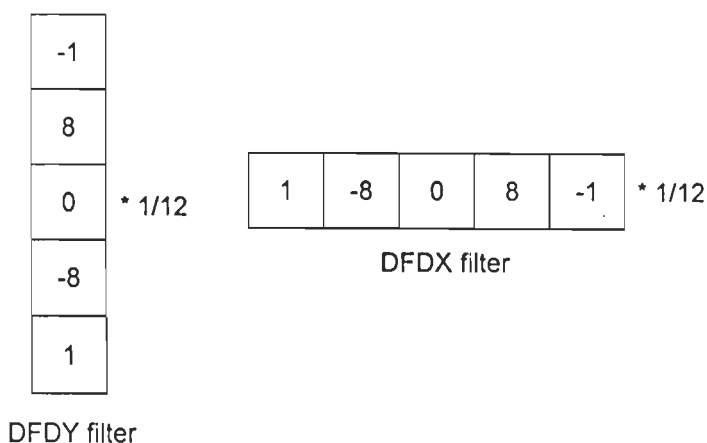
Figure 4.8: The vertical (DFDY) and horizontal (DFDX) gradient filters used in ILWIS (ILWIS Manual, 2001).

4.4.3 Relative Relief

Relative relief is also an important parameter in landslide hazard zonation and is defined as the difference in maximum and minimum elevation values within an area or facet. In a raster GIS, the relative relief can be calculated using "rank-order filter" which arranges the pixel values within the specified window (*e.g.,* 3 × 3 pixels, 5 × 5 pixels, *etc.*) and returns a map with minimum, maximum or median value at the centre pixel (ILWIS, 2001). As the relative relief is a rather regional attribute, the 6 m resolution DEM was coarsened and resampled to 30 m resolution. A 3 × 3 pixels window has been applied to this DEM to generate a minimum and maximum elevation map. The minimum elevation value map is subtracted from the maximum elevation value map to get a relative relief map for 90 m × 90 m area. This map is further resampled to 6 m pixel size using nearest neighbour method for its integration with the database for LHZ studies. It has been found that the relative relief ranges between 0 m and 490 m. The data layer is finally sliced into five classes at 30 m relative relief differences (Fig. 4.11). The relative elevations above 120 m are grouped into a single class. The majority of the area is found to lie within relative relief range of 31-60 m.

4.4.4 Shaded Relief Model

Ruggedness of the terrain can be easily perceived through differential illumination of terrain slopes using a Shaded Relief Model (SRM), which represents the terrain under artificial illumination with grey tone variations. The SRM can be generated using following formula:

$$SRM = (-Cos(\alpha) \times Sin(\beta) \times DXmap - Cos(\alpha) \times Cos(\beta) \times DYmap) / (DXmap^2 + DYmap^2)^{1/2}$$

(4.5)

where, α is sun-angle and β is sun-azimuth. The *DXmap* and *DYmap* represent the variation in gradient in X and Y directions, respectively. The SRM has solely been used here for a better visualisation of various thematic layers (*e.g.,* Fig. 4.6, Fig. 4.7, Fig. 4.12, Fig. 4.14).

4.5 Lithology

The lithological units exposed in the study area have been discussed in Section 3.2.5. These lithounits differ in their composition, compactness, fracture pattern and shear strength. Hence, lithology is an important parameter for landslide hazard zonation, as it controls the susceptibility of various lithounits to landslide activity. Besides, lithology has also been considered for preparation of thematic cost map, as it has a bearing on the cost related to blasting and excavation in the route planning (see Section 5.2.5 of Chapter 5).

As discussed earlier, the regional geological map published in Valdiya (1980) has been used as the basic source map. The rock groups and formations have been reclassified into five major lithounits, *viz.,* (a) quartzites with slates, (b) schists and gneisses, (c) limestones and greywackes, (d) granite-granodiorite-gneisses and (e) granites. The geological map has been co-registered with the geo-coded topographic map (master). The lithological boundaries of different lithounits have been digitised in segment mode and transformed to polygons. Finally, the polygons have been converted into raster map (6 m pixel size) as shown in Figure 4.12.
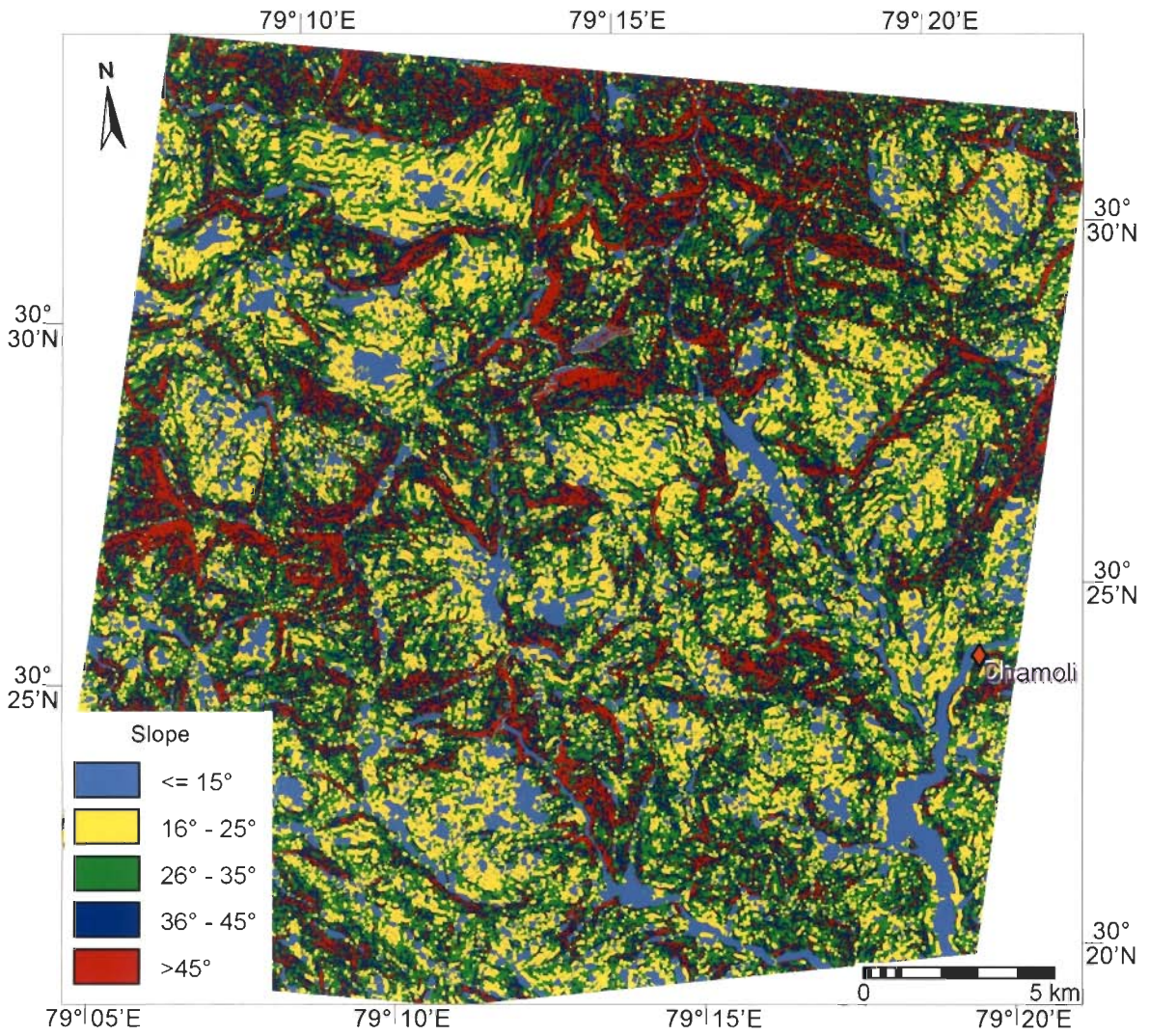
Figure 4.9: Classified slope map generated from the DEM and used in Landslide Hazard Zonation.
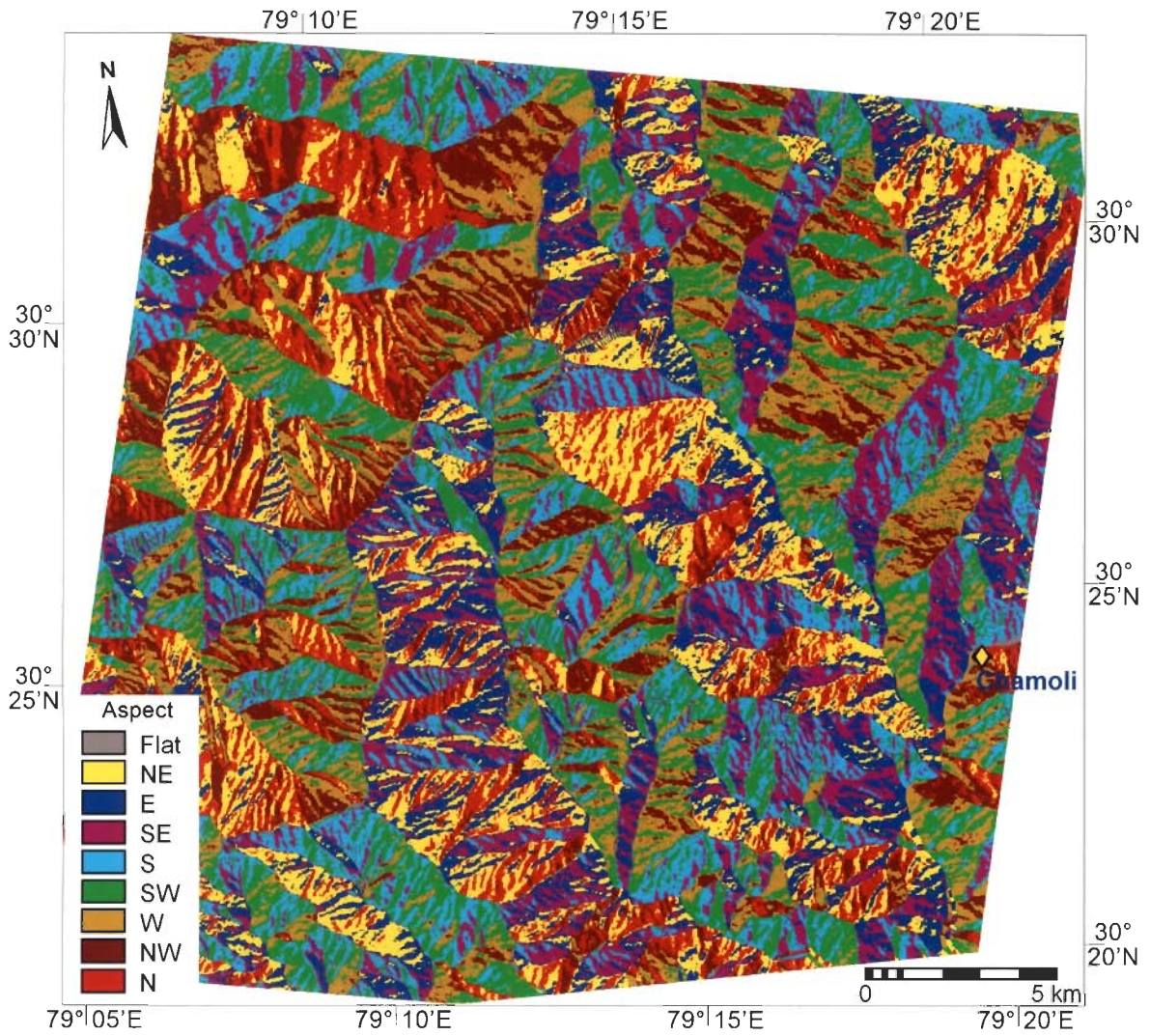
Figure 4.10: Aspect map of the study area generated from the DEM.
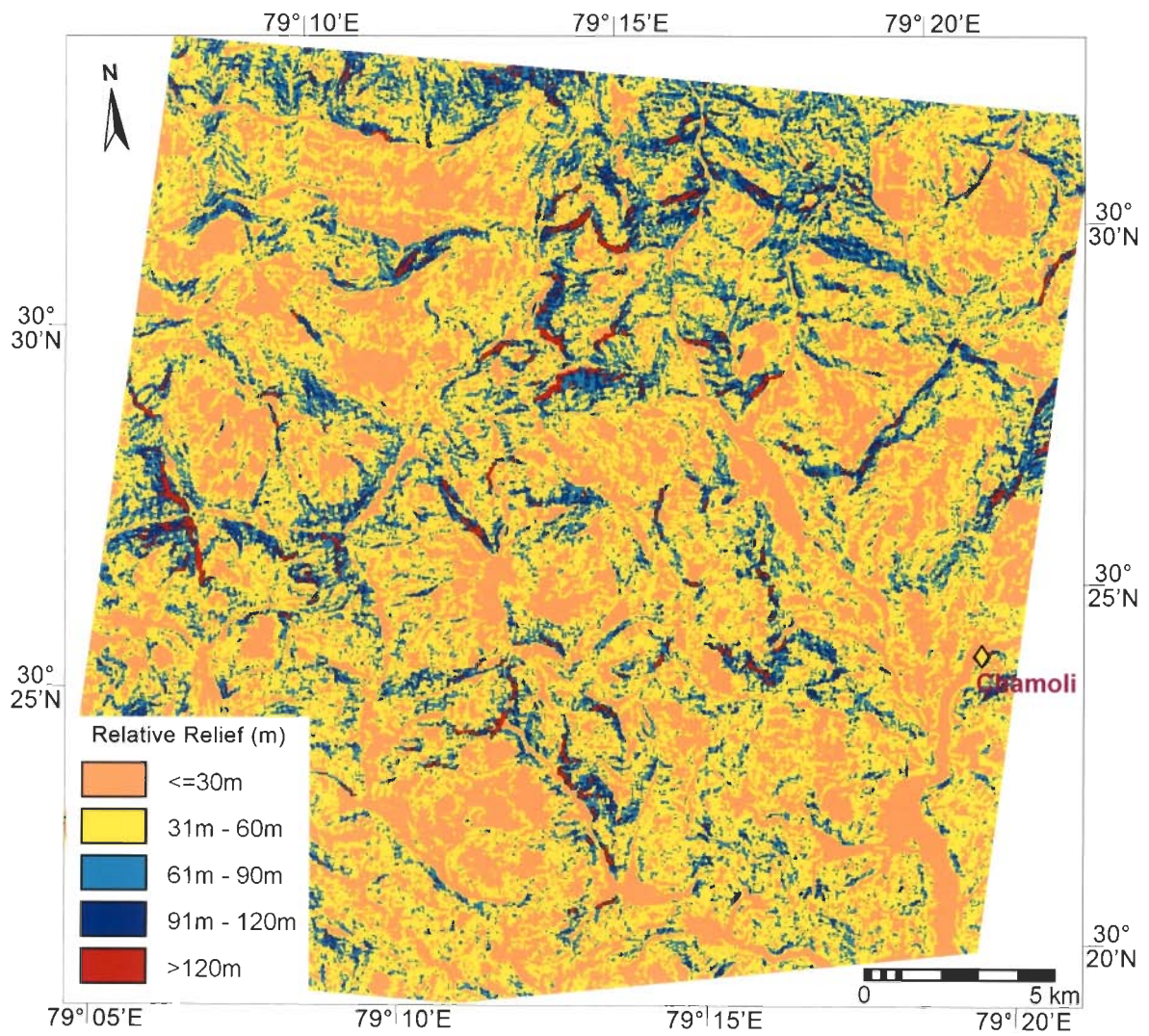
Figure 4.11: Relative relief map.

4.6 Structural Features

Structural features discussed here include thrusts, faults and lineaments, which have an important role to play in landslide hazard zonation. These structural features describe the zone/plane of weakness, shearing and tectonic activity along which landslide susceptibility is higher. The map showing structural features has been prepared by integrating the structural tectonic features in the geological map (Valdiya, 1980) with the structural lineament information as interpreted from remote sensing data.

4.6.1 Thrusts and Faults

A large number of thrusts and faults occur in the study area. Among these, the Munsiari Thrust and the Vaikrita (Main Central Thrust) are the major thrusts passing across the area. These thrusts have great importance as these are marked by large shear zones. The positions of thrusts and faults have been digitised from the geo-referenced regional geological map and locally verified through field visits (Fig. 4.12).

4.6.2 Lineaments

The term lineament is used, in a geomorphological sense, as "a mappable simple or composite linear feature of a surface, whose parts are aligned in a rectilinear or slightly curvilinear relationship and which differs distinctly from the pattern of the adjacent features, and presumably reflects subsurface phenomena" (O'Leary et al., 1976). Hence, the lineament includes all structural, topographical, vegetational, soil and lithological alignments, which are likely to be the surface expression of buried fractures and structures. Generally, the lineaments are related to the fracture systems, discontinuity planes, faults and shear zones in the rocks. On a photograph or an image, lineaments (photo-lineaments) can be easily identified by visual interpretation using various image interpretation elements, such as tonal variation, texture, pattern, association, etc.

In this study, lineaments have been identified from visual interpretation of edge-enhanced IRS-1C LISS-III image. Edge enhancement can be performed using a number of filtering techniques (for details see Gupta, 2003; Jensen, 1996; ERDAS, 2001). The LISS-III image has been processed using 3 × 3 edge-enhancement filter to enhance the high-frequency features. The filtered image has then been added back to the original image to produce the edge-enhanced image, which has been used for interpretation of lineaments. The interpreted lineaments have been digitised on-screen (Fig. 4.13).

4.6.3 Preparation of Buffers along Structural Features

Various structural features (thrusts, faults and lineaments) are combined into a single segment file and converted to raster format. Generally, the incidence of landslide decreases with the increase in distance from the structural features. The "distance" function (ILWIS, 2001) has been applied to the above rasterised structural features to find out the shortest distance of each pixel in the map to any of these structural features (thrusts, faults or lineaments) and a buffer zone has been created around each structural feature. The buffer zone is categorised into seven equal-distance classes of 504 m each, using "slicing" operation. Figure 4.14 illustrates the classified buffer map of structural features in the study area.

4.7 Drainage

The drainage map has been generated by digitising drainage lines from the geo-coded toposheets. It has been used for the preparation of drainage density map and drainage order map. The drainage density map has been used as hydrogeological input for landslide hazard zonation (Section 4.10). The drainage order map has been used for considering the cost of bridge construction during route planning (see Section 5.2.3 of Chapter 5).
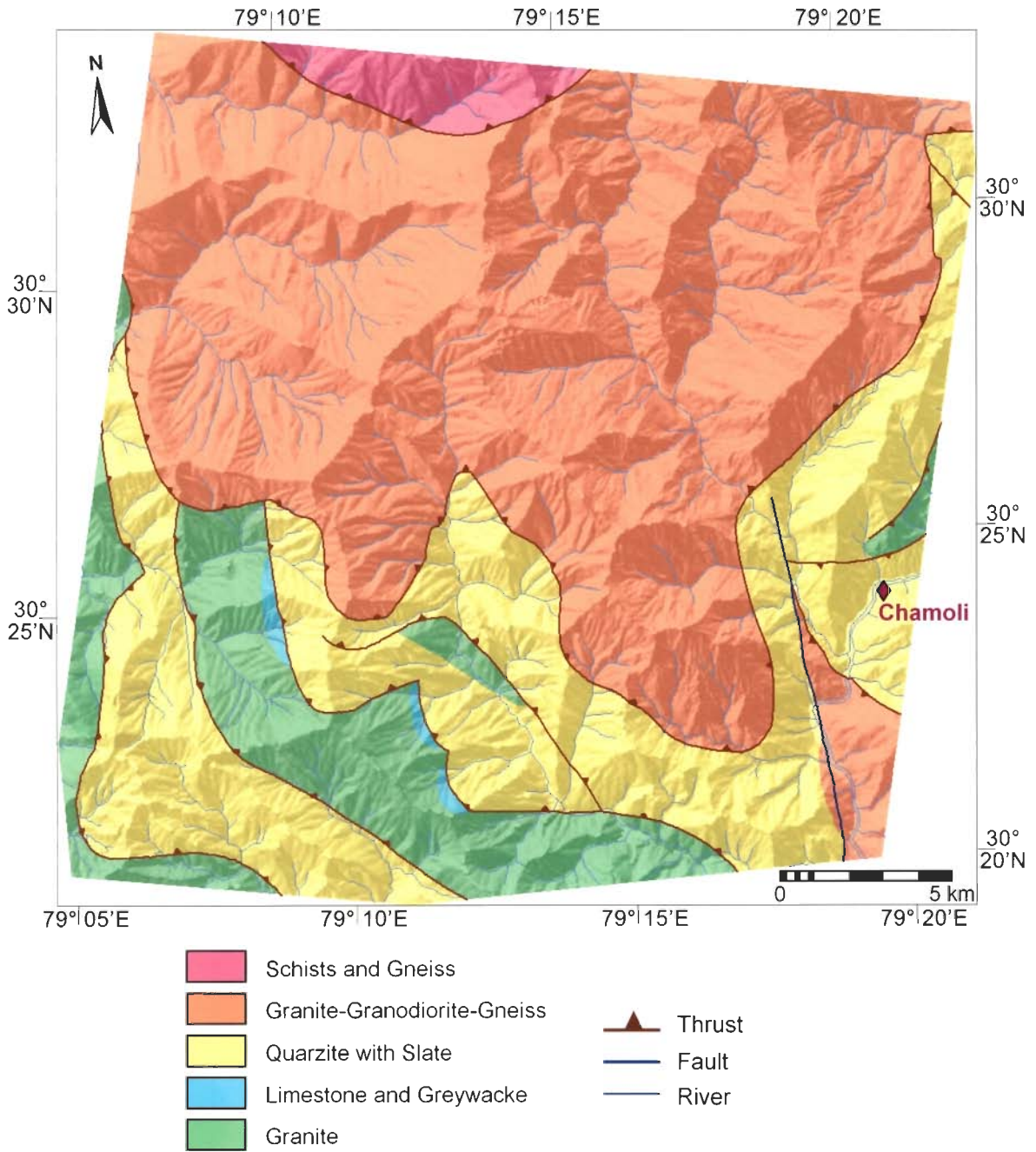
Figure 4.12: Map showing lithounits along with thrusts and fault based on geological map after Valdiya (1980) (the SRM forms the background).
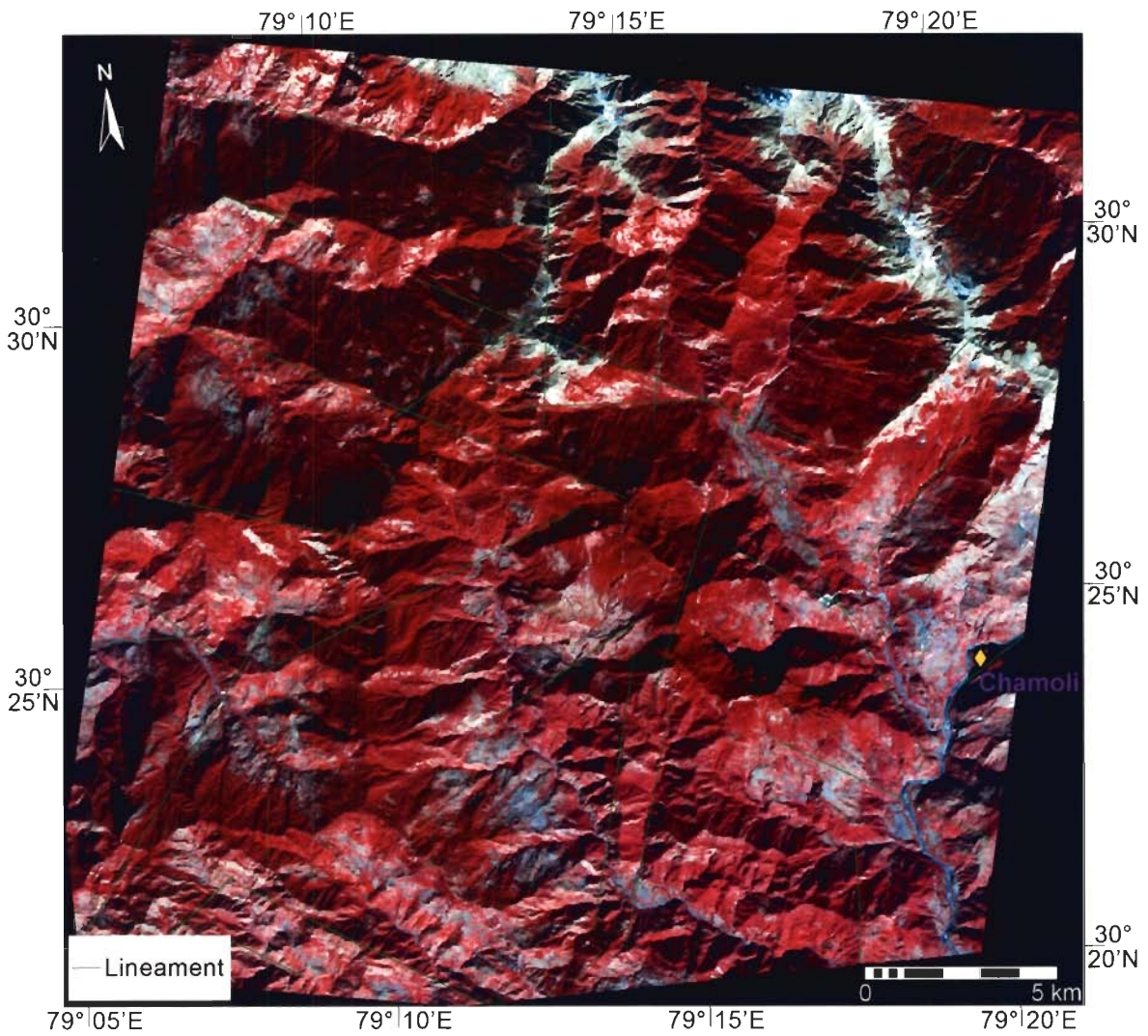
**Figure 4.13: Lineaments interpreted from the edge-enhanced
IRS-1C LISS-III colour infrared composite.**
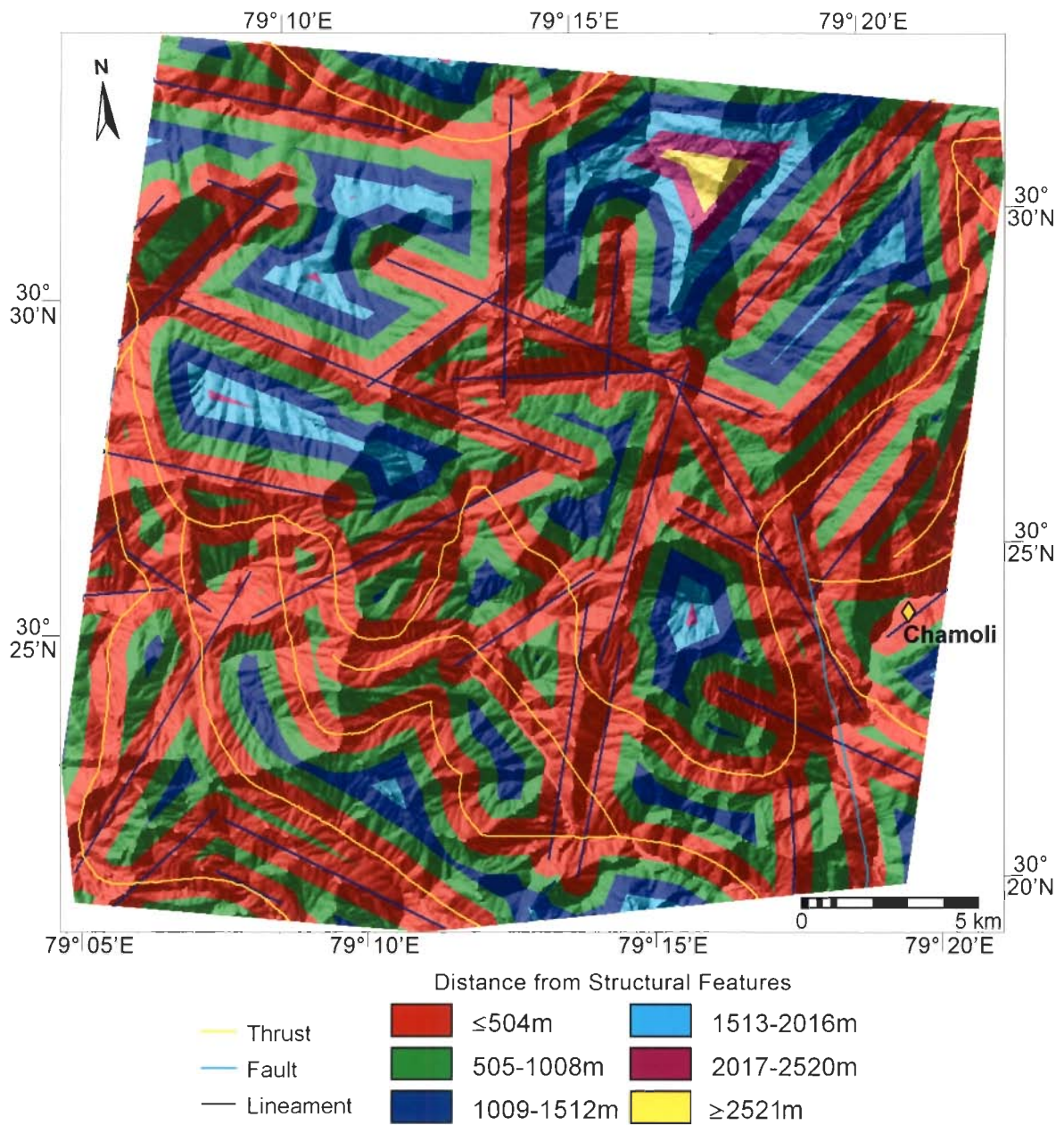
Figure 4.14: Buffer map of structural features (thrusts, faults and lineaments) (the SRM forms the background).

4.7.1 Drainage Density

Drainage density is defined as the cumulative length of drainage per unit area. It provides a measure of ground water infiltration *vis-à-vis* surface run-off occurring in an area. In mountainous areas, it is difficult to estimate the ground water conditions directly, therefore, drainage density is used as an indirect input parameter of ground water conditions. Low drainage density implies low surface run-off and higher infiltration to groundwater, which may increase slope instability in the region (*e.g.,* Sarkar and Kanungo, 2004).

In this study, drainage density has been determined by considering the length of drainage in a raster format with grid size of 252 m × 252 m (which appears appropriate for the study area) and is an integer multiple of 6 m raster cell size considered for all other thematic data layers. The drainage density values are further categorised into low, medium and high to generate the drainage density data layer (Fig. 4.15).

4.7.2 Drainage Order

Strahler's (1964) drainage order system is a simple method of classifying stream segments based on the number and type of tributaries in the upstream. A stream with no tributaries (headwater stream) is considered as a first order stream. A segment, downstream of the confluence of two first order streams is a second order stream (Fig. 4.16). Thus, an nth order stream is always located downstream of the confluence of two $(n-1)^{th}$ order streams.

Drainage order can also be related to the width of channel (*e.g.,* the width of the drainage generally increases with the increase in drainage order). The data on the width of drainage (channel) is required to calculate the likely cost of the bridge construction during route planning. Therefore, the digitised drainage map has been edited for its attribute information as per Strahler's (*op. cit.*) system to prepare a drainage order map (Fig. 4.17).

The map has been rasterised subsequently for its use as an input for thematic cost calculation during the route planning exercise (see Section 5.2.3 of Chapter 5).

4.8 Landuse/Landcover Map

The knowledge of spatial landuse/landcover information is essential for proper management, planning and monitoring of natural resources. For example, it is a desired input for many agricultural, geological, hydrological and ecological models. Also, any natural hazard study, such as landslide hazard zonation is dependent on the availability of accurate and up-to-date landuse/landcover information (*e.g.,* Gupta *et al.*, 1999; Saha *et al.*, 2002).

Due to synoptic view, map like format and repetitive coverage, satellite remote sensing imagery is a viable source of gathering quality landuse/landcover information at local, regional and global scales (Csaplovics, 1998; Foody, 2002). Moreover, remote sensing data are particularly useful for mapping in mountainous regions like the Himalayas, as these areas are generally inaccessible due to high altitudes and ruggedness of the terrain. Over the years, a number of studies to map landuse/landcover using remote sensing data in high mountain areas have been reported with varying degrees of success. This may be due to a large number of factors that influence the remote sensing data processing and interpretation. These include the presence of shadows due to high altitude of the terrain, cloud cover, low sun angle, steep slopes and differential vegetation cover. Therefore, due to changes in environmental conditions, spectral characteristics also change from one region to another (Arora and Mathur, 2001). Hence, classification only on the basis of spectral data from a sensor alone may not be sufficient to gather effective landuse/landcover information. A classification approach that incorporates data from other sources may be more effective than that is based solely upon one sensor multi-spectral data. The ancillary data from other sources may be acquired from topographic maps (Bruzzone *et al.*, 1997), geological (Gong, 1996) and other maps. The most useful
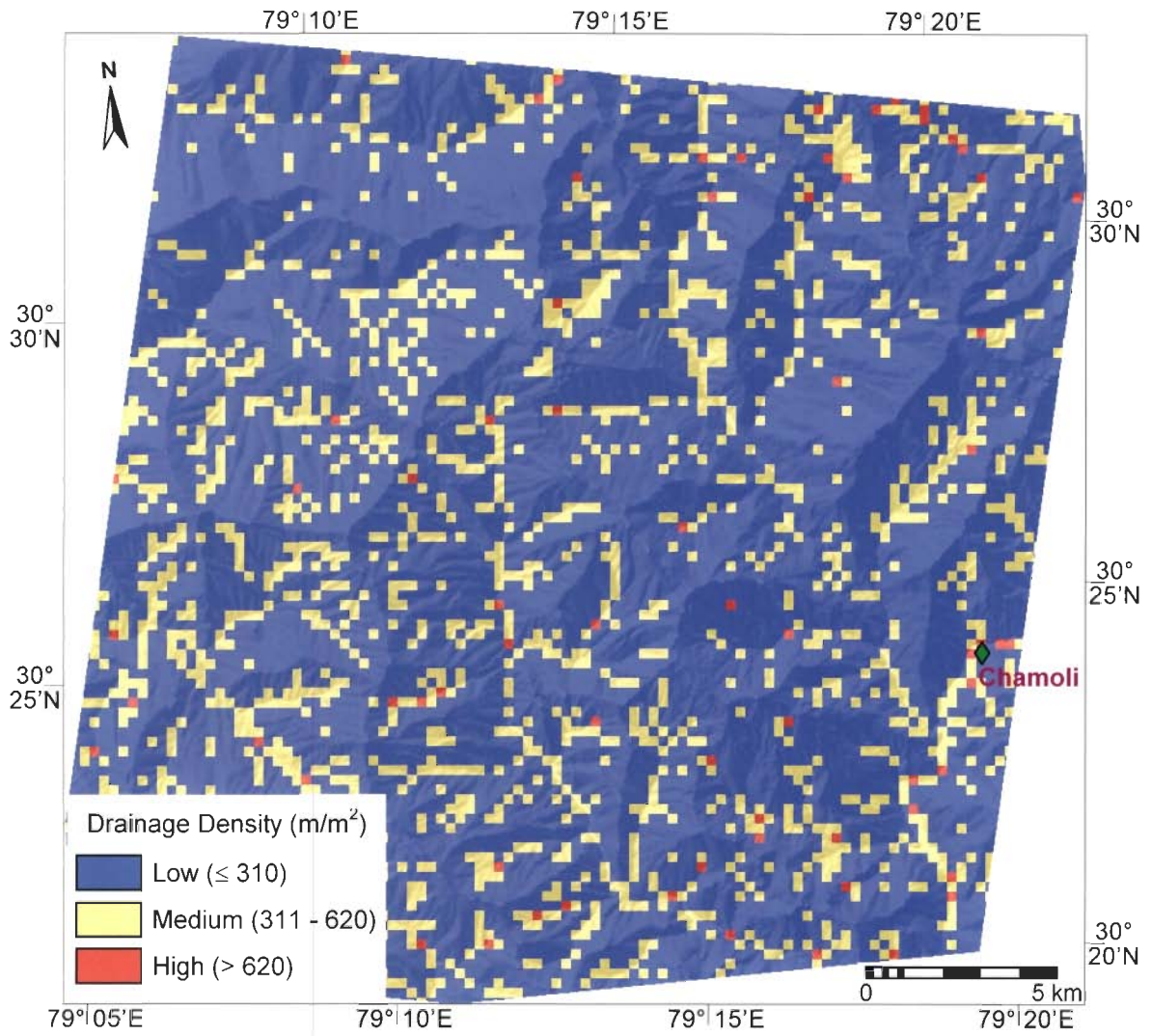
Figure 4.15: Drainage density map (calculated on a grid of 252 m × 252 m) (background is the shaded relief model).
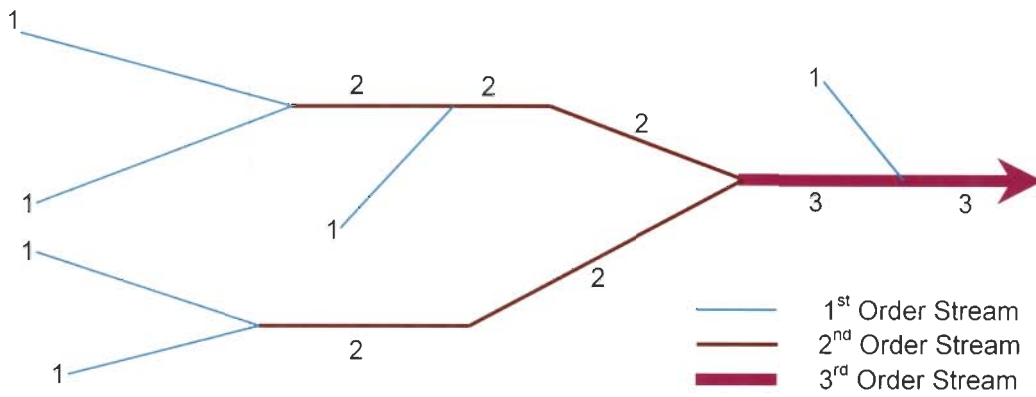
Figure 4.16: The drainage order scheme (Strahler, 1964).
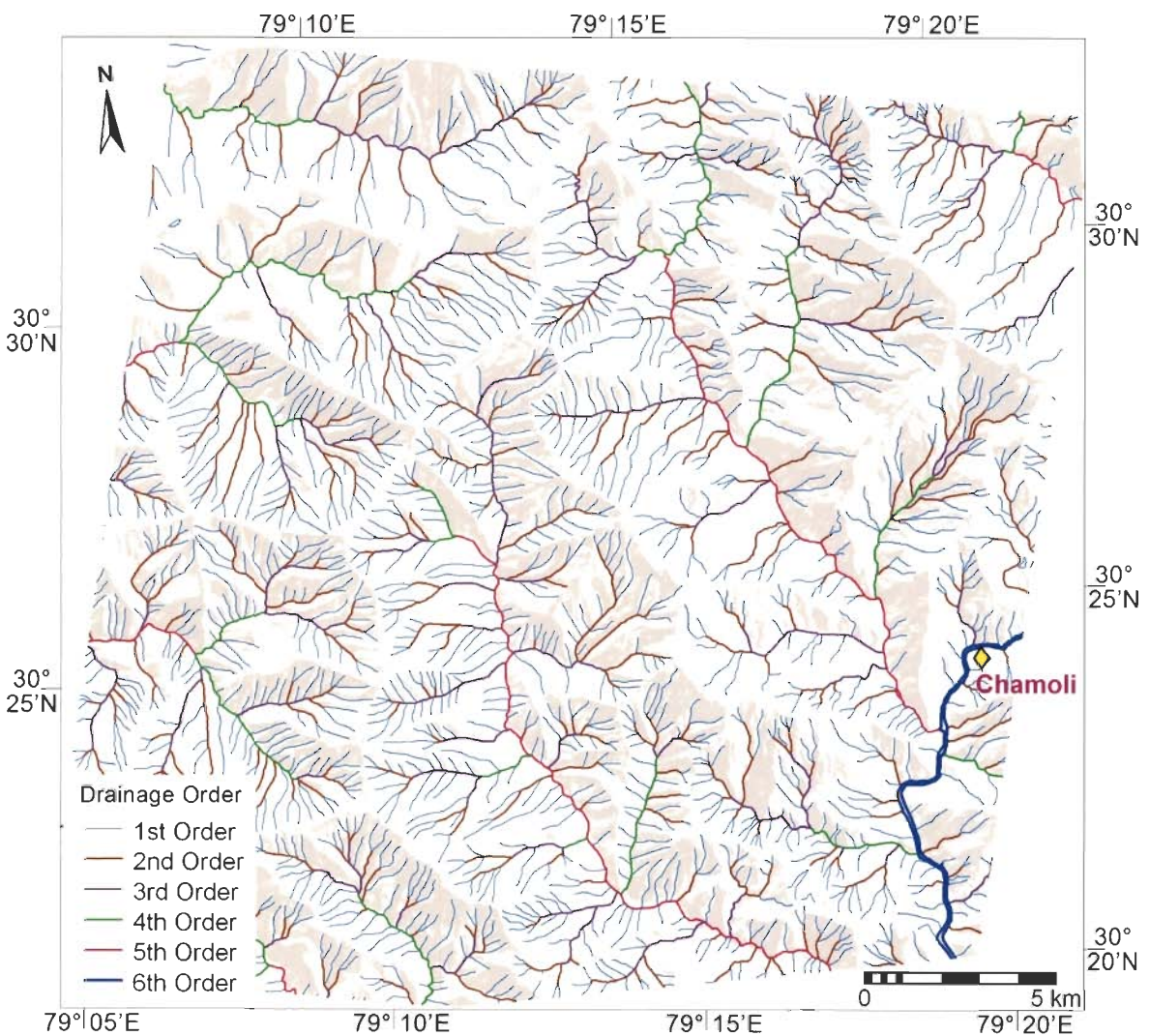
Figure 4.17: Drainage order map (background is the shaded relief model).

information that can be generated from topographic maps is the DEM, which along with its derivatives, such as slope and aspect, provide the basis for multi-source classification (Strahler *et al.*, 1978; Jones *et al.*, 1988; Frank, 1988; Janssen *et al.*, 1990). Data from different remote sensing sensors may also be combined to produce multi-sensor classification for vegetation mapping (Michelson *et al.*, 2000). Moreover, a number of derivatives of multi-spectral images, such as Principal Components Analysis (PCA) and Normalised Difference Vegetation Index (NDVI) may also be incorporated in the classification process to enhance the quality of landuse/landcover information from remote sensing data in mountainous regions (Eiumnoh and Shrestha, 2000).

In mountainous regions, such as the Himalayas, shadow is the major source of ambiguity in extracting landuse/landcover information from remote sensing data. Although, there is no suitable method to completely remove the effect of shadow, several alternatives exist to minimise its effect in order to improve classification from remotely sensed data. Many of the methods are based on shaded relief models that are produced from DEM. However, many studies (*e.g.*, Kawata *et al.*, 1988; Civco, 1989; Colby, 1991; Curran and Foody, 1994), have shown that due the presence of errors in creating DEMs and the way the DEM is applied in the classification process, the correction for shaded slopes may get over-estimated. To counteract this problem of over-correction, the use of NDVI image as an additional layer has been recommended, since the band ratio derivatives may help in nullifying the topographic component to some extent (Holben and Justice, 1981; Apan, 1997); however, NDVI alone may not completely remove the shadow effect. Recently, Eiumnoh and Shrestha (2000) exploited the advantages of incorporating both NDVI and DEM in the classification process and showed a significant improvement in the classification accuracy.

In this study, the IRS-1C LISS-III sensor data has been used as the primary data source with NDVI and DEM as the additional data layers to implement multi-source landcover classification. The logical channel approach (Tso and Mather, 2001) has been

used to select the best band combination. Separability analysis on the basis of transformed divergence has also been performed to examine the significance of various spectral and ancillary bands in the classification process. The classification has been performed using the most widely used Maximum Likelihood Classifier (MLC). The LISS-III multi-spectral (23.5 m spatial resolution) image has been used as the primary data to produce landuse/landcover classification and the PAN image (5.8 m spatial resolution) has been used as the reference data for generating training and testing datasets. This is in accordance with other studies on landuse/landcover classification of remote sensing data (*e.g.,* Fisher and Pathirana, 1990, Foody and Arora, 1996; Shalan *et al.*, 2003), where finer resolution datasets have been used as reference data. The preparation of reference data has been ably supported with field surveys and previous knowledge of the study area. The GPS survey has been carried out to obtain accurate location of landuse/landcover classes for their easy demarcation on geo-rectified LISS-III and PAN images.

4.8.1 Methodology

A number of steps are involved in performing multi-source classification. These include: pre-processing of LISS-III image to correct for atmospheric errors, registration of LISS-III and PAN images, generation of ancillary data layers (NDVI and DEM), image classification and accuracy assessment (Fig. 4.18). All the processing steps have been implemented in ERDAS Imagine and ILWIS software and are briefly described here. The details of atmospheric correction, registration of images and DEM generation have already been described in the previous sections.

4.8.1.1 NDVI

As the study area is dominated by different types of vegetation, NDVI has been used as an ancillary data layer in the classification process to enhance the separability among various vegetation classes, and also to reduce the shadow effect due to topography.
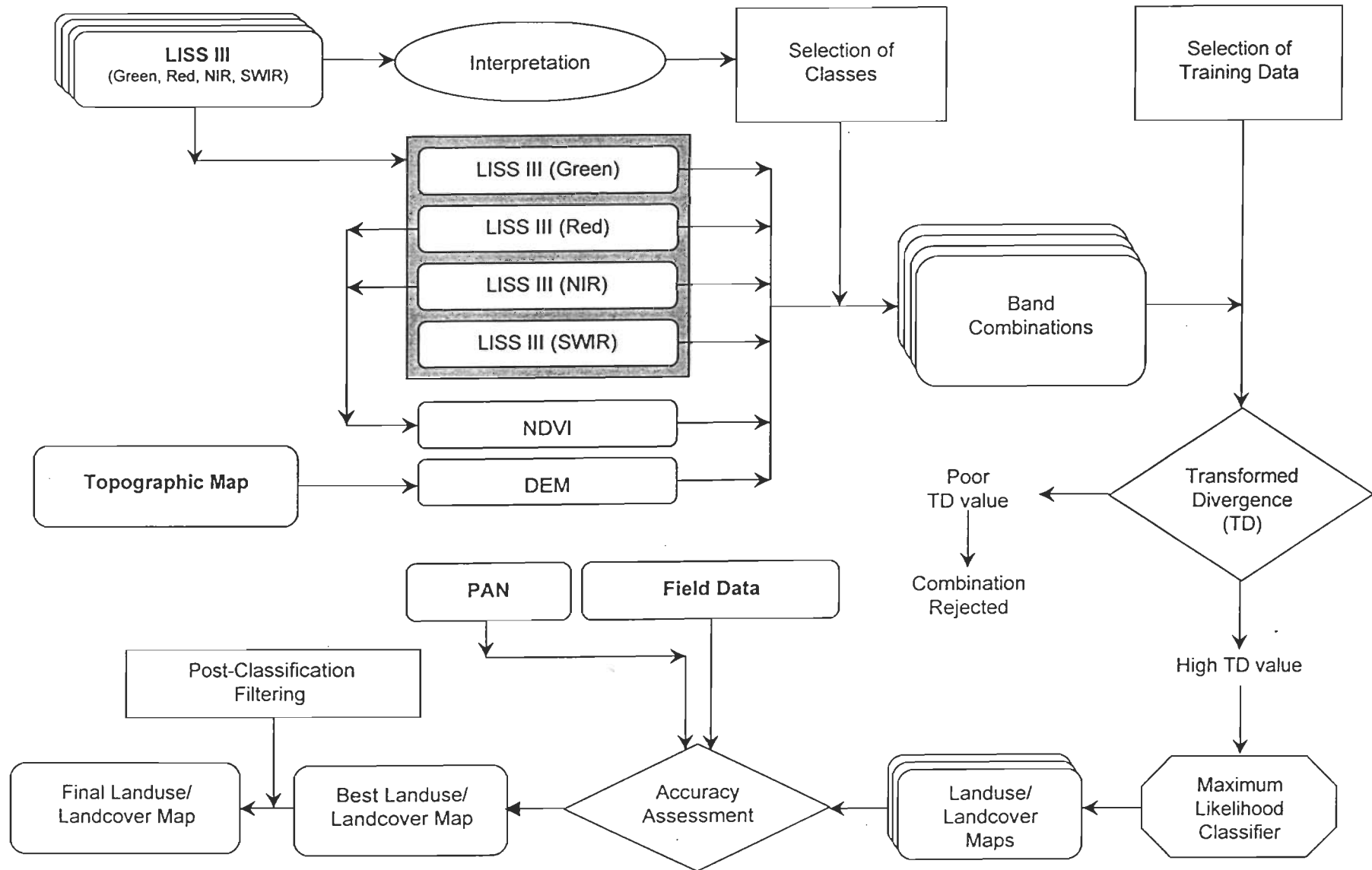
Figure 4.18: Multi-source landuse/landcover classification scheme used in this study.

The NDVI is defined as,

$$NDVI = \frac{(NIR - Red)}{(NIR + Red)} \qquad (4.6)$$

The Red and NIR bands of LISS-III image have been used to derive NDVI data layer. Figure 4.19 shows the NDVI data layer draped over the DEM of the study area. The pixel values of the NDVI data layer image range from -1 to 1 with higher values indicating increasing biomass. In the NDVI data layer thus created, the pixel values range from -0.36 to +0.62. The positive values represent various types of vegetation classes. Near zero and negative values indicate non-vegetation classes, such as water, snow and barren land.

4.8.1.2 Image Classification

A series of image classification operations have been performed to produce the landuse/landcover map from LISS-III image and ancillary data, which are described below:

a) *Selection of a landuse/landcover classification scheme*

A classification scheme defines the number of landcover classes to be considered to perform remote sensing image classification. Sometimes, a standard classification scheme, such as Anderson's landuse/landcover classification system (Anderson *et al.*, 1976) may be used, while at other times the number of landuse/landcover classes may be chosen according to the requirements of the specific project for a particular application. In this study, based on Anderson's classification system, nine landuse/landcover classes have been defined. Some of these classes as they appear in the field are shown in Figure 4.20. Detailed description of all the classes along with their interpretative characteristics on the colour infrared composite of LISS-III image (Fig. 4.2) and PAN image (Fig. 4.21) is provided in Table 4.2.
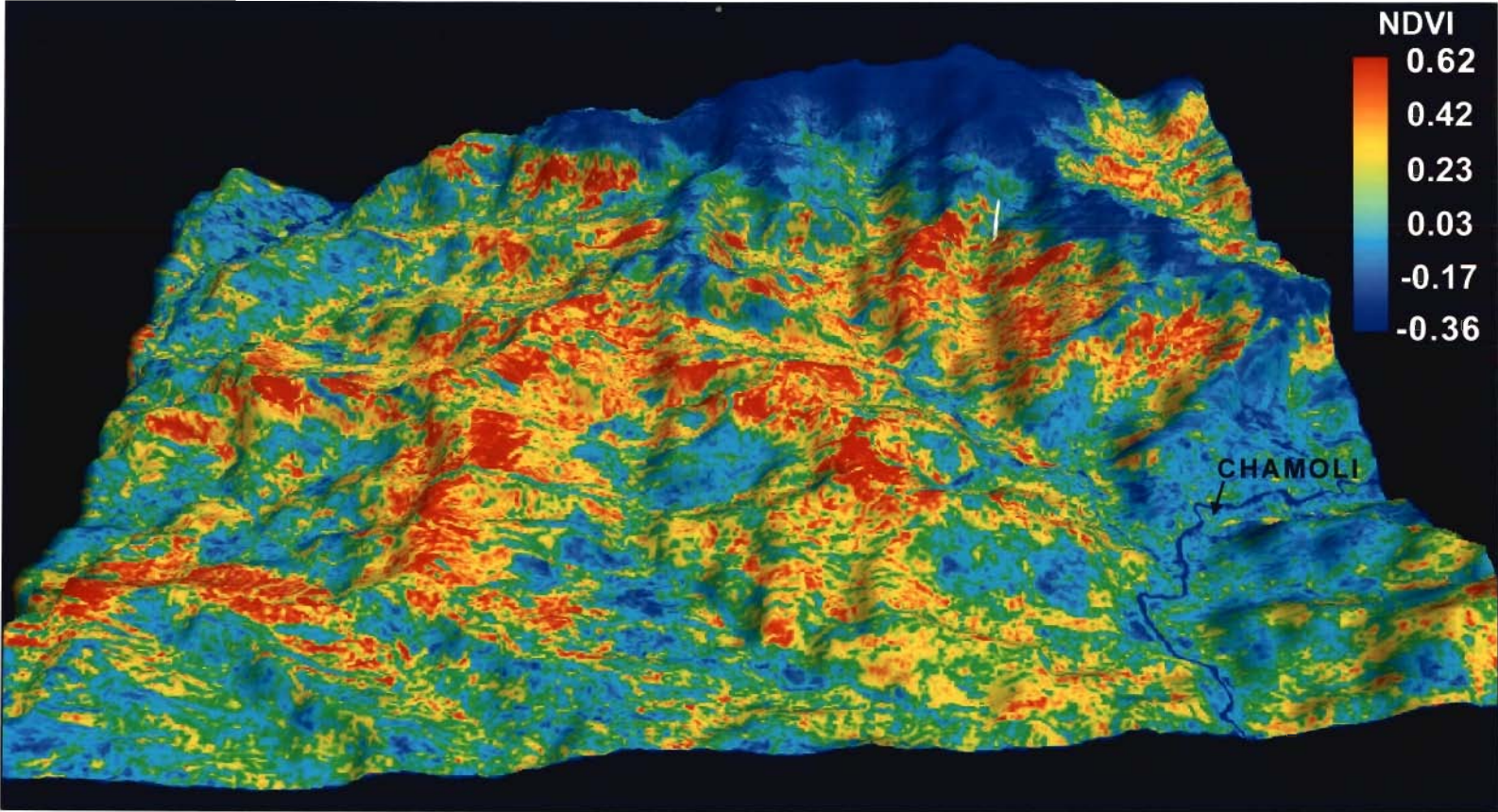
Figure 4.19: Normalised Difference Vegetation Index (NDVI) image generated from IRS-1C LISS-III data draped over DEM.

**Figure 4.20: Field photographs showing various landuse/landcover classes
(Df – Dense forest; Sv – Sparse vegetation; Ag – Agriculture; Fl – Fallow land;
Bl – Barren land; St – Settlements; Rs – River sediments; Ld – Landslide
debris; Wb – Water body; Sn – Snow).**
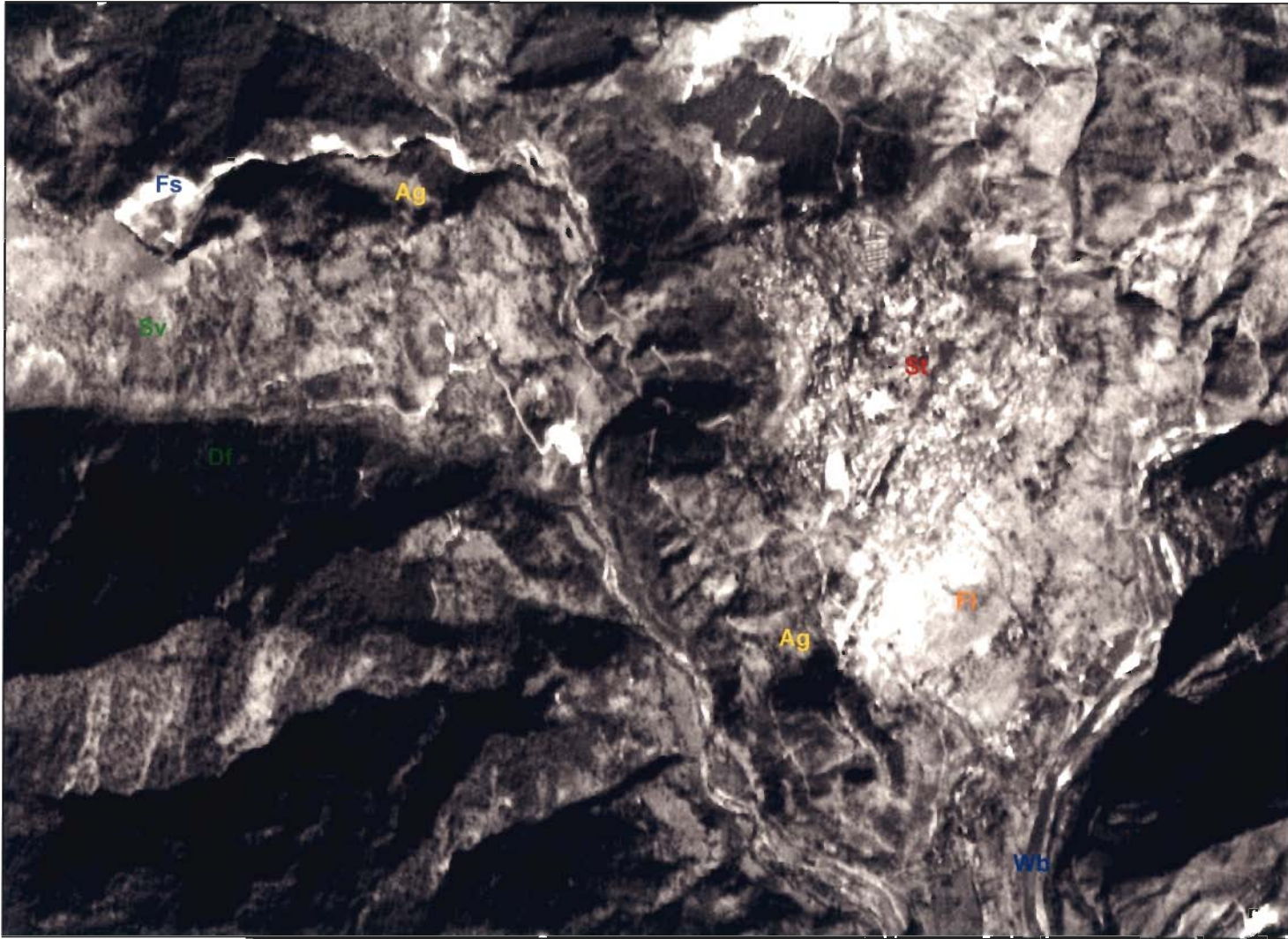
**Figure 4.21: A sub-scene of IRS-1C PAN image showing various landuse/landcover classes
(Df – Dense forest; Sv – Sparse vegetation; Ag – Agriculture; Fl – Fallow land;
St – Settlements; Fs – Fresh sediments; Wb – Water body)**

Table 4.2: Characteristics of landuse/landcover classes

Landuse/ landcover class	Description	Interpretation on LISS-III colour infrared composite	Interpretation on PAN image
Dense forest	Tall dense trees	Dark red with rough texture	Dark tone with rough texture
Sparse vegetation	Low vegetation density with exposed ground surface	Dull red to pinkish	Light tone with dark patches
Agriculture	Crops on hill terraces as step cultivation	Dull red and smooth appearance	Step like arrangement of fields
Fallow land	Agricultural fields without crops	Bluish/greenish grey with smooth texture	Bright tone with smooth texture
Barren land	Exposed rocks without vegetation	Yellowish	Very bright tone
Settlements	Towns and villages; block like appearance	Bluish	Typical blocky appearance with light tone
Fresh sediments	Fresh landslide debris and river sediments on the bank	Cyanish	Bright tone
Water body	Rivers and lakes	Cyanish blue to blue according to the depth of water and sediment content	Dark tone
Snow	Snow covered areas on high altitude mountains	Bright white	Very bright tone

b) *Formation of training dataset*

Training data extraction is a critical step in a supervised image classification process. As the success of a classification highly depends on the quality of the training data, these must be selected from the regions that are representative of the landuse/ landcover classes under investigation. Data should thus be collected from relatively homogeneous areas consisting of those classes. The collection of training data is generally a costly affair and, therefore, the size of the training data set must also be kept small. On the other hand, the number of pixels constituting the training data set must be large enough to accurately characterise the landuse/landcover classes. As a rule of thumb, the number of training pixels for each class may be kept at 30 times the number of bands under

consideration (Mather, 1999). In this study, the training data set consists of about 1% of the total pixels in the LISS-III image. For each class, the number of training pixels (Table 4.3) has been adopted in accordance with the proportion of area covered by the respective classes on the ground. Similar to other studies, the fine spatial resolution PAN image and topographic map have been used as reference data (ground truth) to delineate the training pixels on the LISS-III image. First, the PAN image has been visually interpreted based on the characteristics defined in Table 4.2 to delineate the nine landuse/landcover classes identified above. In case of confusion in identifying the classes, field verification has been carried out. The PAN image derived landuse/landcover information has been used to demarcate training areas on LISS-III image. The histogram plot of majority of training areas shows normal distribution, which is a requirement of the maximum likelihood classifier used in this study.

Table 4.3: Number of training pixels for each landuse/landcover class used in classification

Landuse/landcover class	Number of training pixels
Dense Forest	3779
Sparse vegetation	1087
Agriculture	461
Fallow Land	1335
Barren Land	1907
Settlements	494
Fresh sediments	401
Water body	618
Snow	1642
Total	**11724**

c) Separability analysis

The input datasets for multi-source classification consist of six data layers (four bands of multi-spectral LISS-III image, two ancillary data sources - NDVI and the DEM). For convenience, Green band, Red band, Near Infrared (NIR) band, Shortwave Infrared (SWIR) band, NDVI and DEM have been numbered as 1, 2, 3, 4, 5 and 6 respectively, in this study. A separability analysis has been performed using the training dataset to identify the combination of bands that produces the highest discrimination between the landuse/landcover classes. Separability is a statistical measure devised on the basis of spectral distances computed from a combination of bands. From a number of separability measures, the Transformed Divergence (TD) has been used in this study (Janssen *et al.*, 1990). The TD values range from 0 to 2000 with a value close to 2000 indicating the best separability. The values between 1800 and 2000 are generally considered adequate for the selection of appropriate band combinations. Since, the focus of the present study is on the inclusion of ancillary data in the classification process, the average TD values of various band combinations that include ancillary data, have been computed. Various five-band combinations that produced average TD values near to 2000 were considered appropriate for classification and are reported in Table 4.4.

**Table 4.4: Various band combinations and their average TD values
(Bands 1, 2, 3, 4: LISS-III bands; Band 5: NDVI; Band 6: DEM)**

Band combinations	Average TD
1, 2, 3, 4, 5	1985
1, 2, 3, 4, 6	2000
1, 2, 3, 5, 6	1977
1, 2, 4, 5, 6	2000
1, 3, 4, 5, 6	1998
2, 3, 4, 5, 6	1993

Although all the five-bands combinations are equally good, the band combination consisting of 1, 2, 3, 4 and 6 bands has resulted in the highest average TD value, indicating that LISS-III image together with DEM has produced the best separability among various pairs of landuse/landcover classes. Further, since no significant variation in the average TD values has been observed, all the five-band combinations as well as the complete data set (1, 2, 3, 4, 5 and 6) have been used to perform the classification.

d) Maximum likelihood classification (MLC)

Numerous image classifiers have been developed and applied for remote sensing data, each having their own merits and demerits in terms of efficiency and accuracy. The MLC has been found to be the most accurate and commonly used classifier, when data-distribution assumptions are met. This classifier is based on the decision rule that the pixels of unknown class membership are allocated to those classes with which they have the highest likelihood of membership (Foody *et al.*, 1992). The detailed formulation of this classifier may be found in Richards and Jia (1999). MLC has been used here to produce landuse/landcover maps using different band combinations, as described in the previous section.

4.8.1.3 Classification Accuracy Assessment

No image classification is said to be complete unless its accuracy has been assessed. To determine the accuracy of classification, a sample of testing pixels is selected on the classified image and their class identity is compared with the reference data (ground truth). The choice of a suitable sampling scheme and the determination of an appropriate sample size for testing data plays a significant role in the assessment of classification accuracy (Arora and Agarwal, 2002). The pixels of agreement and disagreement are generally compiled in the form of an error matrix. It is a $c \times c$ matrix (c is the number of classes), the elements of which indicate the number of pixels in the testing data. The

columns of the matrix depict the number of pixels per class for the reference data, and the rows show the number of pixels per class for the classified image. From this error matrix, a number of accuracy measures, such as overall accuracy, user's and producer's accuracy, may be determined (Congalton, 1991). The overall accuracy is used to indicate the accuracy of whole classification (*i.e.*, number of correctly classified pixels divided by the total number of pixels in the error matrix), whereas the other two measures indicate the accuracy of individual classes. User's accuracy is regarded as the probability that a pixel classified on the map actually represents that class on the ground or reference data, whereas producer's accuracy represents the probability of a pixel on reference data being correctly classified.

In this study, the landuse/landcover information interpreted from the PAN image together with the field data has been used as reference data to generate the testing data set. A total of 200 testing pixels for each class have been randomly selected, which are larger than 75 to 100 pixels per class as recommended by Congalton (1991) for accuracy assessment purposes. For effective comparison, the same testing dataset has been used to evaluate different landuse/landcover classifications. From this testing dataset, overall accuracy and producer's accuracy have been computed.

The overall accuracy of various landuse/landcover classifications obtained from different band combinations is shown in Table 4.5. The classification based only on spectral data of LISS-III image has produced an accuracy of 86.94%, which is more than the minimum accuracy criterion of 85% overall accuracy, as reported in USGS landuse/landcover classification system (Anderson, 1976). On inclusion of NDVI data layer with spectral data, this accuracy has marginally dropped to 84.78%, however it increases remarkably to 91.00% when DEM and NDVI data layers are included in the classification process. The highest accuracy of 92.06% has been obtained with the five-band combination (*i.e.*, band combination 1, 2, 4, 5, 6) that contains both NDVI and DEM

datasets, thus producing a considerable increase of 5% accuracy over the landuse/landcover classification map produced only using LISS-III data.

Table 4.5: The overall accuracy for landuse/landcover classifications produced from data using different band combinations. Bands 1, 2, 3, 4, 5, and 6 have been defined in the text. (Note: Highest accuracy in bold face)

Band combination	Overall accuracy (%)
1, 2, 3, 4, 5, 6	91.00
1, 2, 3, 4, 5	84.78
1, 2, 3, 4, 6	91.06
1, 2, 4, 5, 6	**92.06**
1, 3, 4, 5, 6	91.72
1, 2, 3, 5, 6	85.00
2, 3, 4, 5, 6	89.33
1, 2, 3, 4	86.94

To assess the accuracy of individual landuse/landcover classes, producer's accuracies have also been determined for the classification providing the highest overall accuracy (*i.e.,* using band combination 1, 2, 4, 5, 6). As an example, the error-matrix for the best-classified image has been given in Table 4.6. These accuracy values have been compared with those obtained from the classification produced by using only LISS-III spectral data (Table 4.7). A glance at the values of the producer's accuracy values shows improvement in the accuracy of most of the classes when NDVI and DEM data layers are incorporated in the classification process. This illustrates that the misclassifications between the classes have been reduced. In particular, the classification accuracy of the classes, namely sparse vegetation, agriculture, fallow and barren land, settlements and snow has shown a substantial increase ranging from 1.5% to 20%. Two explicit reasons may be stated for this increase in accuracy. First, the class barren land has been considerably misclassified with the classes settlements and water body, when only spectral data are used. Since, at higher elevations, the presence of these classes is rare, the addition of DEM has reduced this misclassification. Secondly, due to the presence of shadows in

the region, the classification using only spectral data shows misclassification of fallow land and sparse vegetation to the class forest. The addition of NDVI image and DEM has reduced the shadow effect and thus these classes have been appropriately classified.

Table 4.6: Error matrix of the classified image obtained from classification of data with 1, 2, 4, 5, 6 band combination

Classes in the classified image	Classes on reference data									
	1	2	3	4	5	6	7	8	9	Row total
1. Dense forest	199	0	0	0	0	0	0	3	0	202
2. Sparse Vegetation	0	180	0	0	2	0	3	0	0	185
3. Agriculture	1	18	195	0	0	1	1	4	0	220
4. Fallow Land	0	2	5	143	0	8	0	3	0	161
5. Barren Land	0	0	0	0	198	0	2	0	2	202
6. Settlements	0	0	0	56	0	184	3	6	0	249
7. Fresh sediments	0	0	0	1	0	7	191	15	0	214
8. Water body	0	0	0	0	0	0	0	169	0	169
9. Snow	0	0	0	0	0	0	0	0	198	198
Column total	200	200	200	200	200	200	200	200	200	1657/1800

Table 4.7: Producer's accuracy of individual classes derived from classifications from data using 1, 2, 3, 4 band combination *vis-à-vis* 1, 2, 4, 5, 6 band combination. 1, 2, 3, 4, 5, and 6 bands have been defined in the text.

Classes	Producer's accuracy (%)	
	1, 2, 3, 4 bands	1, 2, 4, 5, 6 bands
Dense Forest	99.0	99.5
Sparse Vegetation	76.0	90.0
Agriculture	77.5	97.5
Fallow land	79.5	71.5
Barren land	91.5	99.0
Settlements	85.5	92.0
Fresh sediments	98.0	95.5
Water body	83.0	84.5
Snow	92.5	99.0

On visual comparison of the colour infrared composite (Fig. 4.2) and the landuse/landcover map (Fig. 4.22), it can further be observed that the addition of DEM and NDVI data layers has allowed for the correct classification of shadowed areas to their corresponding vegetation classes, which is not the case when only spectral data has been used for classification. This clearly demonstrates the utility of incorporating NDVI and DEM data layers in the landuse/landcover classification.

4.8.1.4 Post-classification Filtering

Some stray pixels always occur in a landuse/landcover classification produced from remote sensing data. To remove these stray pixels to generate a smooth image, a 3 × 3 pixels majority filter has been applied which assigns the most dominant class to the central pixel.

Some logical operations have also been applied to reclassify the classes in this landuse/landcover classification for their direct use in preparation of landslide hazard zonation map and for thematic cost calculation. Thus, the fallow and barren classes have been grouped together as both have similar susceptibility to landslide hazard. Further, in the classification map, the class 'fresh sediment' comprises both landslide debris and river sediments, as both have similar spectral properties. However, it is necessary to distinguish between landslide debris and river sediments for the purpose of LHZ, as the two have widely different associated landslide hazards. The river sediments occur with almost flat surfaces and landslide debris possesses steeper slopes. Therefore, the class fresh sediment has been decomposed into two classes. A threshold value of topographic slope of 15° has been used to differentiate between the two classes.
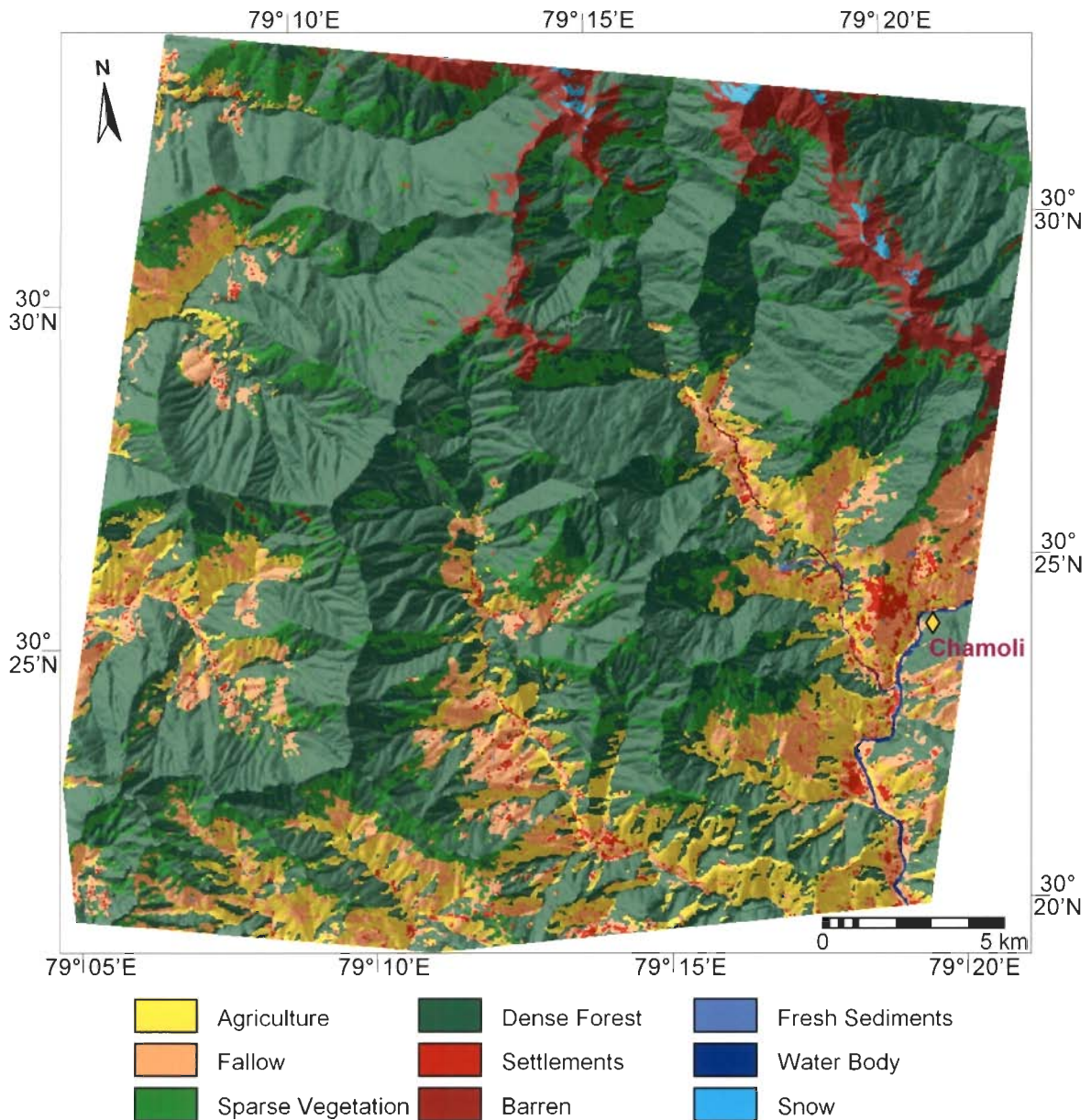
Figure 4.22: Landuse/landcover map possessing the highest accuracy (92.06%) generated from band combinations 1, 2, 4, 5 and 6 (i.e., Green, Red, SWIR band of IRS-1C LISS-III image, NDVI and DEM). A post-classification filtering has been applied (the SRM forms the background).

4.9 Landslide Distribution Map

The identification and mapping of existing landslides is a pre-requisite to perform statistical analysis on the distribution of landslides. Since, in a high-altitude mountainous region, such as the Himalayas, it is not possible to conduct field visits to all the places for physically locating each and every landslide, remote sensing images are highly valuable, as they provide synoptic views for mapping landslides.

The high-resolution PAN image has been used to identify and map the existing landslides. On this image, landslides generally show scar and very light tones (debris - unvegetated). Landslides in barren areas can also be distinguished easily on raw images and/or on contrast stretched images. Besides, old landslides can also be delineated on the basis of shape, landform and drainage.

The technique of PAN-sharpened multi-spectral image products (Welch and Ehler, 1987; EOSAT, 1994; Sabins, 1996; Sharma *et al.,* 1996; Saraf, 2000; Prakash *et al.,* 2001; Sanjeevi *et al.,* 2001; Shanmugam and Sanjeevi, 2001; Gupta, 2003) is very useful in interpretation of features of interest. For generating a PAN-sharpened multi-spectral image, the PAN and multi-spectral images are co-registered and the multi-spectral image is resampled to the spatial resolution of the PAN image. The Colour Infra-Red (CIR) composite of multi-spectral image is transformed into Intensity-Hue-Saturation (IHS) components and the intensity (I) component is replaced with the high-resolution PAN image followed by a reverse transformation. The resultant CIR composite is the PAN-sharpened image that has the advantage of having spectral information from the multi-spectral image and spatial characteristics from the PAN image. This leads to an increase in the interpretability of the image, such as landslide mapping. On the resultant CIR composite, the landslides are depicted in bright-whitish colours that can be easily distinguished from the other features (Fig. 4.23).

In this study, a total of 190 landslides of varying dimensions have been identified using both PAN and the PAN-sharpened LISS images (Fig. 4.23). Many of the landslide locations have also been verified in the field (Fig. 4.24). Each landslide thus identified has been digitised as a polygon (Fig. 4.25) and the layer has been converted to a raster landslide distribution map for further GIS analysis. Field photos of some important landslides have been presented in Figure 4.26.

4.10 Landslide Hazard Zonation (LHZ)

The Landslide Hazard Zonation (LHZ) is an important component for deciding the route development and maintenance cost. A review on various methods of LHZ has been given in Chapter 2. Among the various methods (Table 2.3), the bivariate statistical methods are found to be most suitable for LHZ studies at medium scales. In this investigation, two bivariate statistical methods, namely InfoVal and a modified method of LNRF (named as m-LNHF) have been implemented for the generation of LHZ maps of the area and their results have been compared.

The broad methodology of LHZ map preparation is shown in Figure 4.27. A number of thematic maps (referred to as data layers in GIS terminology) related to the factors affecting the landslide activity (*viz.*, slope, aspect, relative relief, structural features, lithology, landcover and drainage density) have been generated, which have been described in detail in the previous sections. The landslide hazard zonation map has been prepared considering 6 m × 6 m grid size (equivalent to nominal spatial resolution of IRS-PAN image).

4.10.1 Weight Calculation

To evaluate the contribution of each factor towards landslide hazard, the existing landslide distribution data layer (Fig.4.25) has been laid over various thematic data layers separately. The number of landslide pixels falling on each class of the thematic data layers
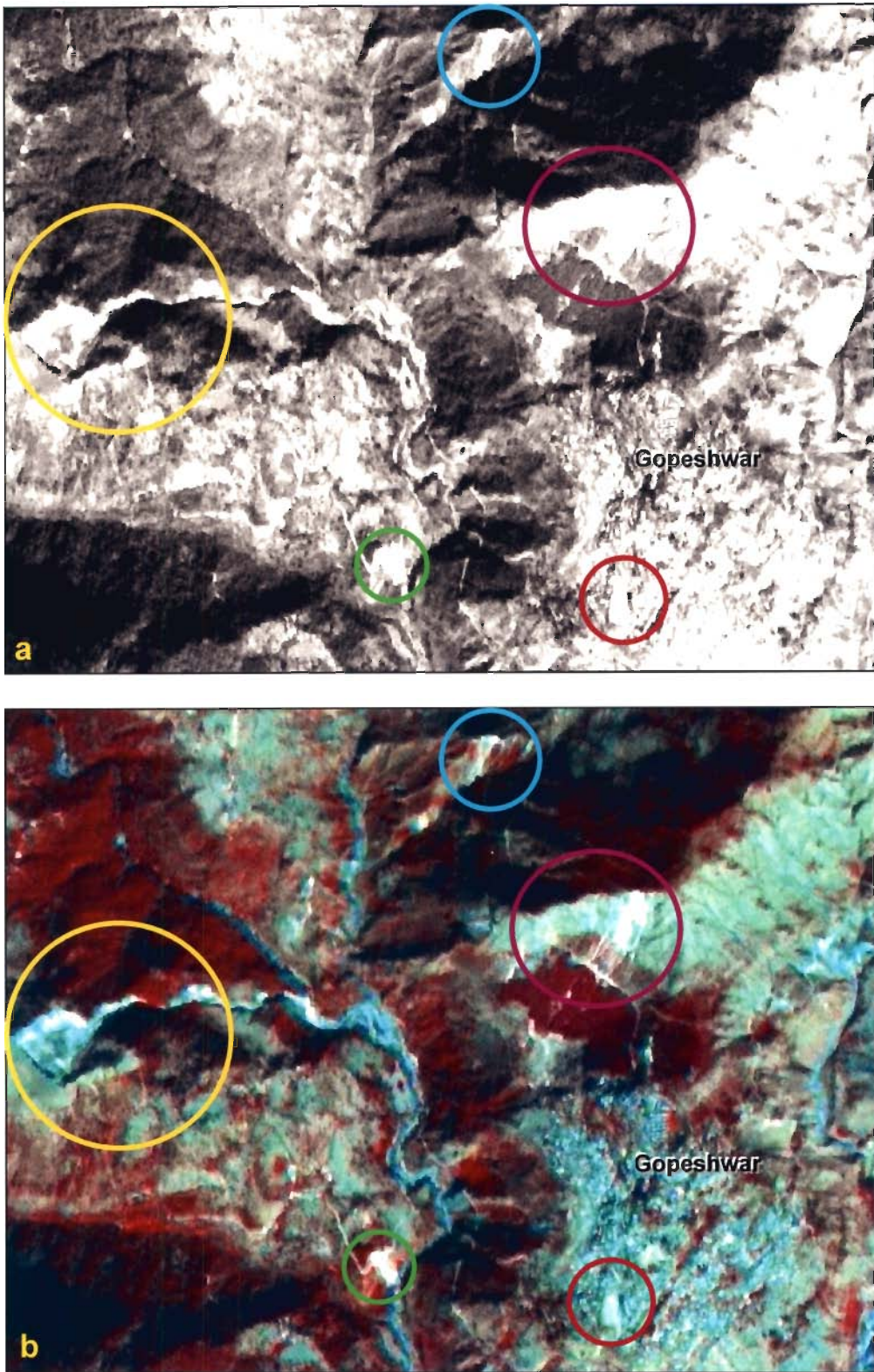
**Figure 4.23: Comparison of (a) IRS-PAN image and (b) PAN-sharpened
LISS-III image for interpreting landslides. The same landslides
are encircled in both the images.**
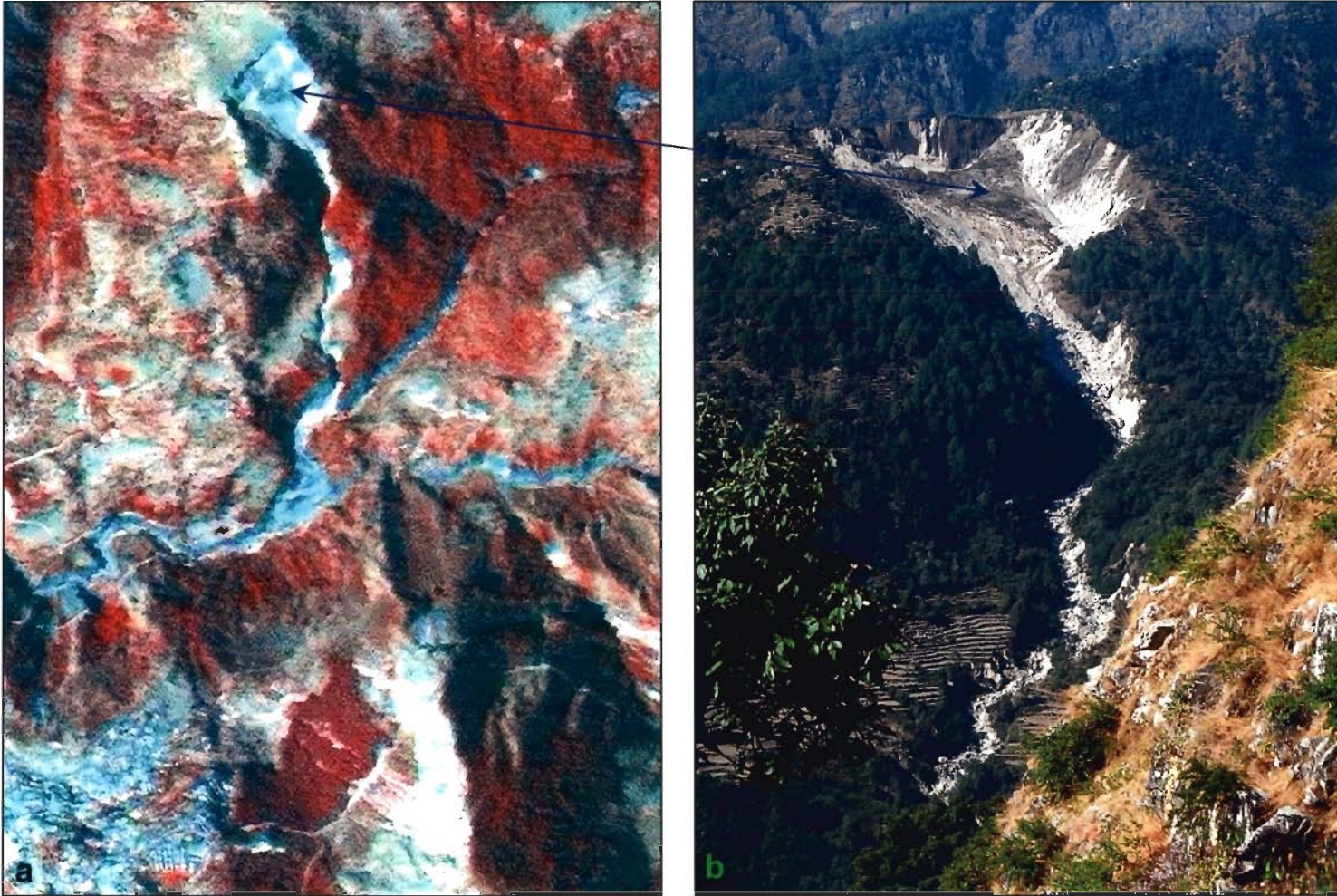
**Figure 4.24: A typical landslide as identified from (a) IRS-PAN image and
(b) the corresponding field photo (indicated by arrow)
(landslide location: 30°25'08"N, 79°17'33"E).**
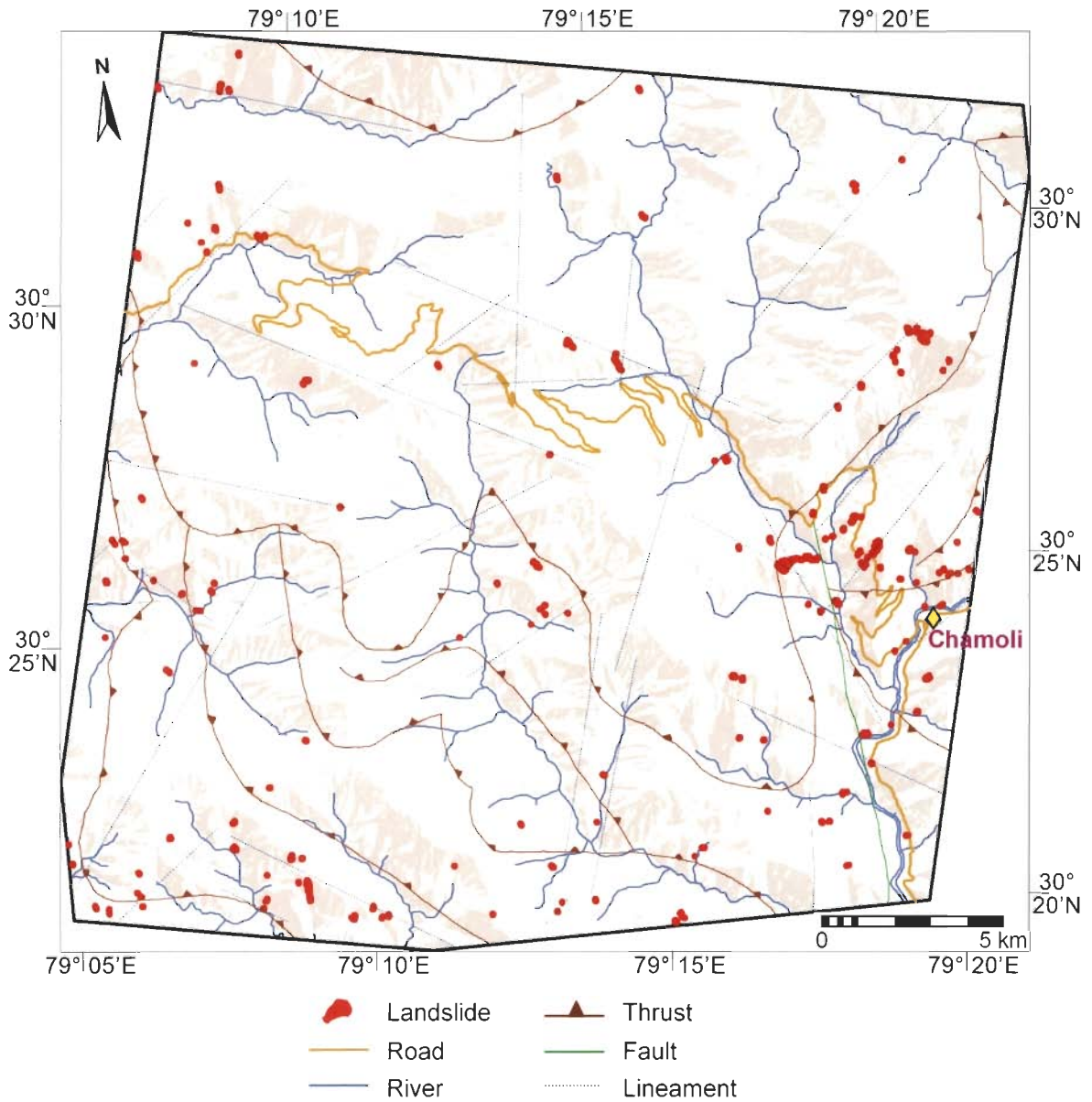
**Figure 4.25: Landslides mapped from IRS-1C PAN and PAN-sharpened
LISS-III image. Structural features have also been plotted
to show their proximity to the landslides.**

(a) Gopeshwar Landslide
(30°25'18"N, 79°19'10"E)

(b) Parariyana Landslide
(30°24'32"N, 79°18'23"E)

(c) Ghingran Landslide
(30°25'38"N, 79°20'56"E)

Figure 4.26: Field photographs of some the major landslides in the study area.
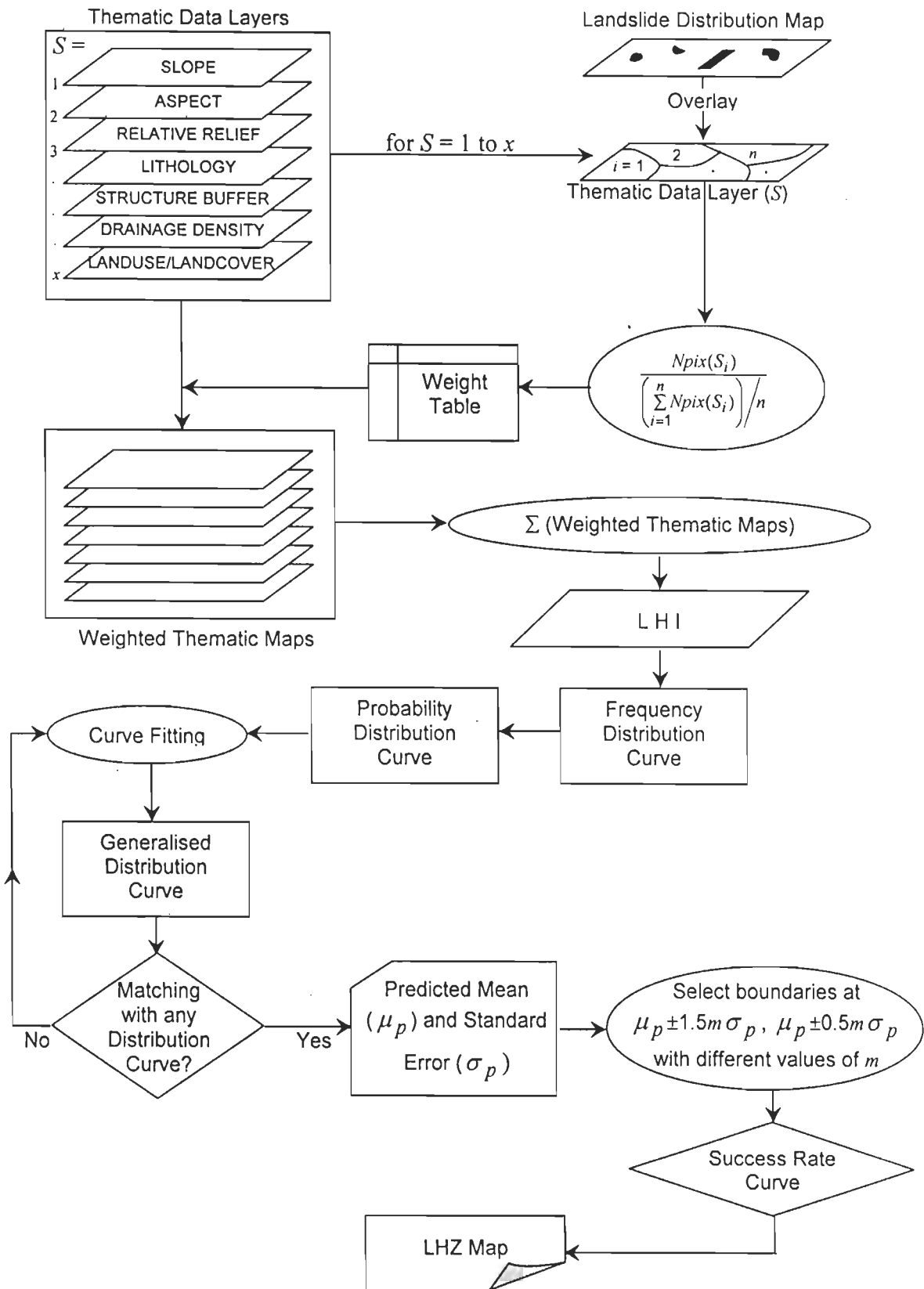
Figure 4.27: Flow diagram showing the LHZ methodology (m-LNHF) adopted in this study. *Npix(S_i)* denotes the number of landslide pixel in *i^{th}* class of *S^{th}* thematic data layer. *m* is a positive, non-zero value.

has been recorded and weight values have been calculated. In the InfoVal method the weights are calculated as per Equation 2.1 (see Chapter 2) and these weights are directly used in computations. In the LNRF method as proposed by Gupta and Joshi (1990), the LNRF values are regrouped into ordinal numbers (0, 1, 2) and then added together in an indexed overlay approach.

However, it is observed that regrouping the LNRF values into ordinal numbers (0, 1, 2) leads to coarsening of approach and reduction in the relative importance of various thematic classes. Hence, in this modified-Landslide Nominal Hazard Factor (m-LNHF) method the computed values as per Equation 2.2 (see Chapter 2) are directly used. The computed weights on the basis of InfoVal and m-LNHF methods are given in Table 4.8.

4.10.2 Integration of Thematic Layers

The computed weights (Table 4.8) have been assigned to the classes of each thematic map to produce weighted thematic map. These maps have been laid over one another, and numerically added according to the following equation to generate a Landslide Hazard Index (LHI) map in GIS:

$$LHI = Sl + As + Rr + Li + St + Dd + Lu \tag{4.7}$$

where Sl, As, Rr, Li, St, Dd and Lu are abbreviated for the weighted thematic maps, *viz.*, slope, aspect, relative relief, lithology, structure, drainage density and landuse/landcover respectively, considered in this study for LHZ. Thus, two LHI maps, one each corresponding to the InfoVal and the M-LNHF methods, have been prepared.

4.10.3 Segmentation of LHI Values and Generation of LHZ Map

a) InfoVal Method

The LHI-values from the InfoVal method have been found to lie in the range between −10.6643 and 8.1220. The cumulative frequency curve of LHI values has been segmented into five classes representing near-equal distribution (as per van Westen, 1997)

to yield five landslide hazard zones, *viz.,* very low, low, moderate, high and very high (Fig. 4.28).

Table 4.8: Relationship of various thematic data layers with landslide occurrences

Classes	Landslide (Pixel)	Area (Pixel)	m-LNHF Weight	InfoVal Weight (*ln*)
a) Slope				
<= 15°	1166	1899852	0.488	-0.219
16° - 25°	2462	4182712	1.031	-0.261
26° - 35°	3307	4286079	1.384	0.010
36° - 45°	2686	2821437	1.124	0.220
>45°	2325	2441452	0.973	0.220
b) Aspect				
Flat	51	48558	0.038	0.318
NE	2188	2156835	1.648	0.283
E	1520	1794493	1.145	0.103
SE	2509	1986783	1.890	0.502
S	2532	2003484	1.908	0.503
SW	2015	2274792	1.518	0.148
W	563	1957136	0.424	-0.978
NW	274	1796658	0.206	-1.609
N	294	1612793	0.222	-1.431
c) Relative Relief				
<= 30 m	2853	4557614	1.194	-0.200
31m - 60 m	5632	7753369	2.357	-0.051
61m - 90 m	2476	2318962	1.036	0.334
91m - 120 m	935	822424	0.391	0.397
>120 m	50	179163	0.021	-1.008
d) Lithology	-			
Schist and Gneiss	0	377411	0	-3.00*
Granite-Granodiorite-Gneiss	3847	8763837	1.610	-0.555
Quartzite with slates	7066	4508249	2.957	0.718
Limestone and Greywacke	0	64767	0	-3.00*
Granite	1033	1917268	0.432	-0.350
e) Structure Buffer			'	
<504 m	9541	8156560	5.591	0.426
505 - 1008 m	1984	4554560	1.163	-0.562
1009 - 1512 m	299	1996254	0.175	-1.630
1513 - 2016 m	122	724353	0.071	-1.514
2017 - 2520 m	0	149956	0	-3.00*
2521 - 3024 m	0	49466	0	-3.00*
3025 - 3528 m	0	383	0	-3.00*
f) Drainage Density				
Low (<= 310 m/m^2)	10421	12654934	2.617	0.075
Medium (311- 620 m/m^2)	1236	2844048	0.310	-0.564
High (> 620 m/m^2)	289	132550	0.073	1.048
g) Landuse/Landcover				
Agriculture	1830	1658013	1.379	0.367
Sparse Vegetation	2082	2071261	1.569	0.274
Dense Forest	685	9342146	0.516	-2.343
Settlements	861	232903	0.649	1.576
Water Body	27	32679	0.020	0.078
Snow	2	39350	0	-2.703
Barren and Fallow Land	3806	2239843	2.867	0.799
Landslide Debris	2608	10515	1.965	5.782
River Sediments	45	4822	0.034	2.502

* Arbitrarily assigned lowest value.
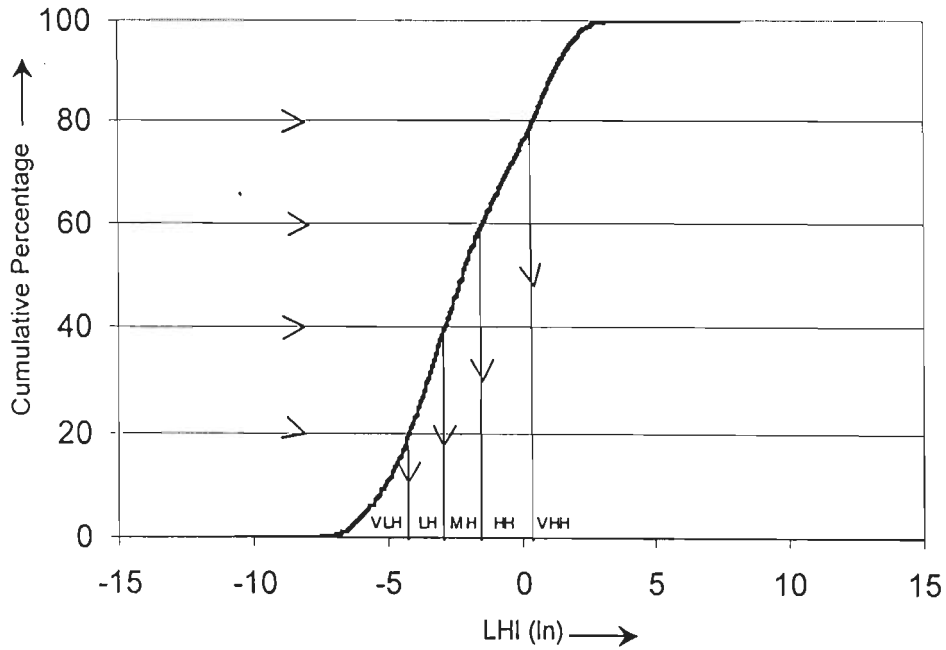
Figure 4.28: Segmentation of LHI values in the InfoVal method.

b) *m-LNHF Method*

The conventional method employed to segment the LHI values for the demarcation of various hazard zones is rather prone to subjectivity. Since, the variations in the weights and the respective central tendencies in the thematic data layers are often large and random; in this particular study, a new probabilistic approach for such segmentation has been employed. On the basis of the normalised frequency distribution of LHI values, the probability of landslide occurrence attached to each LHI value (varying in this area between 2.0319 and 19.6808) has been generated and is depicted in Figure 4.29.

The spikes in the Figure 4.29 are due to the presence of random errors in the data. In an effort to remove this randomness, the data have been sub-grouped into small and equal class-intervals and a trial and error method is employed to obtain the best-fit curve (Fig. 4.30) to this data. The curve is unimodal, negatively skewed and distinctly binomial.
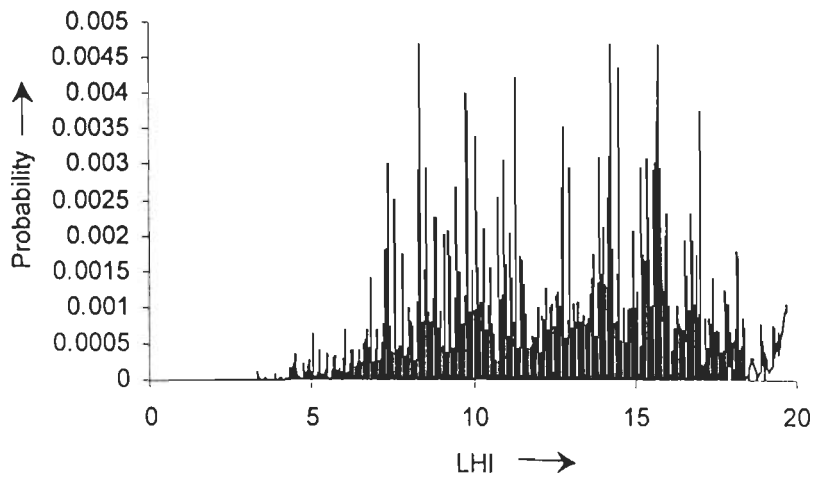
Figure 4.29: Probability distribution curve of LHI values
from the m-LNHF method.
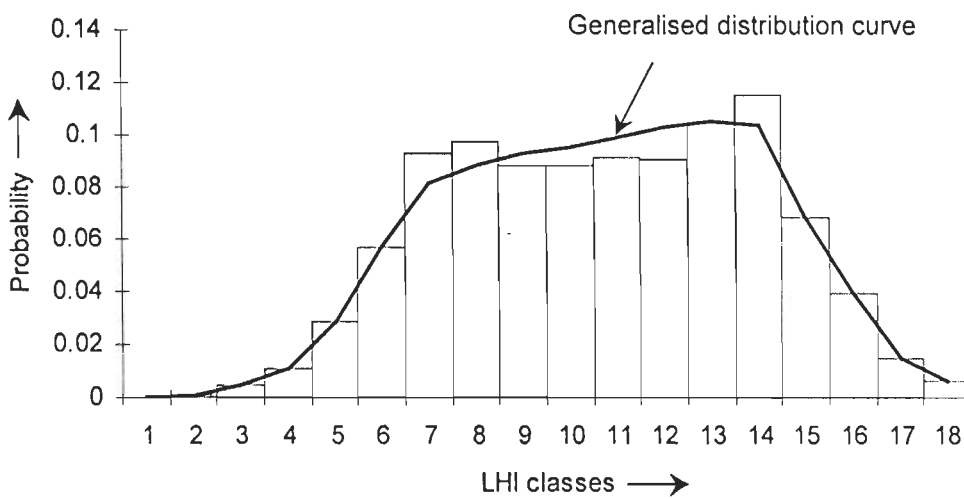
Figure 4.30: Curve fitting in the m-LNHF method.

The mean (μ_p) and standard error (σ_p) predicted from this best fit probability

distribution curve are given in Table 4.9. It is noteworthy that:

a) the predicted mean is equal to the observed mean, and

b) the predicted standard error is significantly less than the observed standard error.

This implies that the best-fit curve derived from the proposed statistical procedure

is reliable and accurate.

**Table 4.9: Statistical calculations for LHI-value
segmentation in m-LNHF method**

Observed Mean (μ_o) = 12.26

Observed Standard Error (σ_o) = 3.22

Number of classes made on probability distribution curve = 18
According to Binomial Distribution:

    Predicted Mean (μ_p) = 12.26

    Predicted Standard Error (σ_p) = 1.98

The LHI values have been segmented into five distinct classes with boundaries fixed at ($\mu_p - 1.5m\sigma_p$), ($\mu_p - 0.5m\sigma_p$), ($\mu_p + 0.5m\sigma_p$) and ($\mu_p + 1.5m\sigma_p$) where m is a positive, non-zero value. The following considerations have been taken into account to select the appropriate value of m in this study.

Based on a given LHZ map, the cumulative percentage of landslide occurrences in various hazard zones ordered from very high to very low can be plotted against the cumulative percentage of the area of the hazard zones. This curve, referred to as the success rate curve in the literature (Chung and Fabbri, 1999; Lu and An, 1999; Chi *et al.*, 2002; Lee *et al.*, 2002b), may be used to decide the suitability of a particular LHZ map.

For different m values, several LHZ maps and the corresponding success rate curves have been prepared. It has been found that at least for the first 10% of the area (*i.e.*, in the very high hazard zone), the success rate corresponding to $m = 1.4$ is the highest. In Figure 4.31, three success rate curves corresponding to $m = 1.3$, 1.4 and 2.0 are shown. The success rate is evaluated on the basis of the fact that more number of landslides per unit area should lie in the very high LHZ as compared to that in a very low LHZ. It can be seen from Figure 4.31 that for 10% of the area, the curves corresponding to $m = 1.3$, 1.4 and 2.0 show the landslide occurrence of 45.5%, 46% and 32% respectively. For 20% of the area,

the corresponding landslide occurrences for these curves are 63%, 62% and 54% respectively. Based on this analysis, the LHZ map corresponding to $m = 1.35 \pm 0.05$ appears to be most appropriate for this study area.
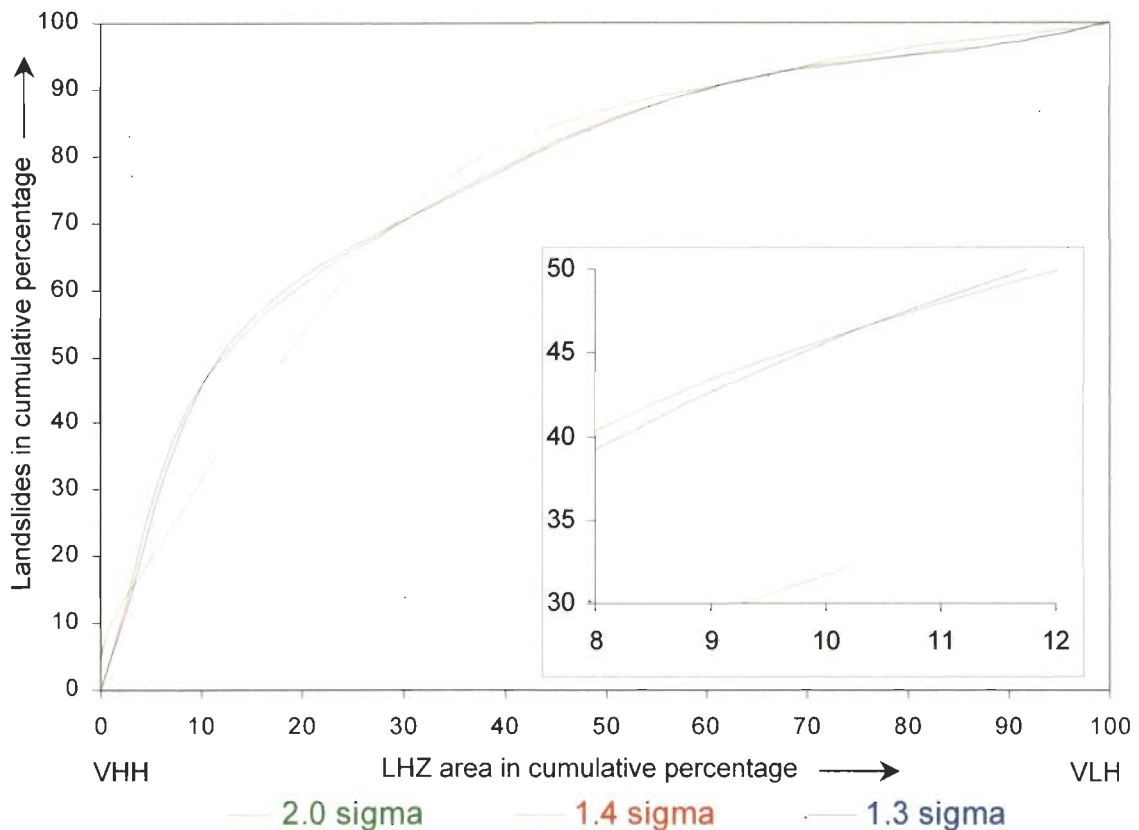
Figure 4.31: Success rate curves to select the best LHZ map in the m-LNHF method.

4.10.4 Comparison of LHZ Maps Generated by InfoVal and m-LNHF Methods

Figure 4.32 and Figure 4.33 show the LHZ maps generated using the InfoVal method and the m-LNHF method respectively. The comparison of two maps on the basis of the methodology of data processing, visual appearance of LHZ maps and their applicability in planning and developmental activities, leads to following three major observations (Table 4.10):

1. The LHZ map is a result of a combination of various factors responsible for landslide hazard, where each factor has relative importance to the probable landslide incidence. The structural discontinuities, such as major faults, thrusts and lineaments are considered to have the most dominant impact on landslide activity and along these zones landslides preferentially occur (Fig. 4.25). In view of this, the buffer zones of structural discontinuities ought to leave traces, called here as "ghost-effect", on the LHZ map. These "ghost-effects" are clearly seen in m-LNHF method derived LHZ map (Fig. 4.33). On the other hand, the LHZ map generated using InfoVal method does not show any "ghost effect" and appears to be relatively homogeneous throughout the area, thereby not showing any influence of major structural zones and discontinuities on landslide hazard zonation (Fig. 4.32).

2. In the InfoVal method, there is a lack of objectivity in dividing the LHI values for generating LHZ map, as the method involves subdividing the cumulative frequency into five near-equal parts. This implies that each of the hazard zones possesses equal areas (≈20%), which is generally not the case in a geologically heterogeneous rugged terrain, such as the Himalayas. The proposed m-LNHF method based on a statistical criterion results in more logical boundaries of various hazard zones with different percentages of areas (*e.g.*, VH (11%), H (28%), M (26%), L (26%), VL (10%)).

3. The major application of LHZ maps is in the field of disaster management and planning developmental activities, which demands that the areas of VH hazard be properly demarcated. The VH hazard zone in InfoVal method is 20%, which is quite large, whereas in the m-LNHF based LHZ map the VH hazard zone is only 11 % of the total area. Therefore, the output information is more focused and realistic, and thus can be of greater practical utility in landslide disaster management and planning developmental activities.
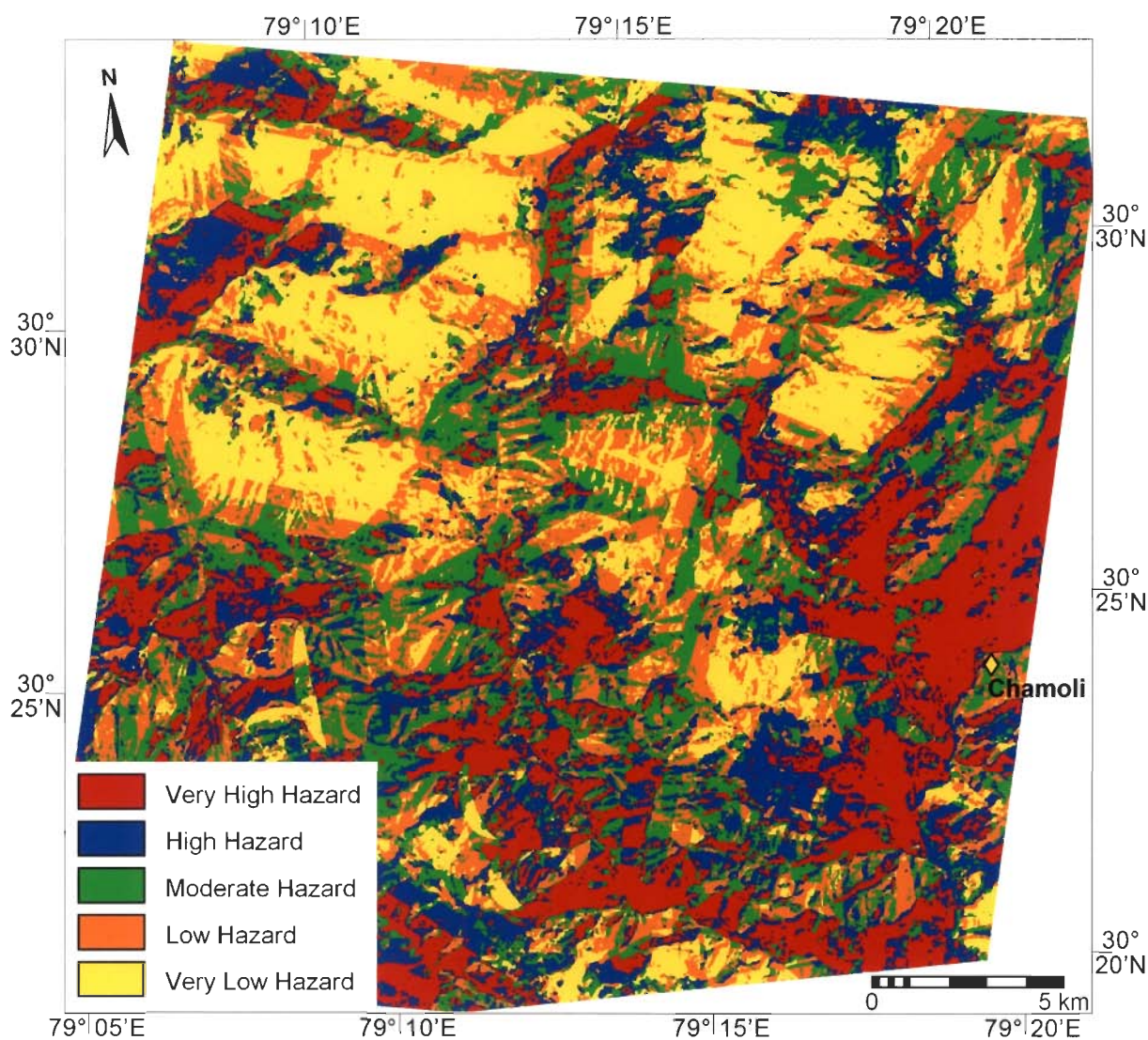
**Figure 4.32: Landslide Hazard Zonation map prepared using
the Information Value (InfoVal) method.**
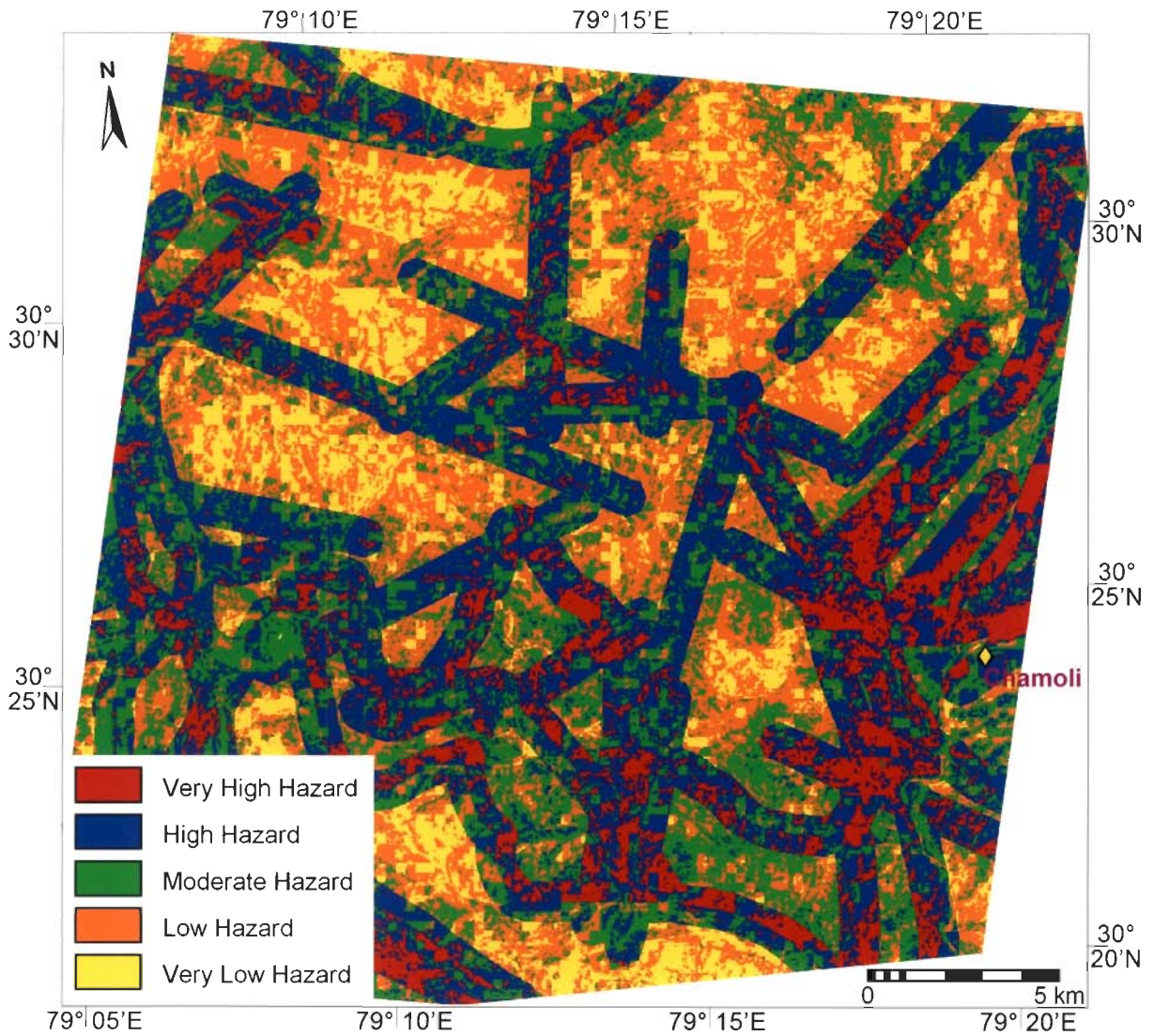
Figure 4.33: Landslide Hazard Zonation map prepared using the Modified-Landslide Nominal Hazard Factor (m-LNHF) method.

Table 4.10: Comparison of the LHZ-maps prepared by the InfoVal and m-LNHF method

InfoVal method	m-LNHF method
1) The LHZ map is relatively homogeneous. The impact of structural discontinuities (which has a very important role in landslide activity) is not obvious.	1) On this LHZ map the bearing of structural discontinuity (faults, thrusts, and lineaments) is quite obvious. There is a "ghost-effect" corresponding to the structural discontinuities, which seems logical in landslide hazard zonation.
2) Each of the VH, H, M, L, VL zones is nearly 20% of the area (with flexibility of some adjustment) (van Westen, 1997).	2) The areas of VH (11%), H (28%), M (25%), L (26%), VL (10%) hazard zones are statistically derived based on probability distribution.
3) The VH hazard zone comprises nearly 20% of the area.	3) The VH hazard zones comprise 11% of the area. As this area is much smaller, the information is more focused which can be of greater practical utility in landslide disaster management.

In the foregoing paragraphs, a detailed description of thematic data layer preparation has been presented. These thematic data layers singly or in combination, pertain to the factors that influence the cost of route development and maintenance. In the next chapters, data integration for thematic cost mapping, which incorporates GIS-based aggregation, is discussed.

Chapter 5

Data Integration for
Thematic Cost Mapping

5.1 Introduction

The conventional route planning is solely based on topographical considerations – gradient and curvature, and the usual practice involves manual marking of the segments of permissible gradients for route alignment on large-scale topographical maps. Such an approach may not be feasible when a variety of other factors, such as geology, landuse/landcover and location of landslide-prone areas are considered. Therefore, to develop an integrated geoenvironmental approach, GIS techniques have the advantages whereby various geological, landuse/landcover and landslide hazard factors may be efficiently integrated for optimum route planning.

In the previous chapter, generation of various thematic data layers proposed to be considered for route planning have been described in detail. These thematic data layers are: landslide distribution, landslide hazard zonation, drainage order, landuse/landcover and lithology, which have a direct bearing on planning a road in hilly area. This chapter deals with integration of above data layers in GIS (Fig. 5.1).

5.2 Thematic Cost – Concept and Computation

The data layers, landslide distribution (size), landslide hazard zonation, drainage order, landuse/landcover and lithology are of a diverse type consisting of measurements at different scales, such as categorical, ordinal and ratio type data (for details see, *e.g.*, Aronoff, 1989). In order to integrate this variety of data, an ordinal weighting-rating is used, and to arrive at a cumulative data layer, the concept of thematic cost is developed here. The thematic cost map is a raster map, where the value at each pixel gives the estimated relative cost of moving through the pixel. The cost is cumulative, having inputs from landslide map, LHZ map, drainage, landuse/landcover and lithology. A higher cost value at a pixel may be related to higher cost of bridge construction, higher cost of road maintenance due to landslides, higher cost of land acquisition, higher cost of blasting, *etc.* Therefore, weighting-rating system in the range of 0 to 9 is used here, with zero signifying minimum cost and 9 implying the highest cost.

An ordinal number (from 0 to 9) is given to each thematic data layer in terms of its relative importance. For example, landslide distribution thematic data layer is assigned the highest weight of 9, followed by LHZ (weight = 8), drainage order (weight = 7), landuse/landcover (weight = 6) and lithology (weight = 4). Similarly, each class in the thematic layer has been given an ordinal rating in the range of 0 to 9 (Table 5.1). The weighting-rating values are based on a comparative study of various thematic data layers and discussions with experts working in the area of transportation engineering. The following describes the logic in brief for weighting-rating values adopted here.

5.2.1 Landslide Distribution

It is considered here that landslide occurrence is the most important parameter in road planning in a mountainous terrain, as landslides lead to recurring problems, such as blockades, disruptions, civic miseries, *etc.*, and greatly increase the cost of transport maintenance. Therefore, the highest weight of 9 has been given to landslide occurrence.
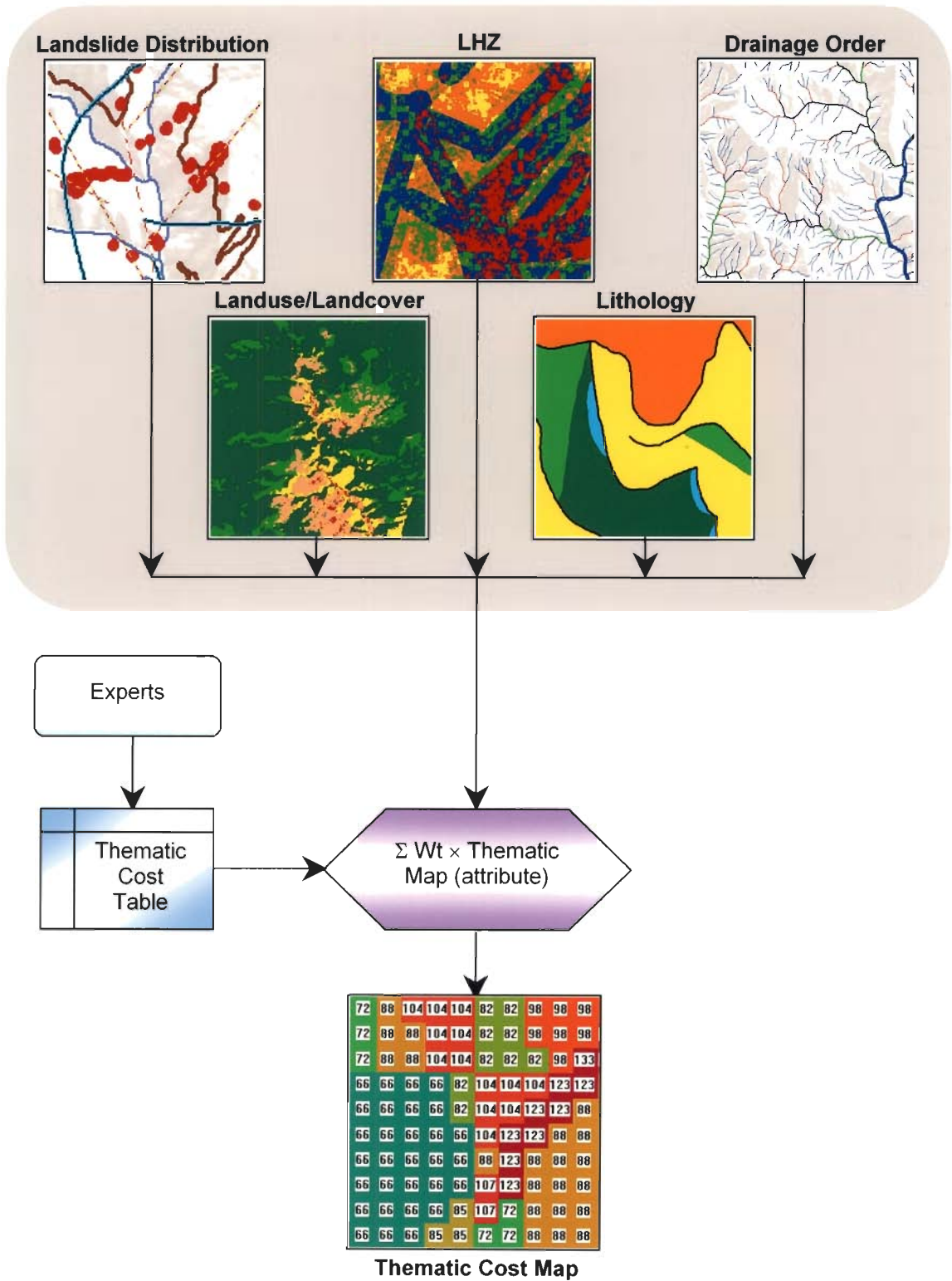
Fig. 5.1: Schematic diagram for generating thematic cost map used in route planning.

There is no doubt that it would be ideal to avoid landslide areas altogether during road planning. However, if the landslides are small in size, it may be possible to apply slope stabilisation measures. Keeping this aspect in view, rating values have been assigned according to the size of the landslides in the region. The landslide distribution map prepared from remote sensing image interpretation (see Section 4.9 of Chapter 4) has been re-classified into six classes, depending upon the size of landslides. Landslides covering more than 400 pixels (1 pixel = 36 m^2) have been assigned infinite value (a very high value for use in algebraic operations in GIS) so that no road can pass through this area. Further, a buffer (50 m) around landslide area has been provided to keep a safe distance from the landslides. If there is no landslide, the pixels have been assigned a zero value, in order to make the pixels favourable for road alignment. The other four landslide classes have been rated (successively 9, 8, 7 and 5) in decreasing order of size.

5.2.2 Landslide Hazard Zonation

The LHZ map is considered here as the second-most important parameter (weight = 8) influencing the thematic cost of road development and maintenance. Each pixel in the landslide hazard zonation map prepared earlier (see Section 4.10 of Chapter 4) carries a value that represents the potential of landslide hazard. The landslide hazard zones have been given rating in an increasing order of the hazard (Table 5.1).

5.2.3 Drainage Order

The drainage order map has been used here to consider the cost of a possible bridge construction. Generally, the width of the river channel increases with increasing order of drainage, and therefore, the cost of bridge construction increases correspondingly. The drainage order map based on Strahler's scheme (see Section 4.7.2 of Chapter 4) has been used here as an input. The first- and second-order drainages have been assigned very low ratings, as these are generally quite narrow, and in most cases the water could be drained using underground pipes, or by providing small culverts. For higher-order drainages, there

may be requirements of bridge construction, the construction cost increasing with the width of the channel. Therefore, higher ratings have been assigned to higher-order streams. The pixels without any channel have been assigned a zero value.

Table 5.1: Weighting – rating scheme of thematic data layer integration

Thematic map	Weight	Rating
1. Landslide (pixels)	9	
>400		∞
>300		9
>200		8
>100		7
<100		5
No Landslide		0
2. Landslide Hazard Zones	8	
Very High		9
High		7
Medium		5
Low		3
Very Low		1
3. Drainage Order	7	
6th Order		9
5th Order		8
4th Order		7
3rd Order		5
2nd Order		2
1st Order		1
No River		0
4. Landuse/Landcover	6	
Snow		9
Landslide Debris		9
River Sediments		7
Settlements (through)		6
Agriculture		4
Fallow Land		4
Barren Land		3
Dense Forest		3
Sparse Vegetation		1
Water Body (Deep)		1
5. Lithology	4	
Granite		6
Granite-Granodiorite-Gneiss		6
Schist and Gneiss		5
Quartzite with Slates		4
Limestone and Greywacke		3

5.2.4 Landuse/Landcover

Landuse/landcover data is required to estimate the cost of land acquisition during route planning. The landuse/landcover map generated using multi-source classification technique (see Section 4.8 of Chapter 4) has been used as an input for the purpose.

In the Himalayas, the snow-covered areas occur at very high elevations and it is difficult to construct and maintain roads at these heights. Further, the road construction over landslide debris could accentuate the problem of slope instability. Hence, snow and landslide debris covered areas have been assigned the highest rating (= 9). The areas covered with river sediments are also not suitable for road construction as these are susceptible to flood inundation and such areas have also been assigned a higher rating(= 7).

Sometimes, a route must pass through a settlement, which means that a higher compensation cost has to be provided in such cases. Hence, a relatively high rating (= 6) is assigned to settlement areas. The agriculture and fallow lands are relatively favourable for road construction in the hills, as this kind of landuse occurs on terraces, which are regions of low relief. The construction cost may also reduce over such areas due to low relief and lower cost of cut-and-fill work; on the other hand, the compensation cost to farmers is also involved. Considering these factors, a rating value of 4 is assigned to fallow and agricultural areas.

Barren areas are relatively favourable for route planning due to the fact that such areas are under government control and, therefore, no compensation cost is involved, and environmental problems like cutting of trees, *etc.*, do not arise. Hence, a relatively lower rating (= 3) has been given to these areas.

Forest areas are also government lands and a road through a forest is also likely to promote tourism. However, many trees may have to be cut-down during road construction through the forest. Keeping in view the above aspects, a rating of 3 has been assigned to forest areas.

Sparsely vegetated areas seem to be the most suitable for road construction. These are government land, relatively stable, and may have minimal environmental problems. Hence, the lowest rating (= 1) has been given to the sparsely vegetated areas.

In the landuse/landcover thematic map, only sufficiently wide water bodies are classed, such as drainage higher than third order. As the cost of bridge construction has already been taken into consideration separately, water bodies have been given the lowest rating (= 1) to avoid over-estimation on this account.

5.2.5 Lithology

Lithology has been considered mainly from the point of view of costs of blasting, excavation, cut-and-fill works, *etc.* Granites and gneisses are compact and hard and hence, a higher rating (= 6) has been given to granitic rocks. Successively lower cost ratings are given to schists and gneisses (= 5), quartzites with slates (= 4), and limestone and greywacke (= 3).

5.3 Thematic Cost Map Generation

For each thematic data layer, there is a weight factor. The classes within each thematic data layer carry rating, which is used as 'attribute data'. The thematic cost map is computed as:

$$\textit{Thematic Cost} = \sum \textit{Weight} \times \textit{Thematic data layer (attribute)} \tag{5.1}$$

Hence, in this case,

$$\textit{Thematic Cost} = [\ 9 \times LD + 8 \times LHZ + 7 \times DO + 6 \times LULC + 4 \times LI\ ] \tag{5.2}$$

where, *LD* is landslide distribution map, *LHZ* is landslide hazard zonation map, *DO* is drainage order map, *LULC* is landuse/landcover map and *LI* is lithology map. Figure 5.2 represents the thematic cost map generated for the study area.
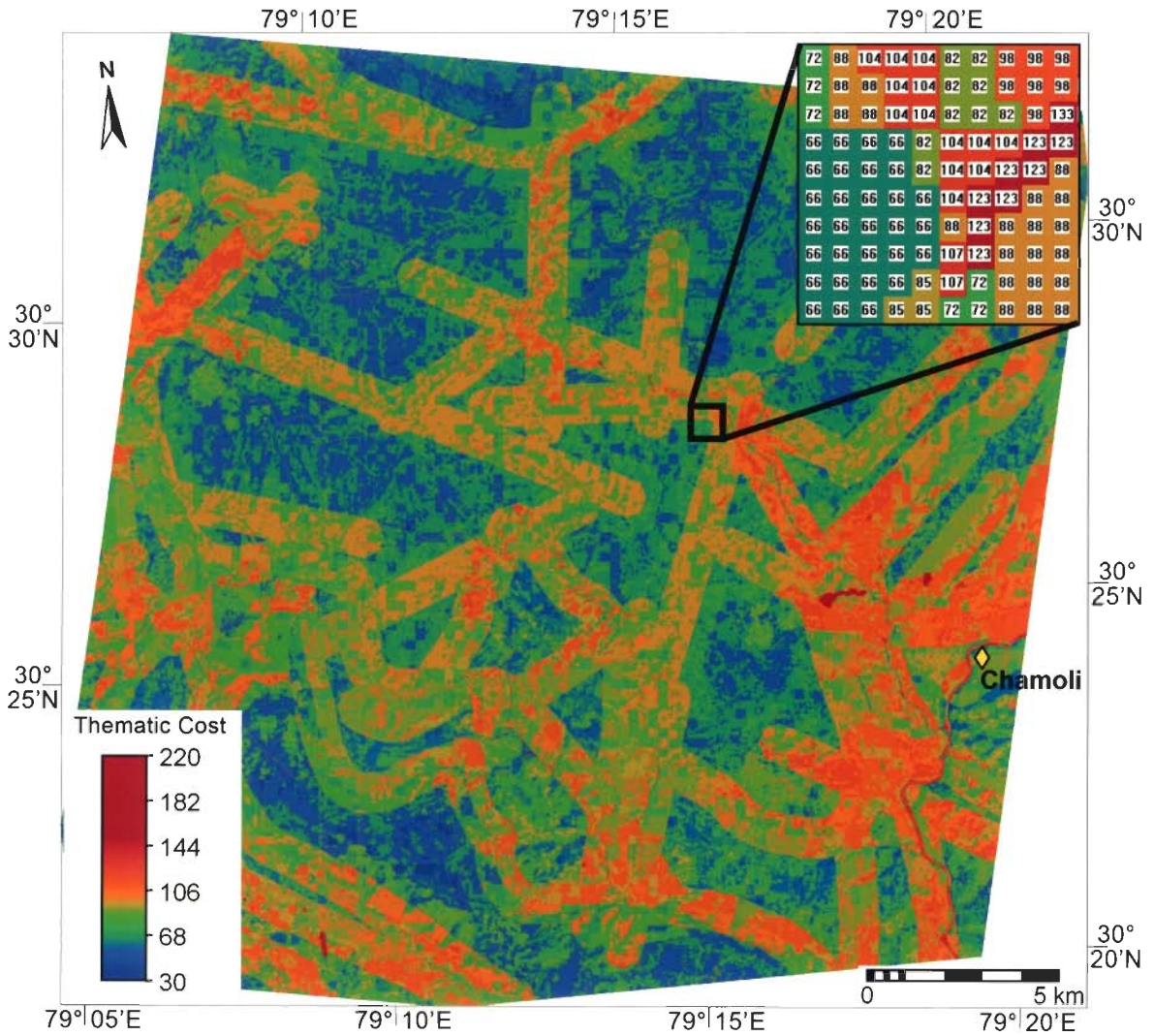
Figure 5.2: Thematic cost map. (Note: In this map, each pixel value indicates relative cost to move through the pixel, higher the value, higher is the cost for route development and maintenance.)

The thematic cost values have been found to vary between 30 and 220. Lower values indicate favourable pixel sites for route planning and higher values indicate relatively unfavourable or less favourable sites. Landslides bigger than 400 pixels have been assigned an abnormally high value, as these pixels are to be completely excluded.

Thus, the methodology described above shows that it is now possible to consider various parameters including landslide distribution, LHZ, landuse/landcover, drainage and lithology collectively for route planning. For route alignment, particularly in a hilly region, topography plays a very important role. The next chapter deals with the methodology incorporating thematic cost factor, distance factor and gradient factor for route planning along with least-cost route selection.

Chapter 6

Route Planning – Methodology and Discussion

6.1 Introduction

The conventional route planning practice for hilly terrains and its limitations have been mentioned in Chapter 1. The practice is based solely on topographic factors such that alternative routes are traced out manually on a contour map. The method is manual and cumbersome. Further, in this method, it is difficult to consider various other important and related aspects in route planning, such as geology, landuse/landcover, slope stability, landslide hazard, *etc.*, in an integrated manner. Remote sensing - GIS techniques, by virtue of their numerous advantages, appear to be very well suited to tackle this problem.

In this chapter, first a review of the published GIS-based route planning methodology is given. This is followed by a detailed presentation of the methodology adopted in this research along with selected examples. This is followed by a discussion and suggestions for future work.

6.2 Route Planning Using GIS – A Review

During the last decade, some attempts have been made to automate the route planning process using GIS technology. A review of a number of papers suggests that the methodologies available for the GIS-based route planning are still at an exploratory stage. Moreover, due to the complexity of procedures involved in route planning, the methods developed have not really been tested in very high altitude rugged terrains, such as the Himalayas. A brief review of the published research in this field is given below.

There are three major aspects of route planning using GIS, which have also been the focus of this research:

a) To generate a thematic cost map which considers relevant parameters for road development and maintenance

b) To consider neighbourhood selection in a raster or grid form

c) To find a least-cost path from the cumulative cost map from a source pixel to a destination pixel

Lee and Stucky (1998) applied viewshed analysis for determining least-cost paths, which can be utilised for civil engineering, military and environmental planning activities, *etc.* They formulated four different types of viewpaths from a digital elevation model: hidden path, scenic path, strategic path and withdrawn path. The visibility cost for various viewpaths, surface distance and gradient, have been used together for calculating the cost of movement from the source to its nearest eight neighbouring pixels. Finally, the least-cost path between source and destination has been found using an iterative searching procedure formulated by Douglas (1994). This procedure uses a spread function that searches for neighbour-pixel to any source pixel that has the lowest value. The procedure continues to search iteratively for the next lowest neighbour until every pixel has been assigned a cumulative cost value from source pixel. Finally, a back-linking is used to find the least-cost path for a specific destination pixel. Lee and Stucky (*op. cit.*) tested their

algorithm for hiking and pipeline scenarios using a 30 m × 30 m USGS DEM and found

out paths with various viewshed patterns listed above. The maximum allowed gradient for

path selection was considered as 50° in their study, which is too high for a realistic road

alignment. Moreover, the study considered only slope, distance and viewshed factors; no

other thematic parameters (land cost, geology, *etc.*) were taken into account.

In a raster GIS, the flexibility in the selection of neighbourhood pattern is rather

limited as compared to a vector GIS. However, the thematic cost calculation is easy to

conceive and manipulate in raster GIS. Moreover, since remote sensing data, which can act

as a link and base to all the datasets, is in raster format, raster GIS is commonly used for

this purpose. In a 3 × 3 pixel matrix, a maximum of 8 neighbourhood directions, and in a 5

× 5 pixel matrix, 16 neighbourhood directions are possible. The use of these

neighbourhoods for cost calculation may, however, result into a rather zigzag and

unrealistic path. To get over this problem to a certain extent, Xu and Lathrop (1994) used

an anisotropic (elliptical) spread function in GRASS (a raster GIS) for neighbourhood path

selection, which could incorporate any number of non-adjacent pixels to make the path

smoother. They showed the implementation of their procedure on an application on

wildfire spread. The limitation of applicability of this method for route planning in a

rugged hilly terrain is the wide variation of gradient and curvature over short distances.

For least-cost route planning, "G-ROUTE" package developed by ITC (Ellis, 1990)

has been used by some workers. The program considers various road construction

parameters, namely distance, roadfill cost, drainage crossing cost, arable land possession

cost and gradient. These parameters are integrated by adding various cost maps and finally

Dijkstra's algorithm is implemented to find the least-cost path. The package uses the

simplest form of neighbouring pattern in 3 × 3 pixel window. An application of "G-

ROUTE" package can be found in Akinyede (1990) for highway route planning. In this

work, major emphasis has been placed on modelling the pavement construction cost,

earthwork cost, drainage crossing cost and maintenance cost. These cost maps have been accumulated and G-ROUTES package has been used to find the least-cost path.

For a real-world problem of pipeline routing in the Caspian sea region, Feldman *et al.* (1995) utilised remote sensing and GIS tool to model costs associated with terrain conditions, geology, landuse, *etc.* The costs have been computed from the experience of various earlier pipeline projects. The Spatial Analyst module of ARC/INFO GIS software has been used to extract the least-cost pipeline route from a cumulative cost surface. It has been shown that the least-cost path derived in this study is 21% longer than the straight-line path between the source and destination, but it leads to a reduction in pipeline construction cost by 14%.

Collischonn and Pilar (2000) presented an algorithm based on dynamic programming to find direction-dependent least-cost path for roads and canals. The algorithm considers costs associated with eight neighbours of a source pixel (3 × 3 pixel window) based on gradient and distance. The main emphasis was given to gradient constraints for the purpose of canal alignment. The algorithm has been tested on a few hypothetical terrains, which indicates that the paths follow the contours (*i.e.,* longer distance) rather than connecting the source and destination by a straight-line path.

In another study, Musa and Mohamed (2002) presented a best-path model for forest road network, in which the road alignment was generated by manual method, field survey and computer-GIS generated method. A comparative study of the routes generated by various methods and the land category covered by each route showed that the computer-GIS generated paths were better and of immense help to the planners.

Yu *et al.* (2003) presented a comprehensive review of the problem on route alignment in GIS and extended the work based on least-cost algorithm for roadways planning. Various possibilities of network neighbours (in 5 × 5 pixel window) have been presented, which are named as per the moves in the game of chess, *viz.,* Rook's, Queen's

and Knight's patterns. A cost function has been derived to cumulate gradient cost and landuse/landcover cost with distance. Finally, Dijkstra's algorithm has been used to find the least-cost path between the source and the destination. Further, a new technique, called Smart Terrain (ST) algorithm, has also been adopted to find the bridges and tunnels using contour information. The methodology has been tested using a 30 m × 30 m USGS DEM and landcover information derived from satellite images. The result shows that the ST algorithm produces more realistic least-cost route by using spatial distance, anisotropic cumulated cost and location of bridges and tunnels. They have also shown improvement in the character of the path after incorporating Knight's pattern. This methodology still produces a zig-zag path and a further improvement has been made in the present work by using a larger window size.

In a more recent study on finding least-cost footpaths in a mountain terrain, Rees (2004) has used an optimised metabolic cost for human locomotion along with a distance function. Dijkstra's algorithm has been used to find the least-cost path between selected locations and compared with the existing footpaths.

6.3 Methodology Adopted

As mentioned earlier, the route planning procedure in GIS can broadly be divided into three basic steps. These are:

a) *Selection of Connected Neighbours:* This step includes the neighbourhood relationship concept in GIS. In a raster or grid based model analysis, each pixel can be represented as a network node. This step involves finding various possibilities of the connected nodes.

b) *Calculation of Neighbourhood Movement Cost (NM-cost):* Once connected neighbours are selected, the next step is to calculate the cost of moving to the connected neighbour from a source. This is termed here as NM-cost and is

computed from three input data: cost related to neighbour-distance, cost related to gradient and the thematic cost.

c) *Selection of Least-Cost Route:* As the route alignment will cover a certain distance, it will pass through pixels and their successive NM-cost values will accumulate to give the total cost. This final step involves finding the least-cost route for which a dedicated computer program has been written in C++.

In the following section, details of all the three basic steps are given. The method helps select an optimal route that is supposed to be the best, as it tries to avoid major landslides and passes through low thematic cost zones, reducing overall road development and maintenance cost. Finally, a few examples have been presented with various terrain and landslide hazard conditions.

6.4 Selection of Connected Neighbours

In GIS, the term neighbourhood is defined as the location within proximity of some starting point or grid cell. Neighbourhood analysis is important in route planning to find various possibilities of movement from a source pixel to its immediate neighbour, so that the cost associated with that connection might be calculated. The neighbourhoods could be of two types: direct neighbour and indirect neighbour.

Direct neighbours are those, which are connected directly (bodily) to the source pixel. In a 3 × 3 pixel window, there are eight direct neighbours, in horizontal, vertical and diagonal connections (Fig. 6.1). An analogy can be established between these connections and the moves in the game of chess (*www.uschess.org*). The vertical and horizontal movements are similar to the moves of Rook and the diagonal movements are similar to those of Bishop. In other words, all the direct neighbours are represented as Queen's pattern of movement (Yu *et al.*, 2003; Xu and Lathrop, 1994). Hence, in such cases the turn angle (angle between an incoming and outgoing paths at a pixel) for the route is restricted to minimum 45° angle.
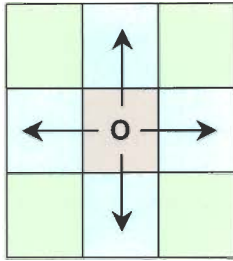
Rook's Pattern
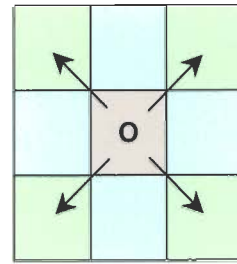
Bishop's Pattern
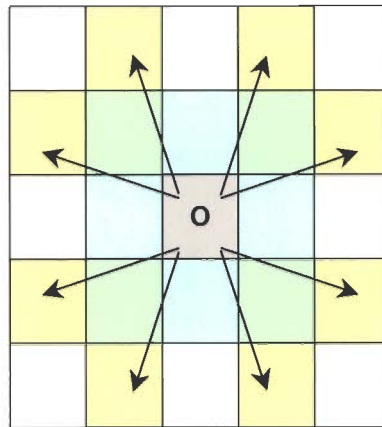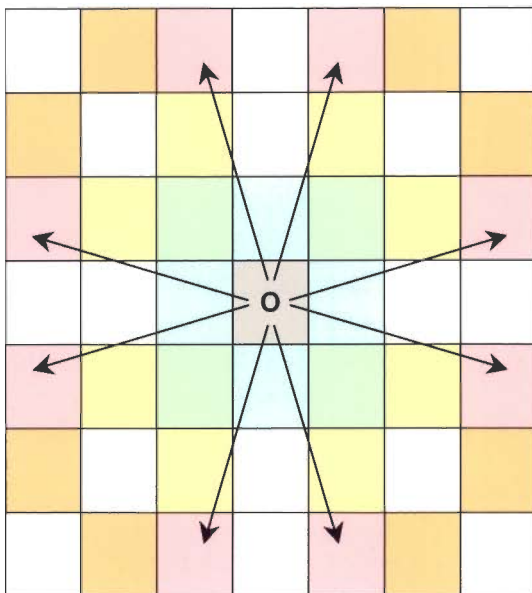
Knight's Pattern
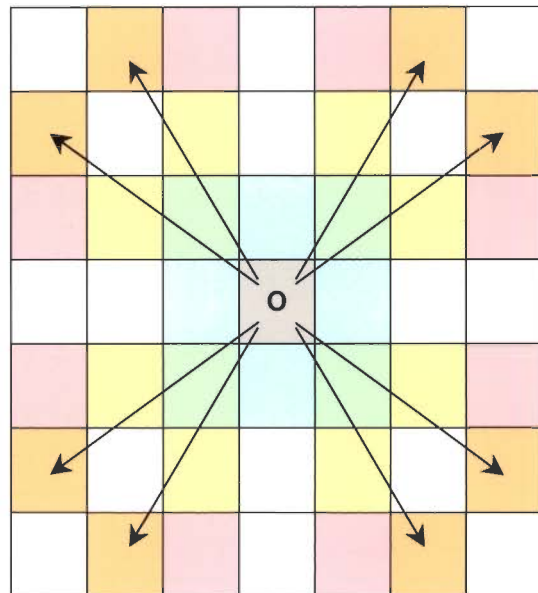
Knight31's Pattern

Knight32's Pattern

**Figure 6.1: Terminology for various neighbourhood patterns.
The neighbourhood patterns of Knight31 and Knight32
have been conceived in this research.**

The turn angle interval may be reduced by considering a larger neighbourhood window. With a 5 × 5 pixel window, eight more indirect neighbourhood connections may be incorporated (Fig. 6.1). The indirect connection means that the pixels are not bodily connected, but a movement through this connection is allowed. These connections can be compared with the move of Knight in the game of chess. The Knight moves two-step straight and one step left or right of the direction of movement, to occupy the new position. Hence, in such cases the turn angle will be further improved to a minimum of 22.5° angle interval. This will make the path smoother avoiding sharp zigzag turns. As the neighbourhood pixel window increases, the minimum turn angle interval is improved further but this will add to the computational cost.

In this study, upto 7 × 7 pixel window sizes have been considered and two new patterns of indirect neighbourhood connections have been conceived. Although, these moves do not exist in the game of chess, these originate from the concept of Knight's movement, and have been named as Knight31 and Knight32 (Fig. 6.1).

Knight31's Pattern:

The Knight31's pattern works in a 7 × 7 pixel window. The movements are such that it moves 3 pixels straight and then one pixel towards left or right.

Knight32's Pattern:

The Knight32's pattern is another new pattern designed for 7 × 7 pixel window. It moves 3 pixels straight and then 2 pixels towards left or right.

The above new patterns would permit smoother turns and gentler gradients in route alignment. To implement the connectivity of possible neighbours in a raster GIS platform, the pixels are represented as nodes. The nodes need to have unique identification numbers and a mathematical relationship is used to find out the neighbourhood with adjacent pixels

(or nodes) (Table 6.1). This process has been adequately programmed in C++ as described in Section 6.7.

Table 6.1: General scheme of node numbering used to represent every pixel of the image under analysis. The mathematical relationships among few neighbours have been shown as example

		Column ($j =$)								
		1	2	3	4	5	6	....	49	50
Row ($i =$)	1	0	1	2	3	4	5	....	48	49
	2	50	51	52	53	54	55	....	98	99
	3	100	101	102	103	104	105	....	148	149
	4	150	151	152	153	154	155	....	198	199
	5	200	201	202	203	204	205	....	248	249
	6	250	251	252	253	254	255	....	298	299
	.	.	.	.	.	.	.		.	.
	49	2400	2401	2402	2403	2404	2405	....	2448	2449
	50	2450	2451	2452	2453	2454	2455	....	2498	2499

Hence,   If area size is N rows × M columns
For i^{th} row and j^{th} column, Node Number = (i – 1) × M + (j – 1)

Some mathematical relations among neighbours:

e.g.,   Node 53 is connected to Node 152 by a Knight's pattern.
              The relation between these two nodes = 152 – 53 = 99 = (2M – 1) where M = 50

Likewise,   Node 205 is connected to Node 152 by a Knight32's pattern.
              The relation between these two nodes = 152 – 205 = – 53 = (– M – 3) where M = 50
                                                      and so on ....

6.5 Neighbourhood Movement Cost (NM-cost)

As mentioned earlier, usually the distance and the gradient are the two major factors that are considered for route alignment. In Chapter 5, the concept of thematic cost map has been introduced, which considers various parameters (*viz.,* landslide distribution, landslide hazard zonation, landuse/landcover, drainage order and lithology) in an integrated manner to provide an estimate of the cost per pixel for road development and maintenance. The thematic cost map is a raster map (see Fig. 5.2), where the value at each pixel gives the estimated relative cost of moving through that pixel. The thematic cost layer does not include costs due to distance and gradient. It is therefore necessary at this stage to consider and incorporate distance and slope factors.

The NM-cost is the cost of moving from the source to the connected neighbour and is based on the costs of neighbour-distance, gradient and the thematic cost. If the topography is perfectly flat, the topographic surface is isotropic, gradient cost will be nil and the NM-cost to move from a source to its connected neighbour is given by:

NM-cost= Distance × Thematic Cost (6.1)

In a real-world problem, the topography is uneven, particularly in a terrain like the Himalayas. The slope of the terrain varies in different directions. Hence, in a real-world situation, the NM-cost must consider this direction-dependency (anisotropy). For an anisotropic surface, the NM-cost may be given as,

NM-cost= Distance × (p × Thematic Cost + q × Gradient Cost) (6.2)

where, *p* and *q* are weights.

6.5.1 Neighbour-Distance

It is the actual distance between successive neighbours in a three-dimensional space. Here simple Euclidean distance is used. In case of raster data, the centre points of

various pixels are used for distance computations. Figure 6.2 schematically describes the method of calculation of distance for any pair of connected pixels in the neighbourhood. In this study, the DEM with 6 m pixel size (see Section 4.3.2 of Chapter 4) has been used for distance calculation.

Assuming a square pixel size for the neighbourhood window (Fig. 6.3), the distance can be calculated for different neighbourhood connections (Yu *et al.*, 2003). For direct horizontal/vertical connection, *i.e.*, Rook's pattern, the neighbour-distance is:

$$ND_{(O, P_i)} = \sqrt{\mu^2 + (H_{P_i} - H_O)^2} \qquad \text{where } i = 1 \text{ to } 4 \tag{6.3}$$

Similarly, for the diagonal direct connection, *i.e.*, Bishop's pattern, the neighbour-distance is:

$$ND_{(O, P_i)} = \sqrt{2\mu^2 + (H_{P_i} - H_O)^2} \qquad \text{where } i = 5 \text{ to } 8 \tag{6.4}$$

For Knight's pattern, which is a kind of indirect connection, the neighbour-distance is:

$$ND_{(O, P_i)} = \sqrt{5\mu^2 + (H_{P_i} - H_O)^2} \qquad \text{where } i = 9 \text{ to } 16 \tag{6.5}$$

Based on above logic, the neighbour-distances for Knight31's and Knight32's patterns, designed in this study, can be formulated as,

Knight31's pattern: $ND_{(O, P_i)} = \sqrt{10\mu^2 + (H_{P_i} - H_O)^2}$ where $i = 17$ to 24 (6.6)

Knight32's pattern: $ND_{(O, P_i)} = \sqrt{13\mu^2 + (H_{P_i} - H_O)^2}$ where $i = 25$ to 32 (6.7)

where, *ND* is the neighbourhood distance between *O* (source) and pixel P_i (connected neighbour); μ is the pixel size and H_O and H_{Pi} are the elevation of source and connected neighbour pixels. Pixel numbers corresponding to *i* are shown in Figure 6.3.

$H_R > H_Q > H_P$
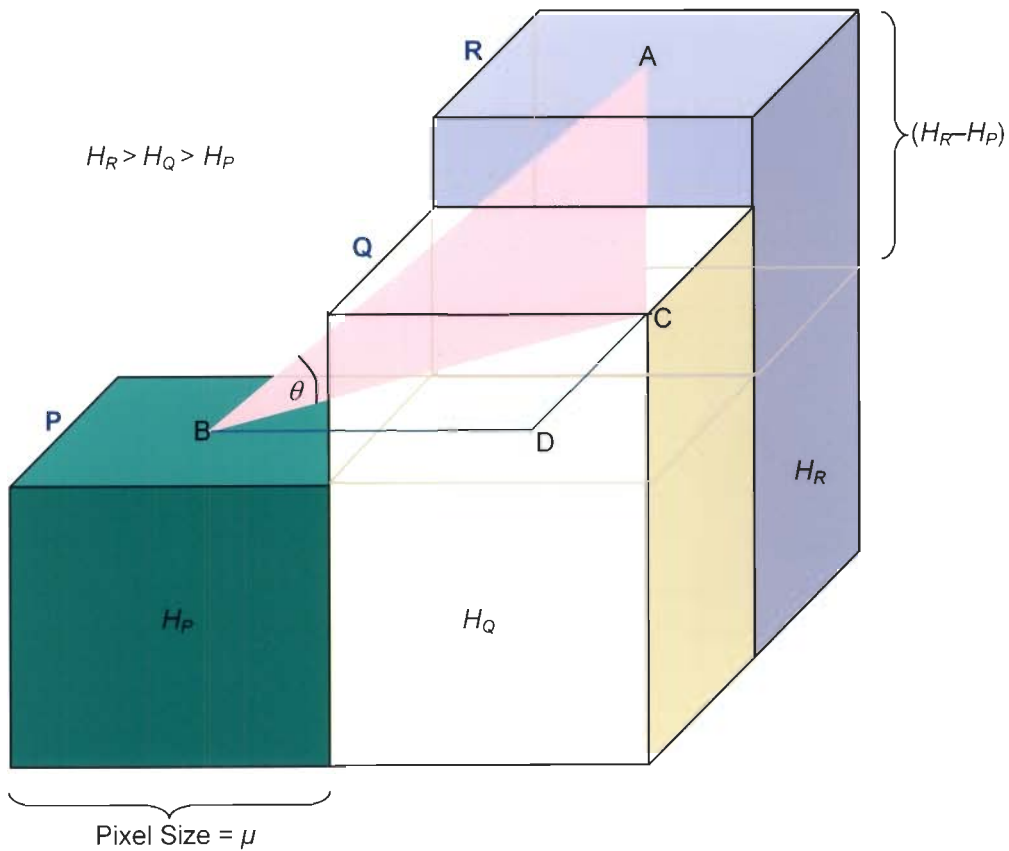
Distance between
pixel P and pixel R $= AB$
                           $= (BC^2 + AC^2)^{1/2}$
                           $= ((BD^2 + CD^2) + AC^2)^{1/2}$
                           $= ((\mu^2 + \mu^2) + AC^2)^{1/2}$
                           $= (2\mu^2 + (H_R{-}H_P)^2)^{1/2}$

Gradient θ $= \tan^{-1} (AC\ /\ BC)$
                           $= \tan^{-1} ((H_R{-}H_P)\ /\ \mu\sqrt{2})$

Figure 6.2: The concept for calculating distance and gradient between two pixel centres in 3-D. H_R, H_Q and H_P denote the elevation of pixels P, Q and R respectively. μ is the pixel size. Point A, B, C and D denote the pixel centres.

	32	23		24	25	
31	33	15	34	16	35	26
22	14	8	1	5	9	17
	40	4	O	2	36	
21	13	7	3	6	10	18
30	39	12	38	11	37	27
	29	20		19	28	

Possible movement from source O to pixel number

Rook's Pattern:	1,2,3,4
Bishop's Pattern:	5,6,7,8
Knight's Pattern:	9,10,11,12,13,14,15,16
Knight31's Pattern:	17,18,19,20,21,22,23,24
Knight32's Pattern:	25,26,27,28,29,30,31,32

Figure 6.3: Various possible neighbourhood patterns in a 7 × 7 pixel window.

6.5.2 Gradient Cost

Gradient or slope is also a key parameter to be considered in route planning in a terrain, such as the Himalayas. The gradient can be defined as the rate of rise or fall along the length of the road with respect to the horizontal (Khanna and Justo, 1987). It is usually expressed as a ratio, *e.g.,* "1 in X" or "1 vertical unit to X horizontal units". For hill roads, it has been categorised into three groups by Indian Roads Congress (IRC, 2001):

a) *Ruling gradient:* The gradient that in normal course should not be exceeded in any part of the road.

b) *Limiting gradient:* It is steeper than the ruling gradient and may be used in restricted lengths where keeping within the ruling gradient is not feasible.

c) *Exceptional gradient:* It is a gradient steeper than the limiting gradient, which may be used in short stretches only in extraordinary situations.

Considering the various requirements for smooth movement of vehicles in a hilly terrain, the IRC has recommended maximum values of gradients for different terrain conditions and are as given in Table 6.2.

Table 6.2: IRC (2001) recommendations on gradients for hill road design

Classification of gradient	Hilly terrain having elevation more than 3000 m above mean sea level	Hilly terrain upto 3000 m height above mean sea level
a) Ruling gradient	2.86° (1 in 20.0)	3.43° (1 in 16.7)
b) Limiting gradient	3.43° (1 in 16.7)	4.00° (1 in 14.3)
c) Exceptional gradient	4.00° (1 in 14.3)	4.57° (1 in 12.5)

The scheme of gradient calculation between two connected neighbours is schematically shown in Figure 6.2. Note that this gradient angle is direction dependent. A vehicle may move to its connected neighbour according to the permissible gradient. To consider this aspect in the present analysis, the gradient angle has been classified into 9 classes and each class has been assigned a relative weight in the scale of 0 to 9. A higher weight implies higher cost arising due to higher gradient. In this study, due to the ruggedness and high altitude terrain conditions, the upper limit of exceptional gradient has been assumed as 12° (which is relatively higher than the IRC recommendation). A gradient greater than 12° has been assigned an infinite cost to eliminate it from the route selection process. The slope classes and corresponding weights have been listed in Table 6.3.

Table 6.3: Nominal cost values assigned to various gradient classes

Gradient classes (in degrees)	Cost
0 – 1	1
1 – 2	2
2 – 3	3
3 – 4	4
4 – 5	5
5 – 7	7
7 – 9	8
9 – 12	9
> 12	∞

6.5.3 Thematic Cost

As mentioned earlier, the value at each pixel in the thematic cost map gives the estimated relative cost per unit distance of moving through that pixel. While considering movement from a source pixel to the connected neighbour, average thematic costs instead of a single pixel cost have been adopted, as any single pixel value will be unrepresentative. In 3 × 3 pixel window, the average thematic cost is a simple average of the two connected pixels. In case of indirect connections (5 × 5 and 7 × 7 pixel window), to compute the average costs, the centre points of the connected neighbours have been joined by an imaginary straight line and all the pixels falling on this line have been used to compute the representative thematic cost for the neighbourhood connection in question. For example, in Figure 6.3 given earlier, thematic cost for a connection between 'O' and '25' has been calculated as an average of costs at pixel numbers 'O', '1', '5', '16', '35' and '25'.

6.5.4 Calculation of NM-cost in Various Neighbourhood Patterns

The NM-cost for various neighbourhood patterns can be formulated for an anisotropic terrain as (after Yu *et al.*, 2003):

a) Rook's Pattern:

In a 3 × 3 pixel window, the vertical and horizontal moves from the centre pixel may be compared with the movement of Rook in the game of chess. The NM-cost for this kind of neighbourhood connection (following Eq. 6.2) can be formulated as:

$$NM-cost_{(O,P_i)} = \sqrt{\mu^2 + (H_{P_i} - H_O)^2} \left(p \times \frac{C_O + C_{P_i}}{2} + q \times \tan^{-1}\left(\frac{H_{P_i} - H_O}{\mu}\right) cost \right)$$

$$(6.8)$$

where, *NM-cost* is the neighbourhood movement cost to move from O (source) to pixel *Pi* (connected neighbour), μ is the pixel size, H_O and H_{Pi} are the elevation of source and pixel

Pi, C is the thematic cost to pass through the pixel under consideration, p and q are weights and i is the neighbourhood pixel number. Here, $i = 1$ to 4 as in Figure 6.3.

b) Bishop's Pattern:

The Bishop's pattern consists of the diagonal movement in a 3×3 pixel window. The NM-cost for this kind of neighbourhood can be formulated as:

$$NM - cost_{(O,P_i)} = \sqrt{2\mu^2 + (H_{P_i} - H_O)^2}\left(p \times \frac{C_O + C_{P_i}}{2} + q \times \tan^{-1}\left(\frac{H_{P_i} - H_O}{\sqrt{2}\mu}\right) cost \right)$$

(6.9)

where $i = 5$ to 8 (see Fig. 6.3), other parameters are the same as in Equation 6.8.

c) Knight's Pattern:

The Knight's pattern can be represented in a 5×5 pixel window. The NM-cost for this kind of neighbourhood can be written as:

$$NM - cost_{(O,P_i)} = \sqrt{5\mu^2 + (H_{P_i} - H_O)^2}\left(p \times \frac{C_O + C_{P_a} + C_{P_b} + C_{P_i}}{4} + q \times \tan^{-1}\left(\frac{H_{P_i} - H_O}{\sqrt{5}\mu}\right) cost \right)$$

(6.10)

where $i = 8$ to 16 (see Fig. 6.3). The value of a and b varies depending upon the neighbouring pixel under consideration, *e.g.,* for $i = 9$, $a = 2$ and $b = 5$ and so on (see Fig. 6.3).

d) Knight31's Pattern:

This is the newly designed neighbourhood pattern for a 7×7 pixel window. The NM-cost for this kind of neighbourhood has been formulated as:

$$NM - cost_{(O,P_i)} = \sqrt{10\mu^2 + (H_{P_i} - H_O)^2}\left(p \times \frac{C_O + C_{P_a} + C_{P_b} + C_{P_c} + C_{P_d} + C_{P_i}}{6} + q \times \tan^{-1}\left(\frac{H_{P_i} - H_O}{\sqrt{10}\mu}\right) cost \right)$$

(6.11)

where $i = 17$ to 24 (see Fig. 6.3). The value of a, b, c and d varies as it depends on the neighbouring pixel under consideration, *e.g.*, for $i = 17$, $a = 2$, $b = 5$, $c = 9$ and $d = 36$ and so on.

e) Knight32's Pattern:

This is another newly designed neighbourhood pattern for a 7×7 pixel window. The NM-cost for this kind of neighbourhood has been formulated as:

$$NM\text{-}cost_{(OP_i)} = \sqrt{13u^2 + (H_{P_i} - H_O)^2} \left(p \times \frac{C_O + C_{P_a} + C_{P_b} + C_{P_c} + C_{P_d} + C_{P_i}}{6} + q \times \tan^{-1}\left(\frac{H_{P_i} - H_O}{\sqrt{13}u} \right) cost \right)$$

(6.12)

where $i = 25$ to 32. The value of a, b, c and d varies and depends on the neighbour pixel under consideration, *e.g.* for $i = 25$, $a = 1$, $b = 5$, $c = 16$ and $d = 35$ and so on (see Fig. 6.3).

In this study, p and q are assigned values of 1 and 8 respectively. This is in view of the fact that while calculating thematic cost layer, a weight of 8 has been given to LHZ (see Table 5.1) and it appears reasonable that a similar weight (= 8) be given to gradient cost to have an equitable weight consideration.

6.6 Selection of Least-Cost Route

Dijkstra's algorithm (Dijkstra, 1959) has been widely used for finding least-cost path. This algorithm is designed for tracing the shortest path in a network with nodes connected by weighted links. In a raster GIS, the centre of each pixel is considered as a node. A few modifications of this algorithm have been reported for specific applications. A* (pronounced "Eh star") algorithm (Tanimeto, 1987) is a variation of Dijkstra's algorithm, which uses some heuristic information related to the node / pixel of interest. As the Dijksta's algorithm is computationally intensive and it requires huge memory to store the data to find the shortest-path, the computational process slows down. To improve the computation efficiency, a parallel Dijkstra's algorithm with constraints has been developed

by Solka *et al.* (1995), which uses the concept of neural network for optimisation. Further, the steering mechanism of a vehicle imposes a minimum turn radius, which may also be incorporated in route planning algorithm (Boroujerdi and Uhlmann, 1998; Winter, 2002).

In this research, the classical Dijkstra's algorithm, described in the next section, has been used to find out the least-cost path as the main emphasis here is on the development of a methodology for route planning in landslide-prone terrain.

6.6.1 Dijkstra's Algorithm

The least-cost route between a source and a destination can be determined using Dijkstra's Algorithm, named after its inventor, the Dutch computer scientist Edsger Dijkstra. Detailed explanation of this algorithm can be found in a number of publications (*e.g.*, Horowitz *et al.*, 2002; Rees, 2004; *www.wikipedia.org/wiki/Dijkstra's_algorithm*; *http://ciips.ee.uwa.edu.au/~morris/Year2/PLDS210/dijkstra.html*, *etc.*). This algorithm is specifically written for a node-based network. To implement the algorithm in a raster based analysis, the centre-point of each pixel has been considered as a node in the network.

According to this algorithm, each pixel in a raster framework should contain two basic information: NM-cost, which comprises of neighbourhood distance, gradient and thematic costs, and a pointer that identifies the connected pixels. These information are updated in an iterative process to find the least-cost path from a designated source to the destination. Rees (2004) has lucidly explained the steps of finding a least-cost path and the same are reproduced below with some modification:

1. Assign a cost of zero to the target pixel (pixel under consideration at particular instance) and an infinite cost to all other pixels in the raster map.

2. Identify all the neighbouring pixels to the target pixel and place them in the list of 'active' pixels. For each of these pixels, calculate and assign the cost of reaching the target pixel, and assign a pointer that points to the target pixel.

3. Find the pixel in the list that has the lowest cost – call this pixel **C**, and call the cost k.

4. Identify the set **S** of all the neighbouring pixels of **C**. For each pixel **C'** in **S** (**C'**s are the connected pixels to **C**), calculate the cost l of moving to **C**.

    4.1 If **C'** is not yet a member of the list, add it to the list with a cost $k + l$ and a pointer that points to **C**.

    4.2 If **C'** is already a member of the list, compare the value of $k + l$ with the provisional cost of this pixel. If $k + l$ is greater than or equal to the provisional cost, do nothing. Else if $k + l$ is less than the provisional cost, change the attributes of the pixel **C'** such that its cost is now $k + l$ and its pointer now points to the cell **C**. This procedure is termed as 'relaxation'.

5. Change the attributes of the pixel **C** from provisional to definite, and remove it from the list.

6. Repeat from step 3 until the list is empty.

The algorithm works only in the case where all the associated costs of neighbourhood connections are positive. It calculates the least-cost route from the source pixel to all the pixels in the raster network. To increase the computational efficiency, the algorithm may be stopped when the pre-defined destination pixel is reached.

6.7 Software to Implement Route Planning Methodology

The methodology for route planning adopted in this study, has been implemented using a dedicated software written in C++. The outputs from the software have been suitably interfaced with ILWIS GIS. This section provides the details of the software and its interface with ILWIS GIS to determine and display the least-cost route for a pair of source and destination points.

6.7.1 Need for the Software

In a standard raster GIS model, each pixel in an image contains single attribute information along with its geographic location. In this study, upto 7×7 pixel window has been considered to incorporate 32 unique neighbourhood movements from a pixel in the map. Hence, in each pixel, there is a need to store 32 NM-cost values in addition to the direction of movement. Therefore, the concept of data structure utilised in this model is not easy to model in an existing raster-based GIS. Moreover, Dijkstra's algorithm consists of a number of complex steps each requiring storage of a large volume of temporary data and pointers. Therefore, a customised software written in any object oriented programming language that could be suitably interfaced with a raster based GIS becomes mandatory to implement a new concept.

6.7.2 Software: Landslide Safe Intelligent Route Finder (LaSIRF)

To perform the least-cost route selection in a raster GIS environment, a dedicated C++ software has been written. The software has been acronymed as "**Landslide Safe Intelligent Route Finder (LaSIRF)**", since the main emphasis of this research is to determine a safe route, which avoids potential landslide-prone areas in a hilly terrain. The program can be compiled and executed by a Windows based MS-Visual C++ compiler. The process is computationally intensive and hence at least 2.4GHz processor with a minimum of 256MB RAM hardware is recommended.

DEM and thematic cost map are the major inputs to LaSIRF to compute the least-cost route between a user-defined source and destination points. The software has four basic modules:

a) DATEXP (for creation of input data file)

b) NMCOST (for computation of neighbourhood movement cost)

c) DIJKSTRA (for finding out least-cost route)

d) INTERFACE (for interfacing with ILWIS).

These modules are described as below:

6.7.2.1 Creation of Input Data Files

The DEM and thematic cost map in ILWIS raster format (*.*MPR* and *.*MP#*) have to be exported to ASCII (*.*asc* format for ILWIS ASCII export) for their direct input to LaSIRF. ILWIS ASCII export option is used for this purpose (Fig. 6.4). The DATEXP module reads the ASCII data, converts row/column location of each pixel into a node number (see Table 6.1) and stores the thematic cost and elevation data against each node into a data file (*cost_elev.dat*). The structure of the output data file has been shown in Figure 6.4.

6.7.2.2 NM-cost Calculation

NMCOST module computes the neighbourhood movement cost for each node (or pixel). The module requires '*cost_elev.dat*' file, generated by DATEXP as input, as all the processing is done node wise. For example, it reads the node number of a pixel's 32 neighbours (in 7 × 7 pixel window) and calculates the distance, gradient and thematic cost according to the pattern of connection (*viz.,* Rook, Bishop, Knight, *etc.*). The gradient value is classified and a cost value is assigned to each class according to Table 6.3. The distance, gradient cost and thematic costs are integrated for each pixel, using Equations 6.8 to 6.12 to calculate the NM-cost for various patterns. The output NM-cost values are stored in a data file (*nmcost.dat*). If there is no possible connection between any two nodes or the NM-cost associated is too high, '-1' is assigned to such connections. As Dijkstra's algorithm is based only on 'non-negative' values, these connections are automatically eliminated from the network. Figure 6.5 shows the procedural layout of NMCOST module and the associated output data file structure.

6.7.2.3 Route Finding Using Dijkstra's Algorithm

DIJKSTRA module is the most important part of the software LaSIRF to find the least-cost route between a user-defined source and destination. DIJKSTRA can read the source and destination information in the form of node numbers. A function ROWCOL2NODE supplements the DIJKSTRA to determine the node number of a pixel if the pixel location information is in the form of row and column coordinates. In this case, the size of the map under consideration, in total number of rows and columns, has also to be provided. DIJKSTRA reads the '*nmcost.dat*' file, generated by NMCOST and allocates it in its Random Access Memory (RAM) for fast retrieval and computation. It calculates the least-cost route using Dijkstra's algorithm explained in detail in Section 6.5.1. A number of functions associated with this module and their purpose are explained in Table 6.4. The least-cost route and the cumulative cost for the route are stored in a data file (*result.dat*). The processing steps for this module are given in Figure 6.6.

Table 6.4: Functions created in DIJKSTRA module and their purpose

C ++ functions	Purpose
get_nmcostmatrix()	- This function reads the '*nmcost.dat*' file as a two-dimensional matrix - Store the data in RAM
nmcost_between()	- This function checks if the nodes are connected - If there is a connection, it supplies the NM-cost value to leastcost_path() else '–1' *i.e.* no connection
leastcost_path()	- Iteratively checks the next node to be on the path as per the algorithm. - When destination node is reached, it prints the nodes on least-cost path in '*result.dat*' file

6.7.2.4 Interface of LaSIRF with ILWIS

The INTERFACE module converts the least-cost route stored in the form of nodes in '*result.dat*' file, generated by DIJKSTRA, into ILWIS readable segment file in ASCII (**.smt*). The user has to enter pixel size, number of rows and columns and the projection information for the map being created. These data are required since the thematic cost and
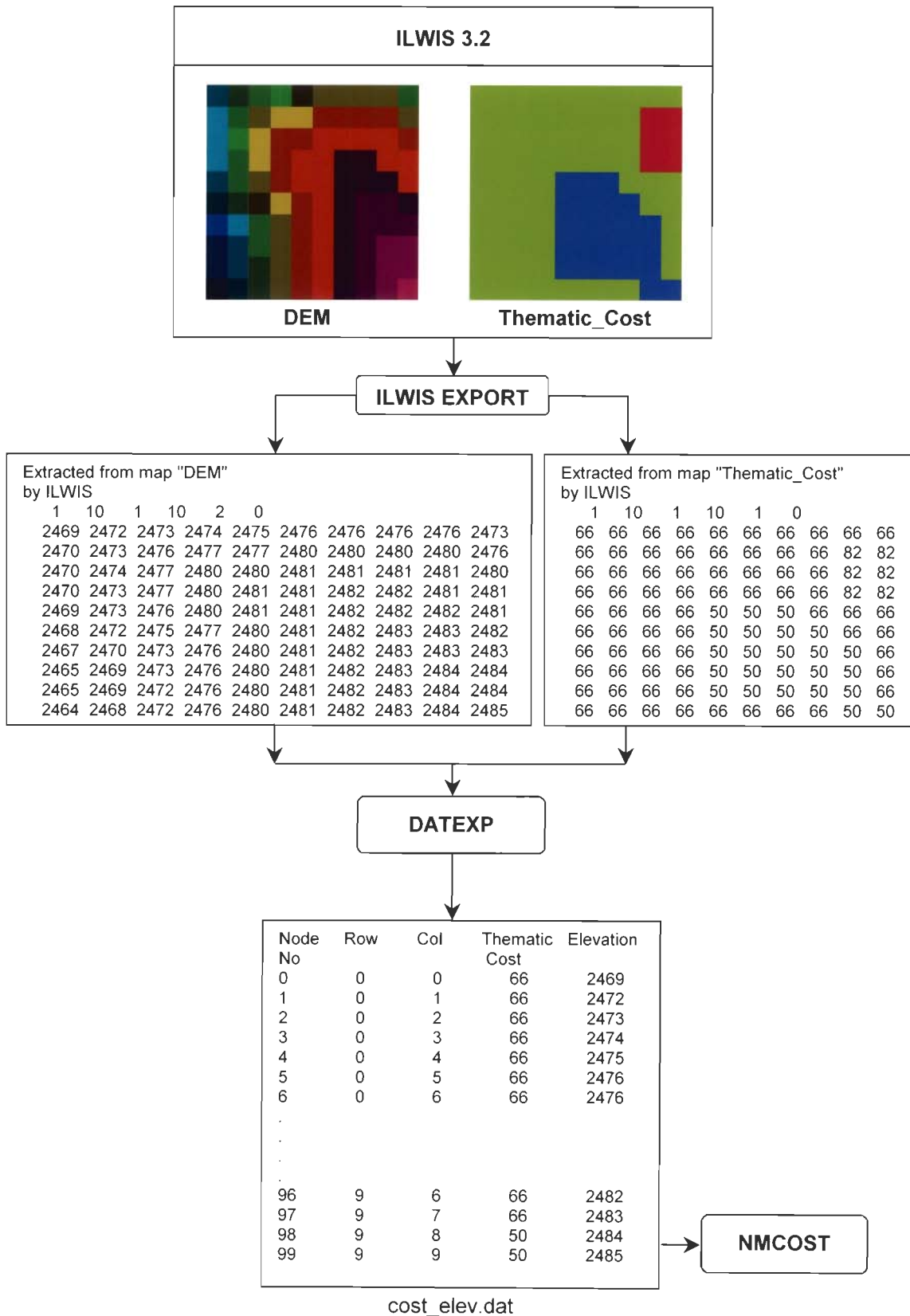
Figure 6.4: Flow diagram showing the steps involved in input data preparation with the help of DATEXP module of LaSIRF. The output from this module 'cost_elev.dat' is used as the input for neighbourhood movement cost calculation in the next step.

	32	23		24	25	
31	33	15	34	16	35	26
22	14	8	1	5	9	17
	40	4	O	2	36	
21	13	7	3	6	10	18
30	39	12	38	11	37	27
	29	20		19	28	

Neighbourhood Relationship

cost_elev.dat

Neighbourhood Pattern Selection

Rook's Pattern   Bishop's Pattern   Knight's Pattern   Knight31's Pattern   Knight32's Pattern

Distance   Gradient   Thematic Cost

Classify

Gradient Cost

NM-cost = Distance × (p × Thematic Cost + q × Gradient Cost)

Node	dir1	dir2	dir3	dir4	dir5	dir6	dir7	dir8	dir9	....	dir30	dir31	dir32
0	-1	-1	456	-1	-1	-1	-1	-1	-1		-1	-1	-1
1	-1	456	456	-1	-1	-1	-1	-1	-1		-1	-1	-1
2	-1	456	-1	456	-1	-1	568	-1	-1		-1	-1	-1
3	-1	456	-1	456	-1	-1	-1	-1	-1		1454	-1	-1
.													
.													
98	306	358	-1	407	500	-1	-1	487	-1		-1	1165	1087
99	407	-1	-1	358	-1	-1	-1	487	-1		-1	1114	1138

nmcost.dat

DIJKSTRA

Figure 6.5: Flow diagram showing the steps of NMCOST module for calculating the neighbourhood movement cost for each pixel/node. The output from this module is used as input to DIJKSTRA module for least-cost route selection.

nmcost.dat

USER

Row, Column

ROWCOL2NODE

Source (node no.)   Destination (node no.)

DIJKSTRA

```
1       Algorithm ShortestPaths(v, cost, cumcost, n)
2       // cumcost[j], 1 ≤ j ≤ n, is set to the cumulative cost of the least-cost
3       // path from node v to node j in a map G with n
4       // nodes. cumcost[v] is set to zero. G is represented by
5       // neighbourhood movement cost matrix nmcost [1 : n, 1 : 32].
6       {
7       for i := 1 to n do
8       { // Initialise S.
9                       S[i] := false; cumcost[i] := cost[v,i];
10              }
11      S[v] := true; cumcost[v] := 0.0;  // Put v in S.
12              for num := 2 to n − 1 do
13      {
14                      // Determine 32 connections from v.
15                      Choose u from among those nodes not
16                      in S such that cumcost[u] is minimum;
17                      S[u] := true; // Put u in S.
18                      for (each w adjacent to u with S[w] = false) do
19                              // Update cumulative costs.
20                              if (cumcost[w] > cumcost[u] + cost[u,w]) then
21                                      cumcost[w] := cumcost[u] + cost[u,w];
22              }
23      }
```

```
result - Notepad                                      _ □ ✕

File   Edit   Format   View   Help

Least-cost path between
Source Node: 81
and
Destination Node: 8
is

81 >> 71 >> 40 >> 30 >> 20 >> 3 >> 4 >> 5 >> 6 >> 7 >> 8

Cumulative cost for the least-cost path is : 8816
```

result.dat

Figure 6.6: Flow diagram showing the steps of DIJKSTRA module of LaSIRF software for calculating the least-cost path.
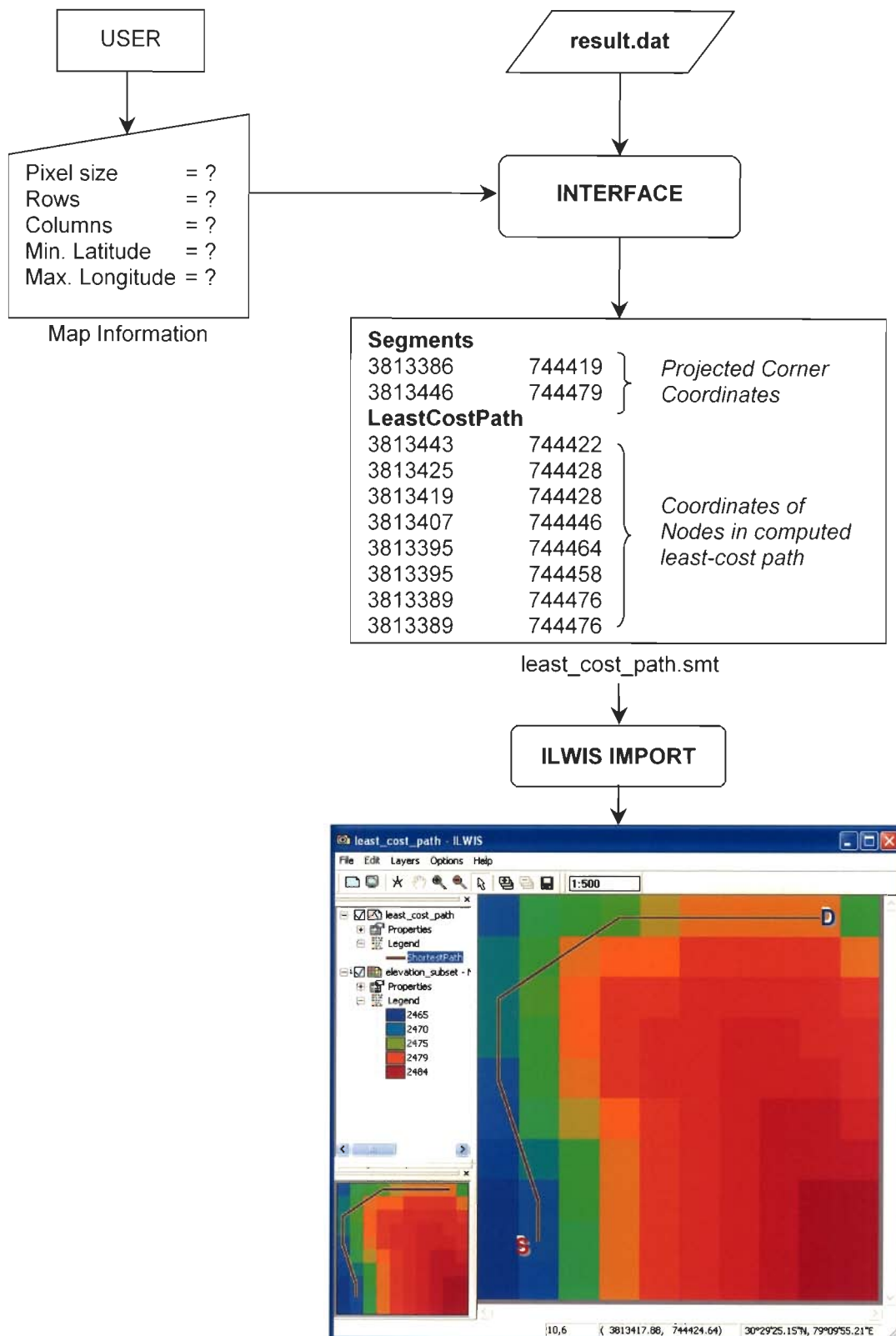
Figure 6.7: Flow diagram showing the INTERFACE module of LaSIRF software. The least-cost path computed by DIJKSTRA is displayed on DEM of the area in ILWIS GIS.

elevation ASCII files are in the form of row and column matrix. The projection information can be readily obtained from the properties of raster maps (in ILWIS). INTERFACE module converts the '*result.dat*' into '*least_cost_path.smt*' file, which can be imported directly through import option of ILWIS and laid over elevation or thematic map to visualise the least-cost route computed (Fig. 6.7).

6.7.2.5 Efficiency of the Software

The efficiency of the program has been tested with sample test areas of 250×250 pixels and 500×500 pixels on an Intel P4 2.8 GHz and 512 MB RAM workstation. It has been found that the LaSIRF software takes 13 minutes and 2 hours 30 minutes respectively to find a route between the diagonally opposite corners for the above two tests areas. The computational time for individual module has been listed in Table 6.5. It can be noted that for multiple route computation, LaSIRF takes relatively lesser time, because once '*nmcost.dat*' file is generated, the DIJKSTRA can compute multiple paths using this data file, which takes a large amount of time to execute.

Table 6.5: Comparative study of efficiency of the LaSIRF program

LaSIRF modules	Test area size in pixels	
	250×250	500×500
DATEXP	14 sec.	1 min.
NMCOST	7 min.	28 min.
DIJKSTRA	5 min. 11 sec.	1 hrs. 45 min.
INTERFACE	2 sec.	5 sec.

6.7.3 Salient Features of the Program

The salient features of LaSIRF can thus be enumerated as,

- The software is fast with reasonable computational efficiency.
- The software can be applicable to a study area of any dimension, though it also depends on the hardware specification.
- The software can be easily interfaced with ILWIS GIS.

6.8 Testing of Route Planning Methodology

In previous sections, the methodology developed for finding the least-cost route in a landslide-prone terrain has been described. The procedure is computationally intensive and time-consuming. Therefore, to test the concept and the methodology in finding safe routes in a landslide-prone rugged terrain, a few test areas of 1.5 km × 1.5 km size, with different combinations of terrain conditions and landslide susceptibility have been selected. The test results are presented below:

Example 1: Case of a major landslide

This test site is located close to Gopeshwar town (Fig. 3.2). The area comprises a hill (altitude ≈ 2100 m) rising towards northeast and gradually sloping towards the west and the southwest. To represent the topography of this area, the DEM in pseudo colour is draped over the shaded relief model as shown in Figure 6.8.

It can be seen from this figure that there are many landslides of differing dimensions in the area. In the northeastern part of the test site, there occurs a major landslide (extent >400 pixels). As an example, the source and destination points have been selected on the east and the west sides of the landslide. At the first instance, the thematic costs are kept zero for all the neighbourhood connections, with the result that only topographic factors (neighbour-distance and gradient) take part in the route finding process. The least-cost path for this case obtained from the algorithm is marked in blue in Figure 6.8. For the same source and destination points, another least-cost path, marked in yellow in this figure, has been found that considers neighbourhood distance, gradient and thematic costs, collectively. It can be seen from the figure that when only the topographic factor is taken into account, the path is shorter (634 m), smoother and consists of less number of turns. However, it passes right through the middle of the major landslide. In contrast, when both the topography and the thematic cost are considered, although the path
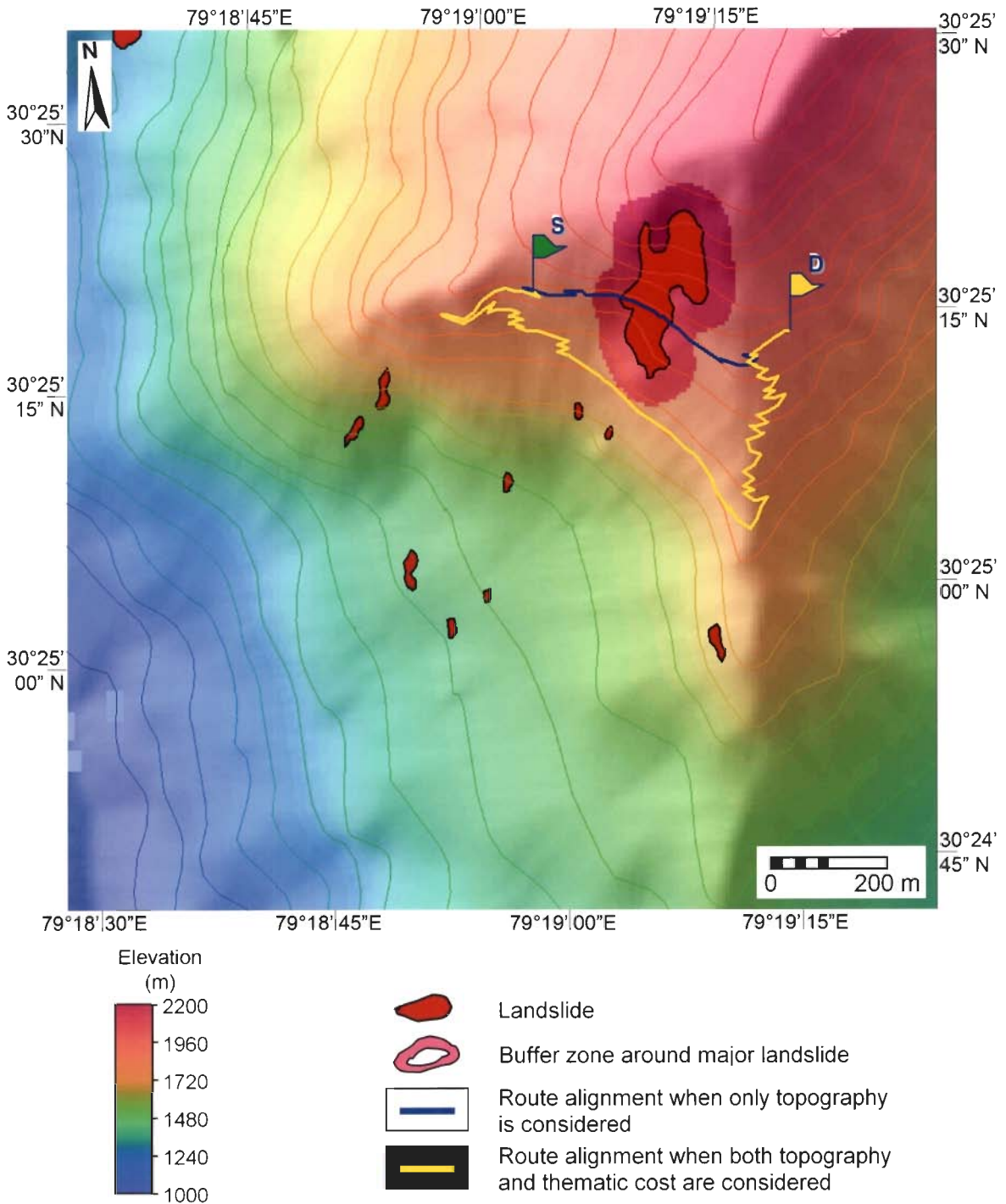
Figure 6.8: Example 1 - Comparison of alternative route alignments in case of major landslide. Note that when only topography is considered, the route passes through the landslide zone, whereas, when the topography and thematic costs both are considered, the route avoids the landslide and the buffer zone around the major landslide. (S – Source, D – Destination)

becomes relatively longer (1892 m), with many curves and hairpin bends, it passes through relatively safer (lower thematic cost) areas avoiding the major landslide.

Example 2: Case of a major landslide and adjacent minor landslides

This example considers the case of major and minor landslides occurring in adjacent areas such that the source and destination points are located across the set of landslides. Figure 6.9a shows the test area, which is situated west of the Gopeshwar town. There is a major landslide along with a debris flow channel that carries the debris to the river valley in the east.

Consider the case that the entire landslide and the associated debris flow track is unsuitable for route location and therefore must be avoided. For such a situation, a buffer zone can be created around the landslide and debris flow track and the entire zone can be assigned a high value in the thematic cost layer. The source and destination points have been selected at nearly same elevation (approximately 1600 m) on either side of the set of major and minor landslides (Fig. 6.9a). The computed route when only topography is considered follows dominantly the contour line and crosses the minor and major landslides right through the middle. When both topography and thematic cost are used, the computed route passes through the minor landslides but avoids the major landslide and its buffer zone, though it takes a longer route to reach the destination point.

Consider another possibility that only the main landslide area is to be avoided and the associated debris flow track on the east can be treated as a minor landslide across which a suitable structure (*e.g.,* a suspension bridge) can be constructed. In this case, the buffer zone is made only around the main landslide area (Fig. 6.9b). A set of the source and destination points has been selected on the northwest and southeast of the major landslide (Fig. 6.9b). It is found that when only topography is considered, the route passes through the major landslide. On the other hand, when both the topography and the thematic cost are considered, the computed route avoids the major landslide and passes over the

debris flow track (over which the feasibility of a suitable structure has been taken into consideration).

Example 3: Case of minor landslides with adjacent areas possessing large variation in thematic cost

This example deals with the situation where there are minor landslides. The test site is located in the northwestern part of the study area. The area comprises an east-west trending valley and is marked by varying thematic cost zones. There occur two minor landslides on the south-facing slope of the hill (Fig. 6.10).

For the sake of example, the source and destination points have been selected on the east and the west sides of the set of landslides (Fig. 6.10). As mentioned earlier, the strategy used in the present study, is that minor landslides can be negotiated (moderate thematic cost). As in the earlier example, computations have been made in two different ways - in the first instance, the thematic cost is made zero all over and only topography is considered, in the second instance, all the factors, *viz.,* thematic cost, gradient cost and distance are considered. It is found that both the computed routes pass through the minor landslides. However, the routes are different. In the first case, the route passes through high thematic cost zones (pink and red) whereas in the second case, it passes through relatively lower cost zones (green and light brown areas).

Example 4: Case of a river crossing

This example of deals with a situation when the route is expected to cross a river. The test area has been culled out from the northwestern part of the study area such that the associated thematic cost has a wide range of values. The thematic cost map is draped over the shaded relief model to show the perspective view. The terrain represents a valley trending NW-SE with the river flowing towards the northwest direction (Fig. 6.11).
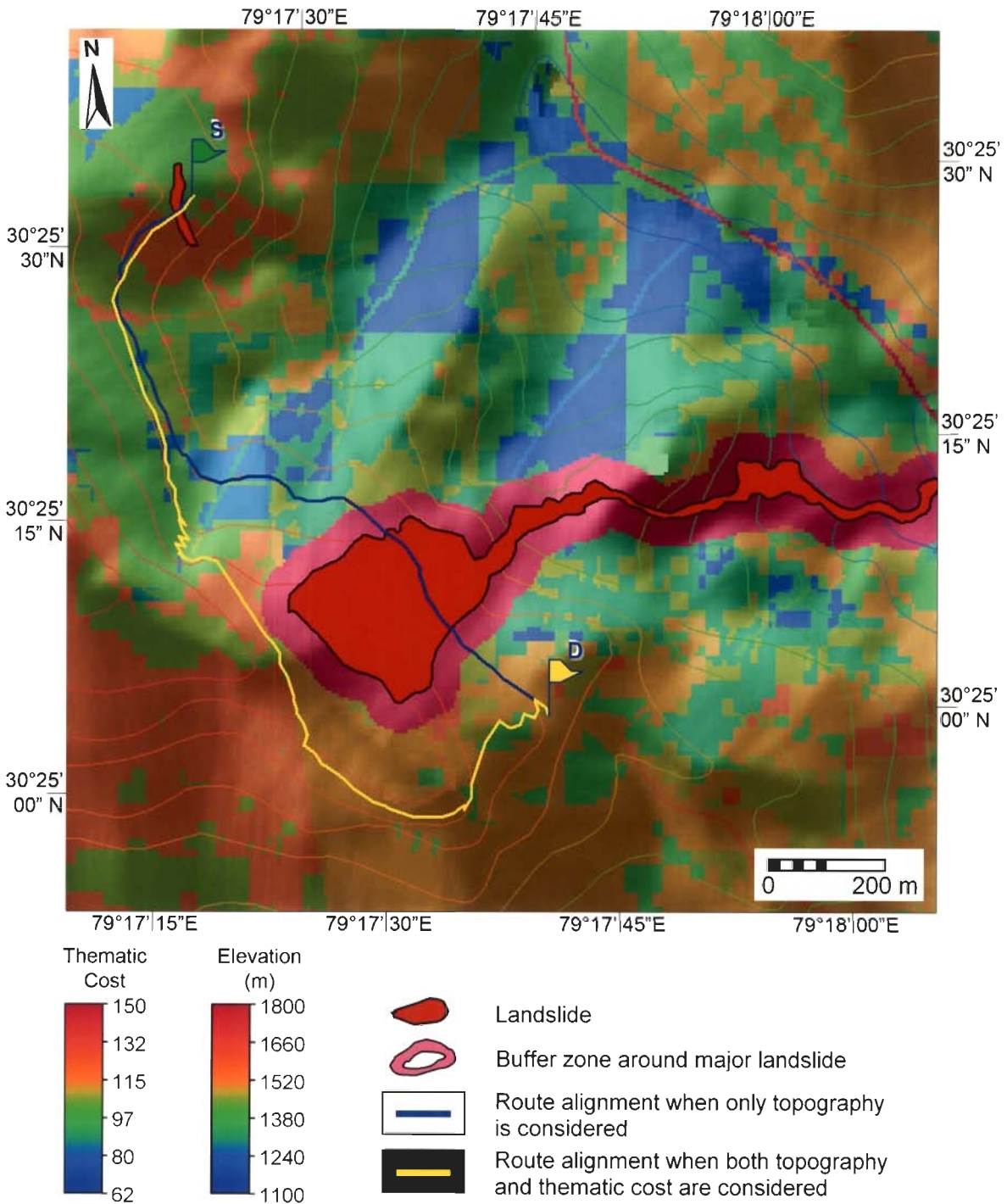
Figure 6.9a: Example 2 - Comparison of alternate route alignments in case of a major landslide and adjacent minor landslide. Note that when only topography is considered, the route passes through the landslides, whereas, when the topography and thematic costs both are considered, the route avoids the major landslide and buffer zone around it. (S – Source, D – Destination)
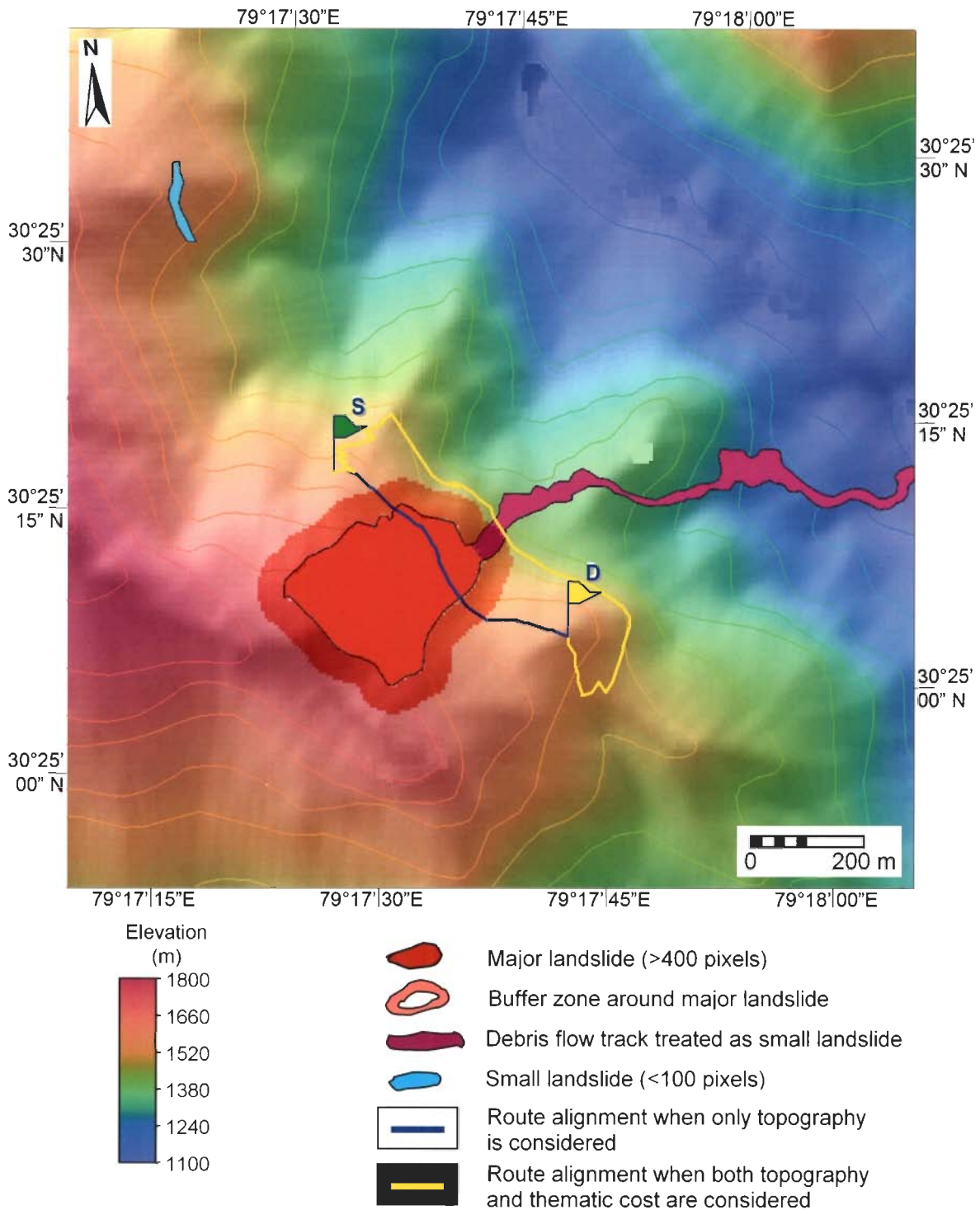
Figure 6.9b: The figure shows another possibility described in Example 2. In this case the debris flow track is treated as a minor landslide, where construction of bridge can allow the debris to pass through. Note that when only topography is considered, the route passes through the major landslide, whereas, when the topography and thematic costs both are considered, the route avoids the major landslide and buffer zone around it and passes through the debris flow channel. (S – Source, D – Destination)
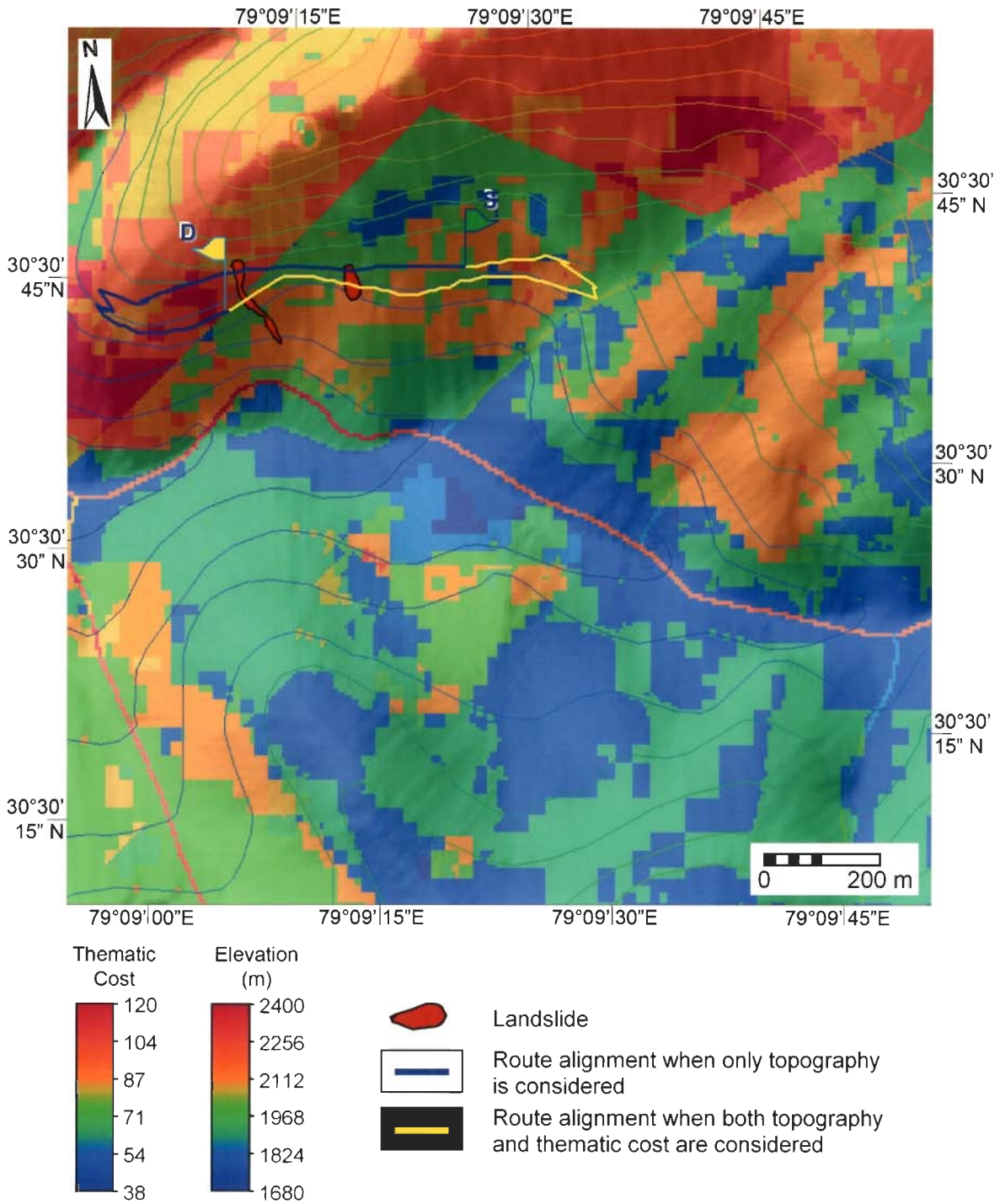
Figure 6.10: Example 3 - Comparison of alternate route alignments. The source and destination points are on either side of minor landslides. If only topography is considered, the route alignment is controlled solely by topography and would pass through minor landslides and high thematic cost zones. When thematic cost data layer is also considered in route selection, the route passes through minor landslides but avoids thematic cost zones. (S – Source, D – Destination)
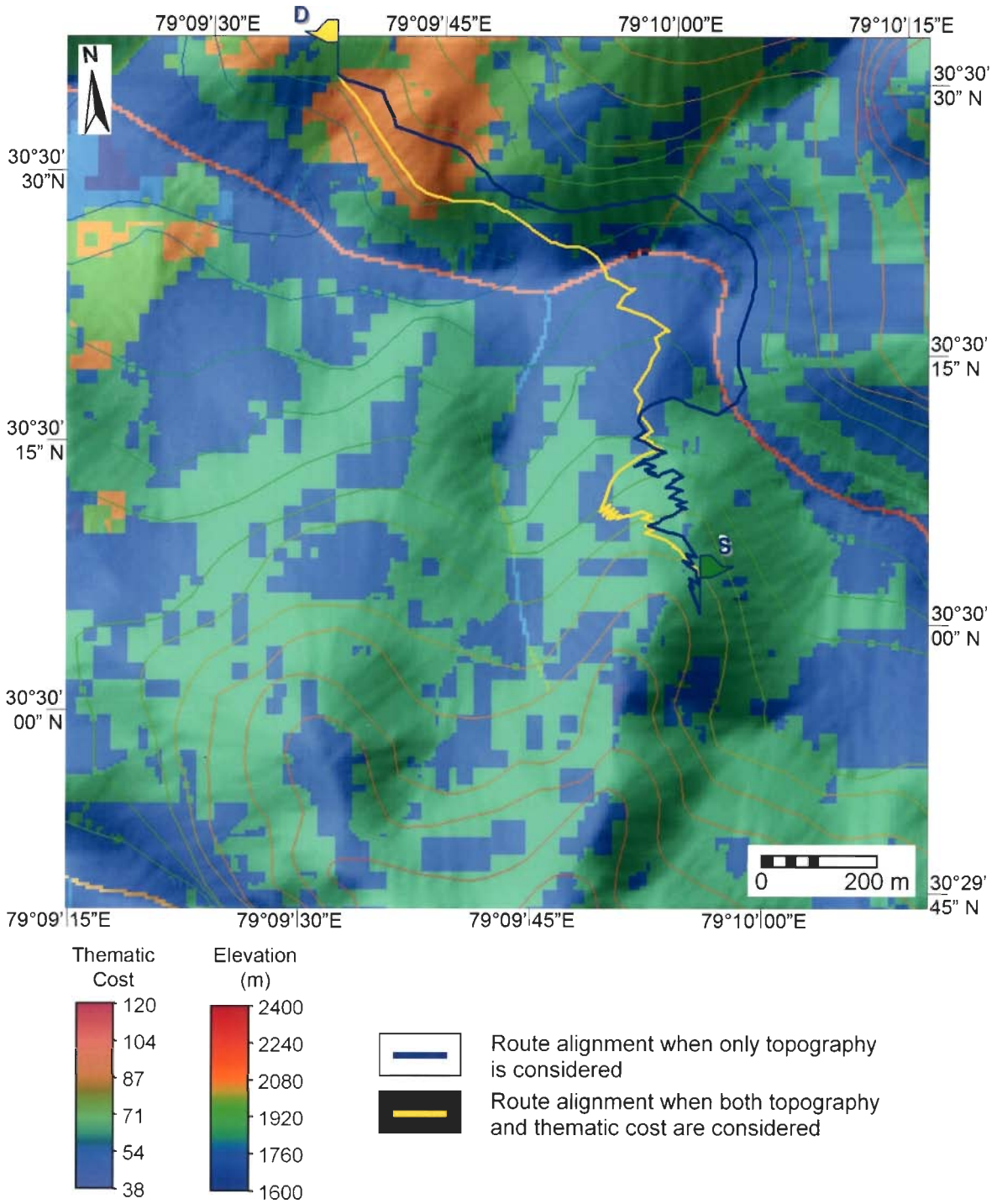
Figure 6.11: Example 4 - Comparison of alternate route alignments for crossing a river valley. The route alignment when only topography is considered follows dominantly the topographic contours. When thematic cost is also integrated with topography, the route alignment is slightly different and passes through the low thematic cost areas. (S – Source, D – Destination)

A set of source and destination points at different elevations, has been selected on either side of the valley. In the first case, when only topography is considered, the computed route follows dominantly the topographic contours. In the case when thematic cost factor is also integrated with topography, the computed route is found to be slightly different and it passes through the low thematic cost areas.

Example 5: Case of no-trespassing zones

This example shows the suitability of the route planning methodology for cases involving no-trespassing zones. The no-trespassing zone could be, for example, due to archaeological-cultural heritage sites, strategic installations, exceptionally high land costs or reserved parks. In such a case, the condition is that the route may touch the boundary of the no-trespassing area, but cannot pass through the area. For this case, a landuse/landcover map has been draped over shaded relief model such that the no-trespassing area is depicted in red colour (very high pixel value) (Fig. 6.12).

The source and destination points have been selected at the corners of two no-trespassing zones. The route computed from thematic cost, gradient cost and distance is shown in yellow and passes outside the periphery of the no-trespassing zones. This example demonstrates the versatility of the methodology developed in this research.

Example 6: Case of significant regional variation in thematic costs

In this example, the area selected is the same as in example 1. The area possesses a large regional variation in thematic cost values, as indicated by yellow-orange-red pixels in the southeastern part and blue-green pixels generally in the northwestern part. The task considered here is to join the southwest corner with the northeast corner. Figure 6.13 shows the thematic cost map draped over the shaded relief model to represent the terrain. The existing landslide zones are assigned higher costs; these are mainly represented in red.

A 50 m buffer zone around major landslides is also provided to keep a safe distance for passing a route. Contour lines are shown in pseudo colour to highlight the topography.

As in the previous examples, the least cost path found by taking into account only topographic factors is marked in blue. For the same source and destination points, another least-cost path has been computed by considering the topographic as well as thematic cost, and is marked in yellow. It can be seen that the path shown in blue passes mostly through areas with higher values of thematic cost, even crossing the major landslide twice on its way to destination. In contrast, the path shown in yellow avoids the higher thematic cost areas and mostly passes through the blue and green regions, *i.e.* the lower thematic cost value regions.

6.9 Summary

Based on the working examples, it can be stated that the proposed GIS-based route planning methodology appears to possess several merits in comparison to the conventional manual route planning practice. These can be enumerated as follows:

- The methodology developed here has been successfully tested for landslide-prone terrain. It has been observed that the routes identified by the proposed methodology in the high-altitude, rugged Himalayan terrain with markedly different landslide susceptibility conditions pass through relatively safe areas avoiding major landslides. Thus, the planning of a road in hilly area using this methodology will result in a safer and cost-effective route involving less recurring costs for road development and maintenance.

- The computer-assisted methodology of route planning is very fast in comparison to the conventional manual practice. The working examples show that for a test area of 1.5 km × 1.5 km, the computer-based least-cost route finding process takes about 13 minutes, and in contrast, the same could have taken many days by the manual approach
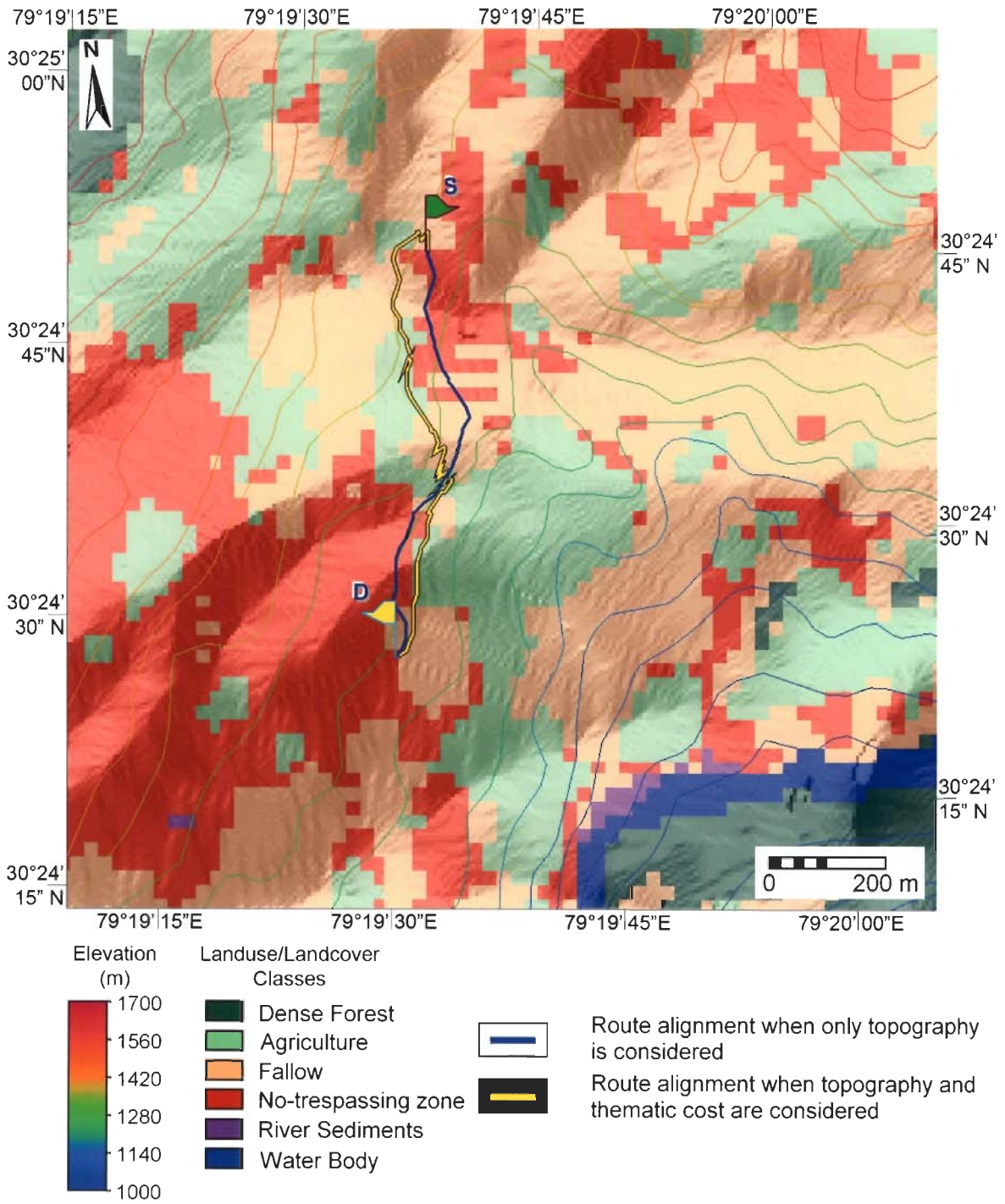
Figure 6.12: Example 5 - Route alignment for connecting no-trespassing zones. (S – Source, D – Destination)
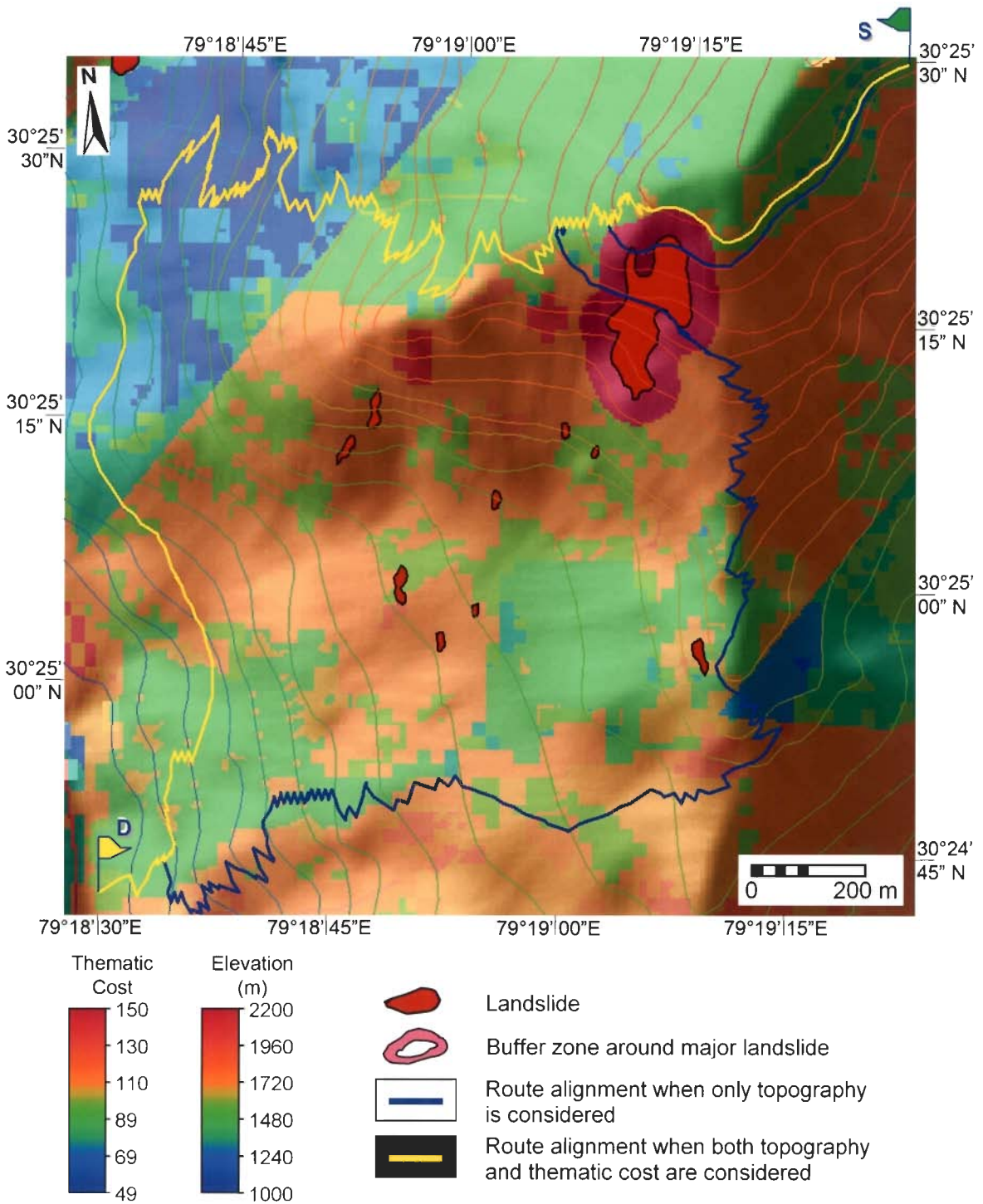
Figure 6.13: Example 6 - Given the task that the northeast corner has to be joined with the southwest corner, this example shows alternative route alignments. When only topography is considered, the alignment passes through higher thematic cost zones and landslide zones; when both the topography and thematic cost are considered, the route passes through mainly lower thematic cost zones and avoids the landslide areas.

even in the presence of all the data in hand. The efficiency of the proposed algorithm can further be increased as the processing technology advances.

- In the GIS-based methodology, it is possible to integrate and analyse various parameters related to road development and maintenance at the same time. For this purpose, the concept of thematic cost has been introduced in this research. In the manual method, it is not possible to consider a large number of parameters at the same time to conduct a purposeful analysis.

- In manual route alignment practice, it is quite possible that an alternate best route gets unknowingly overlooked. In contrast, this methodology uses the Dijkstra's Algorithm for finding the least-cost path. The algorithm is intelligent, fast and efficient and considers all possible combinations of routes between the source and the destination. Therefore, the least-cost path generated by the algorithm would provide the best option with certainty.

- The GIS-based methodology considers the gradient for various direction-dependent connected neighbours, thematic cost and distance in a three-dimensional space. The path gradient can be adjusted as per requirements, depending upon the terrain conditions. Hence, it should be possible to design a more realistic route in an automated way by merely changing some of the parameters, as appropriate.

Finally, it may be emphasised that the thrust of this research is on the methodology development and the list of factors and their weighting-rating can be modified and adjusted, depending upon the local conditions in an area.

6.10 Further Scope

During the course of the proposed route planning methodology, a few important aspects have emerged which may require special consideration in future and are listed as follows:

- Limitations imposed by raster window size have been an important constraint. In this research, it has been possible to use upto 7 × 7 pixel window (in comparison to 5 × 5 pixel window size which was used earlier), which has helped to make the path relatively smoother in the rugged terrain. An increase in the window size to 9 × 9 pixel or higher matrix that may lead to smoother paths with gradual and realistic variation in the path gradient is worth considering, although it may lead to more computational complexity.

- There is a need to make the program more efficient to compute the least-cost path for larger areas (say 10 K × 10 K pixels).

- The interface with the GIS software needs to be further improved, using higher-level programming.

- There is a need to incorporate the possibilities of bridges and tunnels more efficiently.

Chapter 7
Summary and Conclusions

The Himalayan terrain possesses a high susceptibility to landslides, mainly owing to its complex geological setting combined with contemporary crustal movements, high relief and heavy rainfall. Due to the general ruggedness and steep slopes, roads provide the only way of transportation and connectivity in the Himalayan terrain. Invariably, in the rainy seasons some sections of the roads get blocked due to landslides, thereby disconnecting many villages and towns, and a huge amount of money is spent in maintenance of the roads every year. Hence, there is a great need for effective route planning, which is efficient in engineering design as well as considers various geological factors in terms of slope stability and safety.

Objective:

With the advent of satellite data, it has become possible to efficaciously collect and analyse synoptic spatial data, such as on geology, structure, landuse/landcover, drainage, settlements, *etc.* Besides, the advanced GIS computational techniques offer numerous advantages in multi-geodata handling. The main objective of this research is to explore the potential of advanced remote sensing-GIS technology to devise an automatic and intelligent approach for route planning in hilly regions prone to landslides.

Methodology overview:

In order to fulfil the research objectives, the following general methodology has been adopted:

- Selection of a suitable landslide-prone test area in the Himalayas

- Collection of various geo-data including topographic maps, geological maps, remote sensing data, *etc.*

- Pre-processing of remote sensing data for removal of common radiometric and geometric distortions

- Generation of Digital Elevation Model (DEM) from IRS-1C stereo-PAN data

- Digitisation of topographic, drainage and geological maps

- Generation of a number of thematic data layers for various factors related to landslide activity

- Classification of remote sensing data for producing accurate landuse/landcover map

- Preparation of Landslide Hazard Zonation (LHZ) map

- Integration of various thematic data layers in GIS environment to generate a 'thematic cost' map for road development and maintenance

- Computation of 'neighbourhood movement cost' (to move from a source pixel to its possible connected neighbours), considering direction-dependent terrain gradient, distance and thematic cost

- Development and implementation of Dijkstra's Algorithm for least-cost route selection in the region

- Testing of the developed approach in different terrain conditions in the study area

Remote sensing data from IRS-1C LISS-III and PAN sensors have been primarily used for generating various thematic data layers. Survey of India toposheets have been used as base map. Published and field data on geology, structure, landslides, landuse/landcover and GCPs have been collected and integrated with remote sensing data. Various software (ERDAS Imagine 8.6, BLUH and ILWIS 3.2) have been used for data

processing. A dedicated software (LaSIRF) in C++ language has been developed for least-cost path identification and has been suitably interfaced with the ILWIS GIS software.

Study area:

The study area covers a region of about 550 km^2 in Chamoli and Rudraprayag districts of the Uttaranchal state in the Himalayas. The terrain is highly rugged with elevations ranging from about 920 m to 4250 m above mean sea level. The river Alaknanda, with numerous tributaries constitutes the drainage network in the area. Geologically, the region comprises of the Lesser Himalayas and the Higher Himalayas. Structurally, the region is complex due to the presence of various thrusts, faults and intense deformation.

Thematic data layer preparation:

Generation of thematic data layers has been an important task in this research work. A number of thematic data layers, *viz.,* Digital Elevation Model (DEM), lithology, landuse/ landcover, drainage order, landslide distribution and landslide hazard zonation (LHZ) maps have been generated using remote sensing - GIS techniques.

The remote sensing image data has been geometrically corrected and accurately registered with the topographic map using a large number of well-distributed GCPs. The multi-spectral remote sensing data has been corrected for atmospheric path radiance using the 'dark-object subtraction' technique.

DEM: Digital Elevation Model is a basic component in GIS analysis. In this study, two different approaches have been used to generate the DEM: (a) photogrammetric data processing using IRS-1C stereo-PAN satellite data, and (b) digitisation of contours from Survey of India topographic maps. The IRS-1C stereo-PAN data with view angles of –22.27° and +23.20° providing a B/H ratio of 0.84 has been processed with BLUH software to generate the DEM. The software uses automatic image matching and

bundle block adjustment technique to reconstruct the stereo geometry from the image pair. However, it was found that at numerous pixels no image matching was possible due to steep slopes, forest cover and differential snow cover in the region. The point elevation data derived from the stereo pair has been interpolated and resampled to generate the DEM. For accuracy assessment, GCP data has been collected by a field GPS survey. The height accuracy has been estimated to be around ±70 m. Moreover, there are many pixels where no information from the stereo pair is available. Therefore, this DEM could not be used in further investigations.

In view of the above, the conventional topographic map digitisation technique has been implemented to generate the DEM. Contours from the Survey of India topographic map have been digitised, rasterised and interpolated. Various DEM-based derivatives, such as slope, aspect, and relative relief have been generated.

Lithology: The regional geological map has been used as the basic input. The rock groups and formations are reclassified into 5 major lithounits, *viz.,* quartzites and slates, schists and gneisses, limestones and greywackes, granite-granodiorite-gneisses and granites. The geological map has been digitised and co-registered with other thematic layers.

Structural features: Structural features discussed here include thrusts, faults and lineaments, which are very important in landslide studies. These structural features describe the zone/plane of weakness, shearing and tectonic activity along which landslide susceptibility is higher. The map showing structural features has been prepared by integrating the existing geological map with the structural lineaments interpreted from remote sensing data. As the incidence of landslide decreases with increasing distance from structural features, a buffer zone has been created along each structural feature and sliced with respect to distance.

Drainage: Drainage map has been generated by digitising the drainage lines from the toposheets, and has subsequently been used for generating drainage density maps and

drainage order maps. The drainage density map has been used as an input in creation of Landslide Hazard Zonation map, whereas the drainage order map has been used later to consider the cost of bridge construction, if required, during route planning.

Landuse/landcover: Remote sensing data are particularly useful in mapping landuse/landcover in mountainous regions, such as the Himalayas. In such a terrain, the classification of remote sensing data encounters many problems due to the presence of shadows, low sun angle, steep slopes and differential vegetation cover. Therefore in this study, a multi-source classification approach has been adopted. The multi-spectral LISS-III image from IRS-1C together with Normalised Difference Vegetation Index (NDVI) and DEM have been used as the input data sources. Separability analysis based on transformed divergence has been performed to examine the significance of various spectral and ancillary data in the classification process. Logical channel approach has been used to implement multi-source classification using Maximum Likelihood Classifier. IRS-1C PAN image together with the field data served as reference data for generating training and testing datasets. A number of classes having an impact on landslide activities in the region were mapped. These classes are: dense forest, sparse vegetation, agricultural land, fallow land, barren land, settlements, fresh sediments, water body and snow. A high classification accuracy of 92.06% has been achieved. The inclusion of NDVI and DEM has allowed for correct classification of the shadow areas to their corresponding landuse/landcover classes and this has improved the classification accuracy. A post-classification filtering has been carried out to weed out the isolated pixels from landuse/landcover map.

Landslide mapping: As mentioned earlier, in this study particular emphasis has been given to landslides and landslide hazard zonation and their impact on route planning in the region. Therefore, accurate mapping of landslides is very important. In high-altitude mountainous regions, landslides occur at distant and remote places, therefore remote sensing is a very valuable tool in landslide mapping. High-resolution PAN

image and PAN-sharpened multi-spectral image have been used to identify and map the existing landslides. The identification and recognition of landslides have been done based on tone/colour, shape, landform, drainage and vegetation. A total of 190 landslides of varying dimensions have been mapped in the area from remote sensing data. Many of these landslides have been field-checked.

Landslide hazard zonation: First, a detailed review of the techniques of landslide hazard zonation (LHZ) has been carried out. The requirement of input data for LHZ depends upon the scale at which the LHZ map is to be prepared. The various methodologies for LHZ can be grouped into six broad categories: distribution analysis, qualitative analysis, statistical analysis, distribution-free methods, deterministic analysis and landslide frequency analysis. After critically reviewing the methods, the bivariate statistical analysis method for LHZ has been found to be best suited for the present study and subsequently implemented here.

A number of thematic maps, *i.e.,* the data layers related to the landslide activity, *viz.,* structural features, lithology, relative relief, slope, aspect, landcover and drainage density have been generated (as described above) and used as input. To evaluate the contribution of each of the above factors in landslide hazard, weights have been calculated using the existing landslide distribution data layer. The weighted thematic maps so produced have been laid one over another and added to generate a Landslide Hazard Index (LHI) map in GIS. Segmentation of LHI values has been carried out by a new probabilistic approach. The LHI range has been segmented into 5 classes with boundaries placed on the basis of mean and standard error. A number of trials have been done, and the best LHZ map is selected on the basis of the 'success rate curve' method.

Thematic cost mapping:

Geo-environmental factors, such as landslide occurrence, landslide hazard zonation, drainage order, landuse/landcover and lithology have a direct bearing on the cost of road development and maintenance in landslide-prone terrain, such as the Himalayas. The data layers pertaining to these factors can be integrated in GIS using an ordinal weighting-rating system, to arrive at a cumulative data layer, called here as the 'thematic cost map'. The thematic cost map is a raster map where value at each pixel gives the estimated relative cost of passing through the pixel. The cost is cumulative and has inputs from landslide distribution map, LHZ map, drainage, landuse/landcover and lithology. An ordinal number from 0 to 9 has been given to each thematic data layer in terms of its relative importance; similarly each class in the data layer has been given an ordinal number in the range of 0 to 9. The weighting-rating values are based upon a comparative study of various thematic data layers and discussions with experts in the area of transportation engineering, and the logic for weights/ rating has been described appropriately.

As landslides are considered to be the most important factor affecting route planning in this study, the highest weight of 9 has been given to the presence of landslides. It would be ideal to avoid known landslide areas altogether during road planning, though small landslides could still be negotiated after appropriate slope stabilisation measures. Rating values have been assigned according to the landslide size such that large landslides get a very high (∞) value whereas other landslides get decreasing rating values as their size decreases.

Landslide Hazard Zonation (LHZ) is another important consideration in this study. Each pixel in the LHZ map carries a value that corresponds to the potential of landslide hazard. Various landslide hazard zones have been rated according to the severity of hazard.

The drainage order map is involved here to consider the cost aspects of a bridge, if required. Increasing rating values have been assigned to successively higher order streams,

as the bridge span and construction cost is likely to increase with the increase in the width of the river channel.

Landuse/landcover data can be used to estimate the cost of land acquisition and maintenance. Snow and landslide debris areas have been assigned the highest cost rating, and settlements, agriculture land, fallow land, barren land, forest and sparsely vegetated areas receive successively lower cost ratings.

Lithology has been considered to include the cost of blasting, excavation and cut-and-fill works. Granites and gneisses have been given the highest rating, and successively lower cost ratings have been accorded to schists and gneisses, quartzites with slates, and limestone and greywacke.

By integrating the thematic data layers as above, a thematic cost map has been generated such that lower values indicate favourable pixel sites and higher values indicate relatively less favourable sites for route planning.

Route planning methodology:

During the last decade, a few research attempts have been made to develop route-planning approach using GIS technology. A detailed literature review in this regard has been carried out and presented. There appears to be no reported case of any GIS-based study in high-altitude and rugged landslide-prone terrains, such as the Himalayas. The thematic cost map generated earlier in an integrated manner to indicate an estimate of the cost per pixel for road development and maintenance forms the basis of route planning. However, it does not include costs due to distance and gradient. It is therefore necessary to take into account distance and gradient factors in computing the costs. Hence, the GIS-based route planning methodology would involve three main factors - thematic cost, distance, and gradient, which have to be integrated to identify the least-cost route.

For implementing this approach, the following three major steps are involved:

1. Selection of connected neighbours

2. Calculation of neighbourhood movement (NM) cost

3. Selection of least-cost route

Neighbourhood analysis in route planning deals with finding out the various possibilities of movement from the source pixel to its immediate neighbour. In a raster analysis, the connections can be compared with the moves in the game of chess and appropriate terms of Rook's, Bishop's, and Knight's patterns are used. In this study, two new patterns of neighbourhood movement have been conceived (adapted after the Knight's pattern), and named as Knight31 and Knight32 respectively. These new patterns would permit smoother turn and gentler gradient in route alignment, as and where required. To implement the neighbourhood connection in a raster GIS, the pixels are represented as nodes.

The neighbourhood movement cost (NM-cost) is the cost of moving to the connected neighbour from the source, considering the cost of neighbour-distance, gradient cost and thematic cost. Neighbour-distance is the distance between successive neighbours in a 3-D space and is calculated using Euclidean formulae. Gradient cost is very important in route planning in a terrain, such as the Himalayas. Following the Indian Roads Congress (IRC) guidelines (with some modifications), cost values (ordinal numbers) have been assigned to various gradient classes. A higher gradient would beget a higher cost. In considering the thematic cost, a single point value will be unrepresentative when movement from a source pixel to a connected neighbour is being considered. Therefore, the average thematic cost value of all the pixels in the route has been considered during computation. Thus, knowing neighbourhood distance, gradient cost and (average) thematic cost, the NM-costs in various neighbourhood patterns (Rook, Bishop, Knight, Knight31 and Knight32) can be calculated and formulae for the same have been derived.

Dijkstra's Algorithm, which traces the least-cost path in a network of nodes connected by weighted links, has been used in this study. According to this algorithm, each pixel in a raster framework should contain two basic information: NM-cost (which comprises of neighbourhood distance, gradient and thematic cost), and a pointer identifying the pixels connected. These information are updated in an iterative process. The algorithm calculates the least-cost route to all the pixels in the raster network from the source pixel. A dedicated software in C++ has been developed (named LaSIRF) to implement the three steps stated earlier, and has suitably been interfaced with ILWIS GIS.

Examples:

The methodology developed for finding the least-cost route in a landslide-prone terrain is computationally intensive and time consuming. Therefore, to test the concept, methodology and the algorithm, a few test areas of 1.5 km × 1.5 km size with different combinations of terrain conditions and landslide susceptibility have been selected. The following types of examples are presented:

1. Case of a major landslide
2. Case of a major landslide and adjacent minor landslides
3. Case of a minor landslide with adjacent areas possessing large variation in thematic costs
4. Case of a river crossing
5. Case of no-trespassing zones
6. Case of significant regional variation in thematic costs

The above examples demonstrate that the proposed GIS-based route planning methodology can successfully avoid large landslides and high landslide hazard zones, and thus the route can be selected to pass through relatively safer (lower cost) zones. Based on the above application examples, it is concluded that the GIS based route planning

methodology developed here possesses several merits (in comparison to the conventional manual route planning practice):

1. The methodology has been successfully tested in landslide-prone test sites.

2. In GIS-based methodology, it is possible to integrate and analyse various parameters related to route development and maintenance, collectively.

3. The computer-assisted methodology is very fast and efficient in comparison to the conventional manual practice.

4. The computer-based technique checks all the possible combinations of routes between source and destination points (which may not be possible in the manual practice) and therefore, the least-cost route generated by the algorithm would be genuine.

5. The GIS-based methodology considers gradient in various directions and path gradient can be adjusted during route selection, as per the requirements, depending upon the terrain conditions.

In brief, the major contributions can be enumerated as follows:

1. Generation of DEM from satellite stereo data in the Himalayas and its evaluation.

2. Use of multi-source classification approach to minimize the effect of shadows in remote sensing data for landuse/landcover mapping.

3. Development of a new GIS-based statistical approach (m-LNHF) for Landslide Hazard Zonation.

4. Development of a novel and intelligent approach for route planning in landslide susceptible terrain

   - Formulation and use of two new neighbourhood patterns (Knight31 and Knight32).

   - Implementation of Dijkstra's least-cost algorithm in rugged terrain (Himalayas).

It may be emphasised that the thrust of this research is on the development of route planning methodology and the factors, and their weighting-rating can be modified and adjusted, depending upon the local conditions in an area.

Finally, a few points on the future scope, *viz.,* increasing the raster window size for neighbourhood window selection, making the program more efficient and incorporating bridges and tunnels more gainfully, have been suggested.

References

Akinyede, J. O., (1990) A Geotechnical GIS Concept for Highway Route Planning, *ITC Journal*, 3, 262-269.

Aleotti, P. and Chowdhury, R., (1999) Landslide Hazard Assessment: Summary Review and New Perspectives, *Bulletin of Engineering Geology & Environment*, 58, 21-44.

Anbalagan, R., (1992) Landslide Hazard Evaluation and Zonation Mapping in Mountainous Terrain, *Engineering Geology*, 32, 269-277.

Anderson, J. M., Hardy, E. E., Roach, J. T. and Witmert, R. E., (1976) A Land Use Classification System for Use with Remote Sensing Data, *U. S. Geological Survey Professional Paper*, No. 964, Washington DC: Government Printing Office.

Apan, A. A., (1997) Land Cover Mapping for Tropical Forest Rehabilitation Planning using Remotely-Sensed Data, *International Journal of Remote Sensing*, 18(5), 1029-1049.

Aronoff, S., (1989) Geographic Information Systems: A Management Perspective, *WDL Publications*, Ottawa, 294p.

Arora, M. K. and Agarwal, K., (2002) A Computer Program for Sampling Design to Assess Image Classification Accuracy, *Photogrammetry Journal of Finland*, 18(1), 33-43.

Arora, M. K. and Mathur, S., (2001) Multi-source Classification using Artificial Neural Network in a Rugged Terrain, *GeoCarto International*, 16(3), 37-44.

Arora, M. K., Das Gupta, A. S., Gupta, R. P., (2004) An Artificial Neural Network Approach for Landslide Hazard Zonation in the Bhagirathi (Ganga) Valley, Himalayas, *International Journal of Remote Sensing*, 25(3), 559-572.

BLUH Manual (2002) Institute for Photogrammetry and Geoinformation, *University of Hannover*, Germany.

Bonham-Carter, G. F., Agterberg, F. P. and Wright, D. F., (1988) Integration of Geological Datasets for Gold Exploration in Nova Scotia, *Photogrammetric Engineering & Remote Sensing,* 54(11), 1585-1592.

Boroujerdi, A. and Uhlmann, J., (1998) An Efficient Algorithm for Computing Least Cost Paths with Turn Constraints, *Information Processing Letters,* 67, 317-321.

Brabb, E. E., (1984) Innovative Approaches to Landslide Hazard and Risk Mapping. In: *Proceedings 4th International Symposium on Landslides,* Toronto, Canada, 1, 307-324.

Brabb, E. E., (1991) The World Landslide Problem, *Episodes,* 14(1), 52-61.

Bruzzone, L., Conese, C., Maselli, F. and Roli, F., (1997) Multi-source Classification of Complex Rural Areas by Statistical and Neural-Network Approaches, *Photogrammetric Engineering & Remote Sensing,* 63(5), 523-533.

Bughi, S., Aleotti, P., Bruschi, R., Andrei, G., Milani, G. and Scarpelli, G., (1996) Slow Movements of Slopes Interfering with Pipelines: Modeling Vs Monitoring. In: *Proceedings of 15th International Conference OMAE,* Firenze, Italy, June, 1996.

Capecchi, F. and Focardi, P., (1988) Rainfall and Landslides: Research into a Critical Precipitation Coefficient in an Area of Italy. In: *Proceedings of 5th International Symposium on Landslides,* Lausanne, Switzerland, 2, 1131-1136.

Carrara, A. M., Pugliese Carratelli, E. and Merenda, L., (1977) Computer-based Data Bank and Statistical Analysis for Slope Instability Phenomena, *Zeitschrift für Geomorphologie N.F.,* 21, 187-222.

Carrara, A. M., Cardinali, M., Detti, R., Guzzetti, F., Pasqui, V. and Reichenbach, P., (1991) GIS Techniques and Statistical Models in Evaluating Landslide Hazard, *Earth Surface Process & Landforms,* 16, 427-445.

Chavez, P. S. Jr., (1988) An Improved Dark Object Subtraction Technique for Atmospheric Correction of Multispectral Data, *Remote Sensing of Environment,* 24, 459-479.

Cheng, X., Zhang, Y., Dongchen, E., Li, Z. and Shao, Y., (2003) Digital Elevation Model Construction using ASTER Stereo VNIR Scene in Antarctic In-land Ice Sheet, *http://lab.irsa.ac.cn/~xiaoxiao/paper/PID19840.pdf.*

Chi, K-H., Park, N-W. and Lee, K., (2002) Identification of Landslide Area using Remote Sensing Data and Quantitative Assessment of Landslide Hazard. In: *Proceedings of IEEE International Geosciences and Remote Sensing Symposium,* 19 July, Toronto, Canada.

Chung, C-J. F. and Fabbri, A. G., (1999) Probabilistic Prediction Models for Landslide Hazard Mapping, *Photogrammetric Engineering & Remote Sensing,* 65(12), 1389-1399.

Civco, D. L., (1989) Topographic Normalization of Landsat Thematic Mapper Digital Imagery, *Photogrammetric Engineering & Remote Sensing,* 55(9), 1303-1309.

Clerici, A., Perego, S., Tellini, C. and Vescovi, P., (2002) A Procedure for Landslide Susceptibility Zonation by the Conditional Analysis Method, *Geomorphology,* 48, 349-364.

Colby, J. D., (1991) Topographic Normalization in Rugged Terrain, *Photogrammetric Engineering & Remote Sensing*, 57(5), 531-537.

Collischonn, W. and Pilar, J. V., (2000) A Direction Dependent Least-cost-path Algorithm for Roads and Canals, *International Journal of Geographical Information Science,* 14(4), 397-406.

Congalton, R. G., (1991) A Review of Assessing the Accuracy of Classifications of Remotely Sensed Data, *Remote Sensing of Environment*, 37, 35-47.

Cracknell, A. P., (1993) ICORG-92 – Remote Sensing Applications and Geographic Information Systems – Recent Trends – Preface, *International Journal of Remote Sensing*, 14(17), 3077.

Cracknell, A. P., (1998) Synergy in Remote Sensing – What's in a Pixel? *International Journal of Remote Sensing*, 19(11), 2025-2047.

Csaplovics, E., (1998) High Resolution Space Imagery for Regional Environmental Monitoring – Status Quo and Future Trends, *International Archives of Photogrammetry & Remote Sensing*, 32(7), 211-216.

Curran, P. J. and Foody, G. M., (1994) The Use of Remote Sensing to Characterize the Regenerative States of Tropical Forests. In: Foody, G. and Curran, P. (Eds.) *Environmental Remote Sensing from Regional to Global Scales*, John Wiley & Sons, Chichester, UK, 44-83.

Demers, M. N., (2000) Fundamentals of Geographic Information Systems, 2nd Edition, *John Wiley & Sons,* New York, US, 498p.

Dijkstra, E. W., (1959) A Note on Two Problems in Connection with Graphs, *Numerische Mathematik*, 1, 269-271.

Dikau, R., Brunsden, D., Schrott, L. and Ibsen, M. L. (Eds.), (1996) Landslide Recognition: Identification, Movement and Causes, *John Wiley & Sons,* Chichester, UK, 251p.

Douglas, D. H., (1994) Least-cost Path in GIS using an Accumulated-cost Surface and Slope Lines, *Cartographica*, 31, 37-51.

Eiumnoh, A. and Shrestha, P., (2000) Application of DEM Data to Landsat Image Classification: Evaluation in a Tropical Wet-Dry Landscape of Thailand, *Photogrammetric Engineering & Remote Sensing,* 66(3), 297-304.

Elias, P. B. and Bandis, S. C., (2000) Neurofuzzy Systems in Landslide Hazard Assessment. In: *Proceedings of 4th International Symposium on Spatial Accuracy Assessment in Natural Resources and Environment Sciences*, July 2000, 199-202.

Ellis, M. C., (1990) Analytical Free-Range Route Planning "G-Route" GIS Simulation Model, *Technical Note Internal Publication ITC,* Enschede, The Netherlands.

EOSAT, (1994) Merge Process Enhances Value of Data Sets, *EOSAT Notes*, 9, 5.

ERDAS Imagine Field and Tour Guides (2001) *ERDAS, Inc.*, Atlanta, Georgia, US.

Feldman, S. C., Pelletier, R. E., Walser, E., Smoot, J. C. and Ahl, D., (1995) A Prototype for Pipeline Routing using Remotely Sensed Data and Geographic Information System Analysis, *Remote Sensing of Environment*, 53, 123-131.

Fisher, P. F. and Pathirana, S., (1990) The Evaluation of Fuzzy Membership of Land Cover Classes in the Suburban Zone, *Remote Sensing of Environment*, 34(2), 121-132.

Foody, G. M., (2002) Status of Land Cover Classification Accuracy Assessment, *Remote Sensing of Environment*, 80, 185-201.

Foody, G. M. and Arora, M. K., (1996) Incorporating Mixed Pixels in the Training, Allocation and Testing Stages of Supervised Classifications, *Pattern Recognition Letters*, 17, 1389-1398.

Foody, G. M., Campbell, N. A., Trodd, N. M. and Wood, T. F., (1992) Derivation and Applications of Probabilistic Measures of Class Membership from Maximum Likelihood Classification, *Photogrammetric Engineering & Remote Sensing*, 58, 1335-1341.

Frank, T. D., (1988) Mapping Dominant Vegetation Communities in the Colorado Rocky Mountain Front Range with LANDSAT Thematic Mapper and Digital Terrain Data, *Photogrammetric Engineering & Remote Sensing*, 54(12), 1727-1734.

Gansser, A., (1964) Geology of the Himalayas, *Interscience Publishers*, London, UK, 289p.

Gong, P., (1996) Integrated Analysis of Spatial Data from Multisources using Evidential Reasoning and Artificial Neural-Network Techniques for Geological Mapping, *Photogrammetric Engineering & Remote Sensing*, 62, 513-523.

Gupta, R. P., (2003) Remote Sensing Geology, 2nd Edition, *Springer-Verlag*, Berlin-Heidelberg, Germany, 655p.

Gupta, R. P. and Joshi, B. C., (1990) Landslide Hazard Zonation using the GIS Approach – A Case Study from the Ramganga Catchment, Himalayas, *Engineering Geology*, 28, 119-131.

Gupta, R. P., Saha, A. K., Arora, M. K. and Kumar, A., (1999) Landslide Hazard Zonation in a Part of the Bhagirathi Valley, Garhwal Himalayas, using Integrated Remote Sensing- GIS, *Himalayan Geology*, 20(2), 71-85.

Gupta, V., Sah, M. P., Virdi, N. S. and Bartarya, S. K., (1993) Landslide Hazard Zonation in the Upper Satluj valley, District Kinnaur, Himachal Pradesh, *Journal of Himalayan Geology*, 4(1), 81-93.

Guzzetti, F., Carrara, A., Cardinali, M. and Reichenbach, P., (1999) Landslide Hazard Evaluation: a Review of Current Techniques and Their Application in a Multi-scale Study, Central Italy, *Geomorphology*, 31, 181-216.

Holben, B. and Justice, C., (1981) An Examination of Spectral Band Ratioing to Reduce the Topographic Effect on Remotely Sensed Data, *International Journal of Remote Sensing*, 2(2), 115-133.

Horowitz, E., Sahni, S. and Rajasekaran, S., (2002) Fundamentals of Computer Algorithms, *Galgotia Publications*, New Delhi, India, 241-252.

ILWIS Manual, (2001) *ITC*, Enschede, The Netherlands.

IRC, (2001) Recommendations about the Alignment Survey and Geometric Design of Hill Roads, 2nd Revision, *The Indian Roads Congress*, IRC:52-2001.

Jacobsen, K., (1994) Comparison of Mapping with MOMS and SPOT Images. In: *Proceedings of ISPRS Com IV,* Athens, Greece.

Jacobsen, K., (1997) Calibration of IRS-1C PAN-Camera. In: *Proceedings of ISPRS joint workshop "Sensors and mapping from Space",* 29 Sept - 2 Oct, University of Hannover, Germany.

Jacobsen, K., (1998) Mapping with IRS-1C-Images. In: *Proceedings of ASPRS Annual Convention,* Tampa, US.

Janssen, L. F., Jaarsma, J. and Linder, E. van der., (1990) Integrating Topographic Data with Remote Sensing for Land-Cover Classification, *Photogrammetric Engineering & Remote Sensing,* 48(1), 123-130.

Jayaprasad, P., Narender, B., Arya, A. S. and Ajai, (2002) Extraction of Terrain Parameters from IRS-1C PAN Stereo Data using Photogrammetric Techniques, *Current Science,* 82(3), 333-337.

Jensen, J. R., (1996) Introductory Digital Image Processing: A Remote Sensing Perspective, 2nd Edition, *Prentice-Hall,* New Jersey, US, 318p.

Jha, V. K., (1991) Remote Sensing and Aspects of Mass-Movements – A Case Study from Nepal Himalayas. In: Gupta, P. N. and Roy, A. K. (Eds.), *Mountain Resource Management and Remote Sensing,* Surya Publication, Dehradun, India, 79-84.

Jones, A. R., Settle, J. J. and Wyatt, B. K., (1988) Use of Digital Terrain Data in the Interpretation of SPOT-1 HRV Multispectral Imagery, *International Journal of Remote Sensing,* 9(4), 669-682.

Kawata, Y., Ueno, S. and Kusaka, T., (1988) Radiometric Correction for Atmospheric and Topographic Effects on Landsat MSS Images, *International Journal of Remote Sensing,* 9, 729-748.

Khanna, S. K. and Justo, C. E. G., (1987) Highway Engineering, 6th Edition, *Nem Chand & Bros.,* Roorkee, India, 908p.

Kratky, V., (1989) On-line Aspects of Stereophotogrammetric Processing of SPOT images, *Photogrammetric Engineering & Remote Sensing,* 55(3), 311-316.

Kraus, K., (1993) Photogrammetry, Vol. 1, Fundamentals and Standard Processes, *Ümmler,* Bonn, Germany, 397p.

Lee, J. and Stucky, D., (1998) On Applying Viewshed Analysis for Determining Least-Cost Paths on Digital Elevation Models, *International Journal of Geographical Information Science,* 12(8), 891-905.

Lee, S., Choi, J., Chwae, U. and Chang, B., (2002a) Landslide Susceptibility Analysis using Weight of Evidence. In: *Proceedings of IEEE International Geosciences and Remote Sensing Symposium,* 19 July, Toronto, Canada (CD-ROM).

Lee, S., Choi, J. and Min, K., (2002b) Landslide Susceptibility Analysis and Verification using the Bayesian Probability Model, *Environmental Geology,* 43, 120-131.

Lee, S., Ryu, J-H., Won, J-S. and Park, H-J., (2004) Determination and Application of the Weights for Landslide Susceptibility Mapping using an Artificial Neural Network, *Engineering Geology,* 71, 289-302.

Lillesand, T. M. and Kiefer, R. W., (1999) Remote Sensing and Image Interpretation, *John Wiley & Sons*, New York, US, 724p.

Linkwitz, K., (1961) Photogrammetry in Highway Engineering, Translated from *Der Strassenbau*, 10, 610-625.

Lu, P. F. and An, P., (1999) A Metric for Spatial Data Layers in Favourability Mapping for Geological Events, *IEEE Transaction on Geosciences & Remote Sensing*, 37(3), 1194-1198.

Mantovani, F., Soeters, R. and van Westen, C. J., (1996) Remote Sensing Techniques for Landslide Studies and Hazard Zonation in Europe, *Geomorphology*, 15, 213-225.

Mather, P. M., (1999) Computer Processing of Remotely-Sensed Images: An Introduction, 2nd Edition, *Wiley*, Chichester, UK, 306p.

McKean, J., Buechel, S. and Gaydos, L., (1991) Remote Sensing and Landslide Hazard Assessment, *Photogrammetric Engineering & Remote Sensing*, 57(9), 1185-1193.

Michelson, D. B, Liljeberg, B. M. and Pilesjo, P., (2000) Comparison of Algorithms for Classifying Swedish Landcover using Landsat TM and ERS-1 SAR data, *Remote Sensing of Environment*, 71(1), 1-15.

Musa, M. K. A. and Mohamed, A. N., (2002) Alignment and Locating Forest Road Network by Best-Path Modeling Method, *http://www.gisdevelopment.net/aars/acrs/2002/for/092.pdf*.

Nagarajan, R., Mukherjee, A., Roy, A. and Khire, M. V., (1998) Temporal Remote Sensing Data and GIS Application in Landslide Hazard Zonation of Part of Western Ghat, India, *International Journal of Remote Sensing*, 19(4), 573-585.

Naithani, A. K., (1999) The Himalayan Landslides, *Employment News*, 23(47), 20 - 26 February, 1-2.

Navalgund, R. R., (2001) Remote Sensing - Basics and Applications, *Resonance: Journal of Science Education*, 51-60, *http://www.ias.ac.in/resonance/Dec2001/pdf/Dec2001 p51-60.pdf*.

Navalgund, R. R. and Kasturirangan, K., (1983) The Remote Sensing Satellite – A Program Overview. In: *Proceedings of Indian Academy of Sciences; Engineering – Sciences – Remote Sensing – III*, 6, 313-336.

Nilsen, T. H. and Brabb, E. E., (1977) Slope Stability Studies in the San Francisco Bay Region, California, *Geological Society of America Reviews in Engineering Geology*, 3, 235-242.

Okimura, T. and Kawatani, T., (1986) Mapping of the Potential Surface-failure Sites on Granite Mountain Slopes. In: Gardiner, V. (Ed.), *International Geomorphology*, Part 1, Wiley, New York, US, 121-138.

O'Leary, D. W., Friedman, J. D. and Pohn, H. A., (1976) Lineament, Linear and Lineation: Some Proposed New Standards for Old Terms, *Bulletin of Geological Society of America*, 87, 1463-1469.

Pachauri, A. K., Gupta, P. V. and Chander, R., (1998) Landslide Zoning in a Part of the Garhwal Himalayas, *Environmental Geology*, 36(3-4), 325-334.

Pachauri, A. K. and Pant, M., (1992) Landslide Hazard Mapping Based on Geological Attributes, *Engineering Geology*, 32, 81-100.

Prakash, A., Fielding, E. J., Gens, R., Genderen, J. L. van and Evans, D. L., (2001) Data Fusion for Investigating Land Subsidence and Coalfire Hazards in a Coal Mining Area, *International Journal of Remote Sensing*, 22(6), 921-932.

Rao, Y. S. and Rao, K. S., (2003) Comparison of DEMs Derived from In SAR and Optical Stereo Techniques, *http://earth.esa.int/workshops/fringe03/participants/287/paper_ysrao_comp_dems_full_paper.pdf*

Rautela, P. and Lakhera, R. C., (2000) Landslide Risk Analysis between Giri and Tons Rivers in Himachal Himalaya (India), *International Journal of Applied Earth Observation & Geoinformation (JAG)*, 2(3/4), 153-160.

Ravindran, K. V. and Philip, G., (1999) 29 March 1999 Chamoli Earthquake: A preliminary Report on Earthquake-induced Landslides using IRS-1C/1D Data, *Current Science*, 77(1), 21-25.

Rees, W. G., (2004) Least-Cost Paths in Mountainous Terrain, *Computers & Geosciences*, 30, 203-209.

Richards, J. A. and Jia, X., (1999) Remote Sensing Digital Image Analysis: An Introduction, 3rd Edition, *Springer-Verlag*, Heidelberg, Germany, 363p.

Rössner, S., Wetzel, H.-U., Kaufmann, H., Kornus, W., Lehner, M., Reinartz, P. and Müller, R., (2000) Landslide Investigations in Southern Kyrgyzstan Based on a Digital Elevation Model Derived from Stereoscopic MOMS-2p Data, *IAPRS*, 33(B7), Amsterdam, The Netherlands, 1259-1266.

Rupke, J., Cammeraat, E., Seijmonsbergen, A. C. and van Westen, C. J., (1988) Engineering Geomorphology of the Widentobel Catchment, Appenzell and Sankt Gallen, Switzerland. A Geomorphological Inventory System Applied to Geotechnical Appraisal of Slope Stability, *Engineering Geology*, 26, 33-68.

Sabins, F. F., (1996) Remote Sensing Principles and Interpretations, *W. H. Freeman & Co.*, New York, US, 494p.

Saha, A. K., Gupta, R. P. and Arora, M. K., (2002) GIS-based Landslide Hazard Zonation in the Bhagirathi (Ganga) Valley, Himalayas, *International Journal of Remote Sensing*, 23(2), 357-369.

Sanjeevi, S., Vani, K. and Lakshmi, K., (2001) Comparison of Conventional and Wavelet Transform Techniques for Fusion of IRS-1C LISS-III and PAN Images. In: *Proceedings of ACRS 2001 - 22nd Asian Conference on Remote Sensing*, 5-9 November, Singapore, 1, 140-145.

Saraf, A. K., (2000) IRS-1C-PAN Depicts Chamoli Earthquake Induced Landslides in Garhwal Himalayas, India, *International Journal of Remote Sensing*, 21(12), 2345-2352.

Sarkar, S. and Kanungo, D. P., (2004) An Integrated Approach for Landslide Susceptibility Mapping using Remote Sensing and GIS, *Photogrammetric Engineering & Remote Sensing*, 70(5), 617-625.

Shalan, M. A., Arora, M. K. and Ghosh, S. K., (2003) An Evaluation of Fuzzy Classifications from IRS 1C LISS III Imagery: a Case Study, *International Journal of Remote Sensing*, 24(15), 3179-3186.

Shanmugam, P. and Sanjeevi, S., (2001) Analysis and Evaluation of Fusion Techniques using IRS-1C LISS-3 and Pan Data for Monitoring Coastal Wetlands of Vedaranniyam, Tamil Nadu. In: *Proceedings of the National, symposium on advances in remote sensing technology with special emphasis on high resolution imagery & annual convention of Indian Society of Remote Sensing (ISRS)*, 11 - 13 December, Ahmedabad, India.

Sharma, P. K., Chopra, R., Verma, V. K. and Thomas, A., (1996) Flood Management using Remote Sensing Technology: The Punjab (India) Experience, *International Journal of Remote Sensing*, 17(17), 3511-3521.

Solka, J. L., Perry, J. C., Poellinger, B. R. and Rogers, G. W., (1995) Fast Computation of Optimal Paths using a Parallel Dijkstra Algorithm with Embedded Constraints, *Neurocomputing*, 8, 195-212.

Srivastava, P. K., Goswami, A., Alurkar, M. S. and Srinivasan, T. P., (2000) Inflight Geometric Calibration of IRS-1C/IRS-1D Imaging Model: an Experience, *Bulletin SFPT n° 159*, 3, 27-33.

Strahler, A. N., (1964) Quantitative Geomorphology of Drainage Basins and Channel Networks. In: Chow, V. T. (Ed.), *Handbook of Applied Hydrology*, McGraw-Hill, New York, US, Section 4-11.

Strahler, A. H., Logan, T. L. and Bryant, N. A., (1978) Improving Forest Cover Classification Accuracy from Landsat by Incorporating Topographic Information. In: *Proceedings of 12th Symposium Remote Sensing Environment*, Ann Arbor, Michigan, US, 2, 927-942.

Tanimeto, S. L., (1987) The Elements of Artificial Intelligence – an Introduction using LISP, *Computer Science Press*, New York, US, 530p.

Tiwari, R. S., (1981) Surveys for Planning and Alignment of Hill Roads, *340b – Special Course on Hill Roads*, 22 July - 9 August, Department of Continuing Education, University of Roorkee, Roorkee, India.

Tso, B. and Mather, P. M., (2001) Classification Methods for Remotely Sensed Data, *Taylor & Francis*, London, UK, 272p.

Valdiya, K. S., (1980) Geology of Kumaun Lesser Himalaya, *Wadia Institute of Himalayan Geology*, Dehradun, India, 291p.

van Asch, T. H. J., Buma, J. and van Beek, L. P. H., (1999) A View on Some Hydrological Triggering Systems in Landslides, *Geomorphology*, 30, 25-32.

van Westen, C. J., (1994) GIS in Landslide Hazard Zonation: a Review, with Examples from the Andes of Colombia. In: Price, M. and Heywood, I. (Eds.), *Mountain Environments and Geographic Information System*, Taylor & Francis, Basingstoke, UK, 135-165.

van Westen, C. J., (1997) Statistical Landslide Hazard Analysis. In: *Application Guide, ILWIS 2.1 for Windows*, ITC, Enschede, The Netherlands, 73-84.

van Westen, C. J., Soeters, R. and Sijmons, K., (2000) Digital Geomorphological Landslide Hazard Mapping of the Alpago Area, Italy, *International Journal of Applied Earth Observation & Geoinformation (JAG)*, 2(1), 51-59.

Varnes, D. J., (1984) Landslide Hazard Zonation: a Review of Principles and Practice, *UNESCO*, Paris, France, 1-63.

Virdi, N. S., Sah, M. P. and Bartarya, S. K., (1997) Mass Wasting, its Manifestations, Causes and Control: Some Case Histories from Himachal Himalaya. In: Agarwal, D.K., Krishna, A.P., Joshi, V., Kumar, K. and Palni, M.S. (Eds.) *Perspectives of Mountain Risk Engineering in the Himalayan Region,* Gyanodaya Prakashan, Nainital, India, 111-130.

Welch, R. and Ehlers, M., (1987) Merging Multiresolution SPOT HRV and Landsat TM data, *Photogrammetric Engineering & Remote Sensing,* 53(3), 301-303.

Wieczorek, G. F., (1984) Preparing a Detailed Landslide-Inventory Map for Hazard Evaluation and Reduction, *Bulletin of Association of Engineering Geologists*, 21(3), 337-342.

Winter, S., (2002) Modeling Costs of Turns in Route Planning, *GeoInformatica,* 6(4), 345-361.

Xu, J. and Lathrop, R. G., (1994) Improving Cost-path Tracing in a Raster Data Format, *Computers & Geosciences,* 20(10), 1455-1465.

Yin, K. L. and Yan, T. Z., (1988) Statistical Prediction Model for Slope Instability of Metamorphosed Rocks. In: *Proceedings of 5th International Symposium on Landslides*, Lausanne, Switzerland, 2, 1269-1272.

Yu, C., Lee, J. and Munro-Stasiuk, M. J., (2003) Extensions to Least-Cost Path Algorithms for Roadway Planning, *International Journal of Geographical Information Science,* 17(4), 361-376.

Internet Resources:

http://www.nrsa.gov.in

http://www.uschess.org

http://www.wikipedia.org/wiki/Dijkstra's_algorithm

http://ciips.ee.uwa.edu.au/~morris/Year2/PLDS210/dijkstra.html